Coordinated Multi-Point Transmission Aided Cell Switch Off Schemes for Energy Efficient Mobile Cellular Networks

by

Gencer Cili

A thesis submitted to the
Faculty of Graduate Studies and Research
in partial fulfillment of the requirements for the degree of

Master of Applied Science in Electrical and Computer Engineering

Ottawa-Carleton Institute for Electrical and Computer Engineering
Department of Systems and Computer Engineering
Carleton University, Ottawa, Ontario, Canada

Abstract

Due to the increased energy consumption of cellular access networks, energy efficiency of cellular systems should be considered jointly with spectral efficiency to obtain the overall performance metrics and trade-offs. Downlink coordinated multipoint (CoMP) joint transmission aided cell switch off schemes mitigate inter-cell interference and create an energy efficient system by eliminating the need to increase the transmit antenna powers of the active cells serving the users in the switched off cell. However, the performance of this newly proposed scheme is heavily dependent on the accuracy of the selected CoMP joint transmission set. We model the multi-point channel estimation enabled via channel state information reference symbols (CSI-RS) introduced in 3GPP release 10 systems and simulate possible scenarios that would lead to inaccurate transmission set clustering: multi-point channel estimation errors and possible CoMP system delays due to CSI transfers, node processing delays and network topology limitations. Individual and joint impacts of system delays and estimation errors on energy efficiency and capacity performance degradations for various mobility conditions are demonstrated. These technical challenges and the clustering accuracy bottleneck are overcome by users performing multi-point channel estimation and serving eNB performing channel prediction procedures.

Simulations are performed according to realistic large and small scale fading models for multi-point radio links. It is demonstrated that the users being served by larger joint transmission clusters are more vulnerable to performance degradation. Novel multi-point channel estimation schemes are proposed and discussed, where the users with higher clustering degrees enlarge the channel estimation filter lengths for a certain subset of the CoMP measurement set which has high chance of being included in the joint transmission cluster. Multi-point channel estimation accuracy can be maximized when users track each multipath component of channel impulse responses (CIRs) separately, however computation complexity of such schemes are significantly high compared to the methods which just track the superimposed CIRs. Serving eNB can avoid clustering decisions based on outdated CSI feedbacks by predicting the channel conditions on upcoming transmission time intervals (TTIs). To reduce the CoMP clustering accuracy responsibility of the serving eNBs, users can take initiative to influence the clustering decisions by sending selective CSI feedbacks. This novel CSI feedback reporting scheme not only reduces the possible CoMP access network system delays but also reduces the serving eNB processing time for clustering decisions.

Acknowledgements

I would like to express my sincerest gratitude and respect for my supervisors Prof. Halim Yanikomeroglu and Prof. Fei Richard Yu for their dedicated support, guidance, supervision, and motivation throughout the thesis research. Without their contributions, this work would not have been possible. Prof. Yanikomeroglu has been an inspiration for me during the overall research process. His expertise in the field of wireless communications, knowledge of the latest radio technologies and the ability to relate academic research work to industrial implementation proposals helped me significantly extend by telecommunications knowledge. His continuous motivation made it possible to use the thesis research work to create international conference papers and patent filings. Prof. Yu's attention to detail, invaluable suggestions throughout the research, and thorough knowledge of the latest industry trends and academic research topics enhanced the quality of the thesis. His advice about the choice of research topic, suggestions about literatures to review, and technical recommendations for focusing on interesting problems helped majorly expedite the work. Both of my supervisors not only helped me for the research, but also provided invaluable comments about by professional career choices. I am extremely thankful to have the opportunity to work with them throughout this enjoyable and unforgettable journey.

I would also like to thank my former manager from Research in Motion, Hongchang Tian, for providing all the possible support to create an ideal environment for me to work for the RIM Radio SW team and pursue my Master's degree concurrently. Without his understanding, this work would not have been possible. I must also express my appreciation to my former colleague, Hikmet Asmer, for always motivating me to continue my career in the wireless industry and pursue a graduate degree at the same time.

Sincere thanks to my undergraduate supervisor from McGill University, Prof. Jan Bajcsy, for helping me shape my career choices. He will always be my role model due to his intelligence, smart way of thinking, and passion for field of wireless communications.

Last but not the least, I would like to express my special thanks and respect for my parents. There are not enough words to describe my appreciation for all the effort they spent on me. I am extremely grateful for their continuous moral support, patience and love.

Table of Contents

List of Tables

List of Figures

Nomenclature

AIPN	All IP Network
AMC	Adaptive Modulation and Coding
AWGN	Additive White Gaussian Noise
BC	Billing Center
BS	Base Station
C2POWER	Cognitive Radio and Cooperative Strategies for POWER Saving
CAPEX	Capital Expenditure
CDF	Cumulative Distribution Function
CDMA	Code Division Multiple Access
CIR	Channel Impulse Response
CLT	Central Limit Theorem
CN	Core Network
COMP	Coordinated Multi-Point
CP	Cyclic Prefix
CQI	Channel Quality Indicator
CRC	Cyclic Redundancy Check
CRS	Cell Specific Reference Symbol
CS	Circuit Switched
CS/CB	Coordinated Scheduling Coordinated Beamforming
CSI	Channel State Information
CTF	Channel Transfer Function
DCI	Downlink Control Information
DE	Deployment Efficiency
DFT	Discrete Fourier Transform
DL	Downlink
DPS	Dynamic Point Selection

DRX	Discontinuous Reception
DTX	Discontinuous Transmission
EARTH	Energy Aware Radio and Network Technologies
EDGE	Enhanced Data Rates for GSM Evolution
EE	Energy Efficiency
E-NB	Enhanced Node B
E-PDCCH	Enhanced Physical Downlink Control Channel
ES	Energy Saving
E-UTRAN	Evolved Universal Terrestrial Radio Access Network
FDD	Frequency Division Duplex
FDM	Frequency Division Multiplexing
FFT	Fast Fourier Transform
GPRS	General Packet Radio Service
HARQ	Hybrid Automatic Repeat Request
HetNet	Heterogonous Network
HLR	Home Location Register
HSPA	High Speed Packet Access
ICI	Inter Carrier Interference
ICT	Information and Communications Technology
IFFT	Inverse Fast Fourier Transform
IP	Internet Protocol
I/Q	In-phase and Quadrature
ISI	Inter Symbol Interference
ITU	International Telecommunication Union
JT	Joint Transmission
KPI	Key Performance Indicator
LOS	Line-of-Sight
LTE	Long Term Evolution

LTE-A	Long Term Evolution Advanced
MAC	Media Access Control
MIB	Master Information Block
MIMO	Multiple Input Multiple Output
MMSE	Minimum Mean Square Error
NAS	Non Access Stratum
NLOS	Non-Line-of-Sight
OAM	Operations Administration and Management
OFDM	Orthogonal Frequency Division Multiplexing
OFDMA	Orthogonal Frequency Division Multiple Access
OPEX	Operational Expenditure
PA	Power Amplifier
PBCH	Physical Broadcast Channel
PDCCH	Physical Downlink Control Channel
PDF	Probability Distribution Function
PDN-GW	Packet Data Network Gateway
PDP	Power Delay Profile
PDSCH	Physical Downlink Shared Channel
PMI	Precoding Matrix Indicator
PRB	Physical Resource Block
PS	Packet Switched
PUCCH	Physical Uplink Control Channel
PUSCH	Physical Uplink Shared Channel
QAM	Quadrature Amplitude Modulation
QoS	Quality of Service
QPSK	Quadrature Phase Shift Keying
RAT	Radio Access Technology
RB	Resource Block

RE	Resource Element
RI	Rank Indicator
RMS	Root Mean Square
RRC	Radio Resource Control
RRH	Remote Radio Head
RRM	Radio Resource Management
RS	Reference Signal
RSRP	Reference Signal Received Power
RSRQ	Reference Signal Received Quality
SCME	Spatial Channel Model Extended
SE	Spectral Efficiency
SIB	System Information Block
SINR	Signal-to-Interference-plus-Noise Ratio
SON	Self-Organizing Network
TDM	Time Division Multiplexing
TM	Transmission Mode
TTI	Transmission Time Interval
UE	User Equipment
UL	Uplink
UMA	Urban Macro
UMTS	Universal Mobile Telecommunications System
UTRAN	Universal Terrestrial Radio Access Network
VLR	Visiting Location Register
WCDMA	Wideband Code Division Multiple Access
WINNER	Wireless World Initiative New Radio

Chapter 1

Introduction

1.1 Thesis Problem Statement and Motivation

Exponential rise in cellular device usage in the recent years along with the increase in the minimum required received quality of service lead the innovation in the direction of cellular enhancements enabling spectrally efficient systems. Future wireless standards like LTE-A (Long Term Evolution Advanced) and beyond are making significant changes to the overall system architecture, air interface and quality of service offered to the users. Increased complexity of these cellular features and the rising mobile usage rates create a major power consumption burden on the overall systems. As a result, all the key features considered by future wireless technologies should be jointly reviewed under the "green radio" umbrella to check for possibilities of energy saving implementations and increased total system capacity concurrently. Recent development and enhancements in wireless communications do not only focus on increasing the data rates, capacity or spectral efficiency, but also on implementing energy saving methods. This is mostly due to the observation of high energy consumption resulting from information and communications technologies and mainly wireless access networks. The information and communications technology (ICT) is responsible for 2-10% of the global energy consumption and the access networks (GERAN for GPRS, UTRAN for UMTS and e-UTRAN for LTE) are responsible for 60-80% of the whole cellular network energy consumption as mentioned in [1] - [3]. As a consequence, optimizing the wireless access stratum plays a more important role in overall energy savings in cellular architectures compared to the core network energy efficiency.

Fourth generation wireless standards pioneered by LTE (Long Term Evolution) technology utilize adaptive modulation, OFDMA (Orthogonal Frequency Division Multiple Access), and HARQ (Hybrid Automatic Repeat Request) schemes to maximize the observed capacity limits. However, Coordinated Multi-Point (CoMP) transmission technology, which is listed as one of the key features for LTE-Advanced, aims on decreasing the inter-cell interference via coordination among different transmission points to further increase the achieved cell edge data rates. Users will receive data transmission from multiple cells with better SINR (Signal-to-Interference-plus-Noise Ratio) values. This makes CoMP a potential candidate to deliver green radio solutions by decreasing the energy cost per bit, if used correctly.

The thesis aims on performing thorough analysis of CoMP performance in terms of energy efficiency and capacity, investigating joint use of CoMP with existing energy efficient cell switch off scheme, identifying technical challenges and performance bottlenecks for CoMP schemes, creating a framework for time-varying CoMP joint transmission scheme, and developing CoMP adaptive channel estimation and prediction schemes to tackle possible system delays and multi-point channel estimation errors.

1.2 Thesis Contributions

Novel contributions of the thesis which have not been analyzed or proposed in any existing literature, to the best of our knowledge, are listed as follows:

- Individual and joint impacts of channel estimation errors and system delays on DL CoMP performance metrics are evaluated. Impacts of inaccurate CoMP active set clustering due to the multi-point faulty time-varying channel feedbacks on overall system bits/Joule energy efficiency and downlink capacity rates are analyzed. It is shown that the accuracy of the time-varying joint transmission set clustering decisions, in terms of both the member choices and the clustering degrees, is the major performance determining factor for CoMP systems.
- Performance degradation sensitivities of various user locations in the cellular layout are characterized both for low and high mobility conditions. It is demonstrated that the users being served with higher CoMP clustering degrees get affected more severely due to inaccurate joint transmission sets.
- Novel CoMP adaptive multi-point channel estimation filter designs are proposed, where the user equipments (UEs) dynamically change the estimation filter lengths according to the observed CoMP clustering degrees and the probability of each measured point being an active member of the joint transmission set on the upcoming TTI, unlike the single point channel estimation techniques which adapt the filter lengths solely based on the coherence time of the channel and the UE receiver velocity. This method both improves the CoMP clustering accuracy and reduces the channel estimation computation complexity by making sure only the UEs observing higher clustering degrees utilize enlarged estimation filters for points that are more likely to take active role in joint PDSCH transmission.
- A novel multi-point channel feedback reporting method is proposed, where the UE performs down-selection on the joint transmission set for the upcoming TTI to reduce the clustering accuracy burden on the serving eNB. UE performs received power thresholding technique using the estimated multi-

point channel impulse responses and reports CSI feedback only for the points that are likely to be a part of the joint transmission cluster. This scheme reduces the uplink payload required to report multi-point feedbacks, avoids the unnecessary feedbacks to be transferred within the CoMP access network nodes, minimizes CSI processing time at the serving eNB, and yields more up-to-date CSI feedbacks to be used for CoMP clustering decisions.

Additional contributions of the thesis, which can be used to enhance the existing literature, are listed as follows:

- Joint use of the LTE-A feature, CoMP, with the traditional cell switch off scheme is analyzed. Increasing the transmit power method in the remaining active cells during the energy saving period is replaced by the remaining active cells using CoMP joint transmission technique in the downlink to jointly serve the users in the switched off cell. Realistic wireless channel and propagation models are used in accordance to 3GPP specifications and the simulation results demonstrate that the CoMP aided cell switch off schemes not only improve the energy efficiency of the radio access networks, but also increase the user perceived quality of service in terms of received downlink capacity rates with respect to the traditional cell switch off schemes.
- A study on optimal CoMP joint transmission clustering degree choices have been conducted, and it is demonstrated that the serving eNB has to perform threshold-based clustering decisions based on the received DL power values every TTI to balance the trade-off between the capacity and the energy efficiency of the access networks. This technique prevents energy efficiency degradations in the CoMP access network by avoiding inclusion of unnecessary points in the joint transmission cluster, which would lead to additional backhauling and signal processing power consumption that cannot be compensated by enough capacity gains.
- Various multi-point channel estimation/prediction schemes are analyzed to improve the joint transmission set clustering accuracy. Multi-point channel impulse responses can be tracked either by superimposed or decomposed format. Latter mentioned scheme tracks each multipath component of every CoMP measurement set member and yields more accurate estimates, however leads to significantly higher computation times as opposed to the superimposed tracking. It is also demonstrated that the serving eNB can maximize the performance gains by setting the channel prediction range equal to observed system delay between the CSI reports and the PDSCH transmission.

1.3 Publications, Patent Filings and Thesis Organization

The research work presented in this thesis has been published, accepted, submitted, or is in progress for submission. Produced articles are referenced across the chapters according to the following organization:

- Chapter 2 serves as a literature survey and tutorial. Introduction to green radio is presented and existing energy efficient cell switch off schemes are analyzed according to possible trade-offs. Architecture of downlink LTE transmission is explained thoroughly and CoMP joint transmission standardization process is described with respect to the newly introduced radio procedures. Existing CoMP literature is discussed and the technical challenges are identified.
- Chapter 3 describes the cellular system model used in our study, formulates the downlink CoMP performance metrics and presents a performance comparison of the traditional versus CoMP aided cell switch off schemes in terms of energy efficiency and capacity metrics assuming stationary channel conditions. Proof of concept is provided for the serving eNB to form the CoMP joint transmission clusters by thresholding the downlink received powers. Contents of the chapter are published in the following conference paper:
  - **G. Cili**, H. Yanikomeroglu, and F. R. Yu, "Cell switch off technique combined with coordinated multi-point (CoMP) transmission for energy efficiency in beyond-LTE cellular networks," in *Proc. IEEE ICC'12 Workshops,* Ottawa, ON, Canada, June 2012.
- Chapter 4 describes the small scale fading model used in our study, formulates the time-varying CoMP performance metrics, and analyzes the performance sensitivity of the proposed scheme for various users under different channel conditions by taking multi-point channel estimation errors and system delays into consideration. Impacts of the joint transmission clustering accuracy on the achieved CoMP performance gains are discussed. Contents of the chapter are presented in the following conference paper submission:
  - **G. Cili**, H. Yanikomeroglu, and F. R. Yu, "Energy efficiency and capacity evaluation of LTE-Advanced downlink CoMP schemes subject to channel estimation errors and system delay," submitted to *IEEE ICC'13*, Budapest, Hungary, June 2013.

- Chapter 5 describes the stochastic modeling of the channel impulse response and channel transfer function along with possible time-varying channel estimation/prediction schemes. Performance gains due to multi-point channel estimation/prediction procedures are analyzed with respect to energy efficiency and capacity performance metrics. Novel CoMP adaptive channel estimation filter designs and UE aided joint transmission set clustering methods are discussed. Contents of the chapter are presented in the following invention disclosures:

  - **G. Cili**, H. Yanikomeroglu, and F. R. Yu, "UE anchored down-selection for CoMP joint transmission cluster," Filed by Apple Inc., U.S. Patent Application No: 61/674,854 (filing date: July 24, 2012).
  - **G. Cili**, H. Yanikomeroglu, and F. R. Yu, "CoMP adaptive channel estimation prediction filter design," Filed by Apple Inc., U.S. Patent Application No: 61/674,852 (filing date: July 23, 2012).

  A journal paper with the following title is being prepared for submission:

  - **G. Cili**, H. Yanikomeroglu, and F. R. Yu, "Coordinated multi-point adaptive channel estimation and prediction schemes for accurate joint transmission clustering," to be submitted to an IEEE journal, Sept. 2012.

- Chapter 6 highlights the conclusions of the thesis and explains the possible enhancements for future work.

Chapter 2

Overview on Cell Switch Off Methods and CoMP Enhancements

2.1 Analysis of Existing Energy Efficient Cellular Schemes

Recent market innovations for "green radio" are pioneered by EARTH (Energy Aware Radio and Network Technologies) and C2POWER (Cognitive Radio and Cooperative Strategies for POWER saving in multi-standard wireless devices) projects which have strong partners in both academia and the industry. The goal of both projects explained in [4] and [5] can be listed as follows:

- Develop energy saving methods for wireless mobile devices and energy efficient mobile communication systems using cognitive and cooperative radio to decrease the CO_2 emission by the ICT (Information and Communications Technology) industry.
- Propose energy efficient network deployment and resource management schemes without sacrificing the quality of service perceived by the users and the total system capacity.

These innovations lead to new technology requirements for upcoming wireless technologies. Energy saving and low CAPEX/OPEX for the networks are now considered as future technology requirements for 3GPP release 11 and beyond standards by Docomo as mentioned in [6]. As a result, all the key features considered by future wireless technologies should be reviewed under the "green radio" umbrella to check for possibilities of energy saving implementations and design.

2.1.1 Enabling Methods for Green Radio

Various system level approaches are possible to obtain energy efficiency in cellular networks. A detailed survey on motivations for green cellular networks and different methods for energy savings are presented in [7] and categorized under energy savings via cooperative networks, renewable energy resources, heterogonous networks and cognitive radio. Core network operation, sustaining backhaul data traffic, access networks providing radio interface both for user and control planes, and mobile handsets contribute to the overall power consumption of the cellular systems. Energy efficiency approaches were categorized in [8] as: component level, radio interface, and network deployment methodologies.

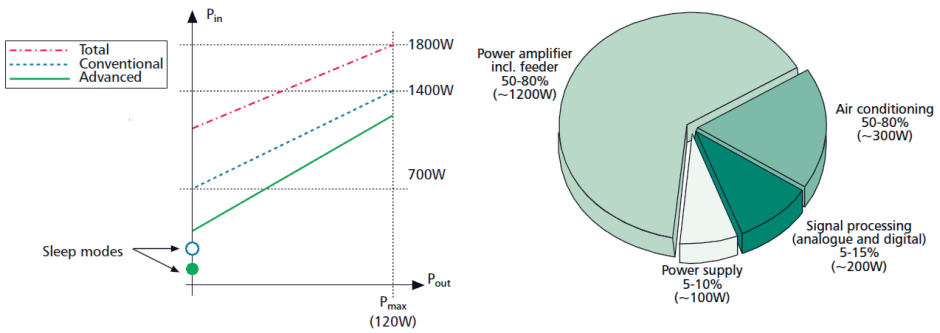

Figure 2.1: Power consumption distribution of radio access networks, adapted from [8] and [9].

Component level energy savings are obtained by focusing on the various power consuming parts of a base station. Figure 2.1 shows that the power amplifiers, air conditioners, power supply and signal processing all consume energy to operate a base station. Component level energy saving focuses on the PA (power amplifier) efficiency to draw less current during operation since the PA consumes between 50-80% of the overall base station power [9]. This is because the power amplification at the base station is essential while serving users facing major path losses. Methods like peak-to-average power ratio reduction, linearity increase, dynamic frequency and voltage scaling according to traffic load, component deactivation for digital/analog inactive base station components, digitally flexible drivers and PAs to control the output power, DC power consumption and linearity are some of the suggested methods. Power amplifier efficiency, the ratio of the input AC power to the downlink transmitted output power, degrades from 50% to 5% as the served number of users in the network decreases [10]. Hence, switching off the base station during low traffic loads can be favorable for overall energy consumption. It is mentioned in [11] that 80-90% of the energy consumed by the power amplifiers are wasted as heat which increases the power consumption of the air conditioning components as well. Power consumption of the signal processors are directly related to the used transmission and modulation schemes. Advanced spectrally efficient modulation schemes lead to higher signal processing powers. It should be noted that even when there is no load in the network, access network still consumes 50% of the peak DC power due to the power supply operating the base station and active air cooling as mentioned in [12] which is shown in Figure 2.1 where the base station still consumes an input power even when the downlink transmitted output antenna power is zero. As a result, main energy saving potentials at the component level are deactivating inactive parts of the digital/analogue circuits, implementing sleep modes during downlink transmission or switching off the base stations completely during the low traffic periods.

Link level energy saving methods contains all the air interface strategies and protocols that can be implemented to save power. Reduced control plane RRC and NAS signaling, MIB (Master Information Block) and SIBs (System Information Blocks) transmission, and synchronization signals will help the network save power during downlink operation. However, this method comes with the risk of bringing the overall network performance down for cell selection, cell acquisition and RRM procedures. Another link level solution to shift the focus from spectral efficiency to energy efficiency is to create micro-sleep modes for discontinuous transmission (DTX) on the downlinks. These deep/micro sleep modes for the base stations are enabled for 3GPP release 8 and further since LTE does not need to transmit the reference symbols continuously unlike UMTS/HSPA protocols where pilot symbols had to be continuously transmitted on the downlink. Discontinuous reception (DRX) operation is already enabled in 3GPP release 8 both for UEs in RRC idle and connected modes. Mobile units monitor paging messages and UL (Uplink)/DL (Downlink) scheduling grants on pre-configured cycles to save power. Same logic can be applied to the base stations where control and user plane data are transmitted on specific periods enabling the transmit circuits to be powered off during sleep modes.

Network level energy savings methods can be applied by deploying heterogonous networks, enabling coordination among the nodes, cooperative relaying and cognitive radio to dynamically adapt to changing traffic loads. Hierarchical deployment of networks via macro, micro, pico and femto cells decrease the propagation distance between the transmit and receive antennas, hence, reduce the required transmit power. Wireless relays, which are cheaper to deploy compared to base stations, do not require any backhaul links or complex routing schemes, create an in-direct multi-hop transmission environment with shorter propagation distances and decrease the burden on the power amplifier components. The challenge for HetNet and wireless relaying schemes is the optimal deployment strategy to balance the trade-off between increasing the outdoor coverage areas via small cells and still keeping the traffic load of the macro-cells at a certain level. As mentioned earlier, if majority of the coverage is sustained by the small cells, the traffic loads and the power amplifier efficiencies of the macro cells reduce and the overall deployment becomes more expensive due to the short range coverages of the small cells and relays. Cooperation among base stations can also help save energy in the cellular system either by load balancing options to decrease the transmission power in the cells with high traffic loads and increasing the transmission power of low traffic cells or by completely shutting of base stations under low traffic conditions and increasing the coverage area of the neighbor cells not to create any coverage

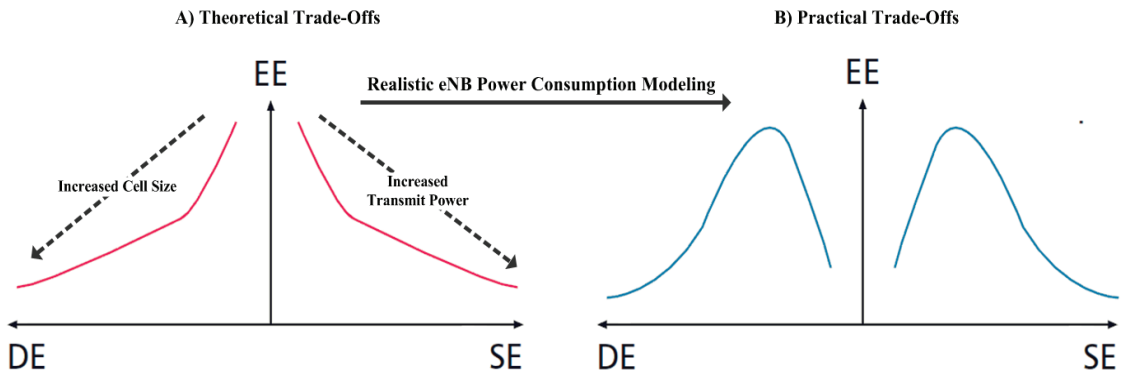

Figure 2.2: Deployment and spectrum efficiency versus energy efficiency trade-off, adapted from [14].

holes. A more environmentalist solution is proposed in [7] to save energy resources and decrease carbon emission is achieved by using alternative "green" resources such as biofuels, solar and wind energy in cellular networks.

Cell switch off scheme is the most promising candidate for energy savings in cellular networks since it provides a holistic approach by combining link, component and network level power saving methodologies. Cell with the low traffic conditions is switched off completely to maximize the component level power savings, and remaining active cells in the network coordinate to serve the users located in the switched off region. Various existing cell zooming strategies are analyzed and discussed in Section 2.1.3. Cell switch off schemes aided with downlink CoMP transmission will be discussed in Chapter 3, which enable the users in the switched off cell to be served simultaneously by multiple radio links.

2.1.2 Energy Efficient Resource Utilization and Performance Trade-offs

Energy efficient cellular methodologies are being standardized by major standardization bodies like 3GPP and ITU and existing key performance indicators like spectral efficiency and deployment efficiency should be jointly considered with the energy efficiency metrics. Standalone methods that aim on improving a certain performance metric and ignoring the remaining metrics are not of interest. Green radio implemented in any aspect of the wireless communication including access network enhancements, core network improvements, protocol stack changes, scheduling implementations or cooperating networks have to be re-considered according to deployment efficiency (*DE*) versus energy efficiency (*EE*) and spectral efficiency (*SE*) versus energy efficiency (*EE*) trade-offs. Deployment efficiency is considered as system throughput per unit deployment cost which can be simply improved by enlarging the cellular coverage of the existing base stations.

Increasing the downlink transmit powers decreases the total number of base stations deployed in the network and save unit cost for both capital expenditure (CapEx) and operational expenditure (OpEx). However, the implementation should be the exact opposite for systems aiming energy efficiency since denser base station deployments correspond to lower transmit powers due to shorter radio links [13]. At first, energy efficiency of the cellular network seems to decrease with lower deployment costs as shown in Figure 2.2a; however the relation between the access network power consumption and the deployment cost should be modeled realistically. Energy consumption and the deployment cost of the networks do not only depend on the transmit power of the base station, P_{TX}, but also on the operational power consumption, P_{OP}, such as the air cooling, signal processing and the power supply as explained in Section 2.1.1. As a result, increased cell sizes do not always yield energy inefficient solutions. Evaluating $EE - DE$ trade-off according to the realistic power consumption models shows that there exists an optimum solution which improves both the performance metrics as shown in Figure 2.2b.

Another performance indicator for cellular systems is the spectral efficiency measured in $\frac{\text{bits/sec}}{\text{Hz}}$, which has always been the main focus of improvement during the wireless evolution. Expressing energy efficiency of the system in bits/Joule, the theoretical relation between spectral and energy efficiency is derived by authors of [14] using Shannon's capacity formula for additive white Gaussian noise (AWGN) channels explained in [15] as:

$$SE = log_2(1 + \frac{P_{TX}g}{W*N_o}) \; ; \tag{2.1}$$

$$EE = Wlog_2(1 + \frac{P_{TX}g}{W*N_o})/P_{TX}g \; ; \tag{2.2}$$

$$EE = \frac{SE}{(2^{SE}-1)*N_o} \; . \tag{2.3}$$

Total bandwidth assigned to the user is expressed as W, channel gain is denoted as g, and noise spectral density is represented by N_o. Theoretical derivation for $EE - SE$ trade-off for an AWGN channel shown in (2.3), which ignored the transmission independent contributors to the overall power consumption in (2.1) and (2.2), suggests monotonically decreasing relation between spectral and energy efficiency performance metrics. In fact, under practical considerations for realistic access network power consumption model in [16], pathloss and propagation schemes, modulation/coding schemes, resource management algorithms, power amplifier linearity/efficiency and multi-user/multi-cell scenarios, $EE - SE$ trade-off leads to a non-monotonic relation shown in Figure 2.2.b.

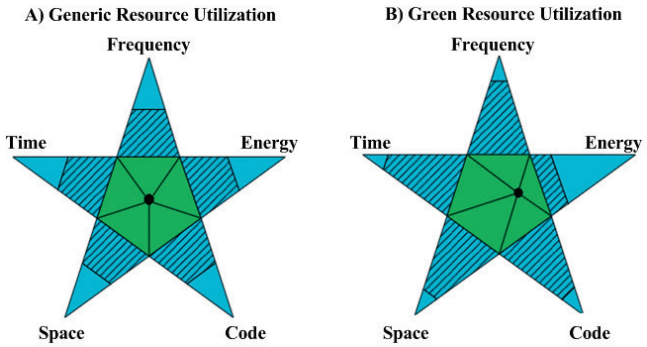

Figure 2.3: Energy efficient wireless resource utilization, taken from [17].

This is the fundamental motivation for developing energy efficient frameworks without sacrificing the user perceived quality of service (QoS) in terms of spectral efficiency and achieved data rates.

Bottleneck for the performance metrics mentioned above is the limitation of wireless resources like time, frequency, space, energy and code. Utilization ratio of these wireless resources can be optimized in favor of certain performance metrics, where Figure 2.3 shows an example green resource trading scheme that improves the energy efficiency by over utilizing the remaining wireless resources. A preliminary framework have been proposed by authors of [17] to find the optimal bandwidth and time resource utilization which results in minimal energy consumption to transmit one bit, $E_{Joule/bit}$. Capacity of the AWGN channel, C, measured in bits/sec is expressed as the inverse of the time it takes to transmit one bit, t_{bit}, as

$$C = \frac{1}{t_{bit}} = W log_2(1 + \frac{P_{TX} g}{W * N_o}). \tag{2.4}$$

Energy consumption of the access network due to the downlink transmit power consumption of the base station is derived using (2.4) as

$$E_{TX} = P_{TX} t_{bit} = \frac{(2^{\frac{1}{W * t_{bit}}} - 1) * W * N_0 * t_{bit}}{g}, \tag{2.5}$$

and the overall energy consumption of the access network is represented as the sum of energy spent for transmission and the energy spent due to the circuitry of the base station, E_{cir}, as

$$E_{Joule/bit} = E_{TX} + E_{cir} = \frac{(2^{\frac{1}{W * t_{bit}}} - 1) * W * N_0 * t_{bit}}{g} + W P_{circ} t_{bit} + P_{sb} t_{bit}, \tag{2.6}$$

where P_{circ} is the transmission independent operational power consumption which scales proportionally with the used frequency bandwidth and P_{sb} denotes the operational power consumption which is independent of the transmission and the utilized bandwidth. It is clear from (2.6) that the operational energy consumption of the

system increases with increasing bandwidth and time resources while the transmitting energy consumption of the system monotonically decreases. As a result there exists an optimum bandwidth and time resource allocation in the system which minimizes the energy consumption depending on the observed channel gain, g. The system implemented in [17] finds the optimum W for a fixed t and vice versa by using the convex energy consumption functions resulting from (2.6) for different channel gains by making sure the user still receives the minimum QoS required in terms of assigned frequency range and the delay observed during transmission. Proposed scheme can be further improved by simulating the large scale pathloss with realistic propagation models instead of the simplistic free space propagation model, including small scale fading in the system and arranging the media access control (MAC) scheduling decisions every TTI according to the green resource trading function.

2.1.3 Analysis and Discussion of Existing Cell Switch-Off Techniques

Various green techniques have been proposed by academia and industry recently for the wireless access networks with different optimization methods using various energy efficiency and trade-off metrics. Although there are methods to sustain long term energy savings by reducing peak user demand as proposed by authors of [18], access network energy savings are mostly implemented by cell size adjustments according to traffic load fluctuations.

An example of energy saving with cooperated base stations scheme is demonstrated in [19] that aims to find which cells in the network should be switched off so that the traffic load is concentrated around the base stations providing highest spectral efficiencies to the served users. The cell sizes in the network are dynamically adapted according to the traffic load fluctuations in the network. A load concentration approach is shown where the cells with the low traffic zoom into zero and the neighbor cells zoom out by using CoMP, relaying approaches or physical adjustment methods including antenna tilts and increased transmit powers to sustain the traffic as shown in Figure 2.4. This is the exact opposite approach compared to the load balancing approach where the high traffic cells used to zoom in to disperse the total traffic in the network. The proposed system comes along with many challenges such as short term traffic fluctuations, risk of coverage holes in the network, and special control channels needed for cooperated signaling and the compatibility limitations due to cells which are incapable of cell zooming. A centralized approach is proposed where the virtual cell zooming server collects all the channel conditions and rate requirements from the users assuming each user can only be served by one base station. The algorithm in the central server loops through all the mobile users, $i \in I$, and assigns

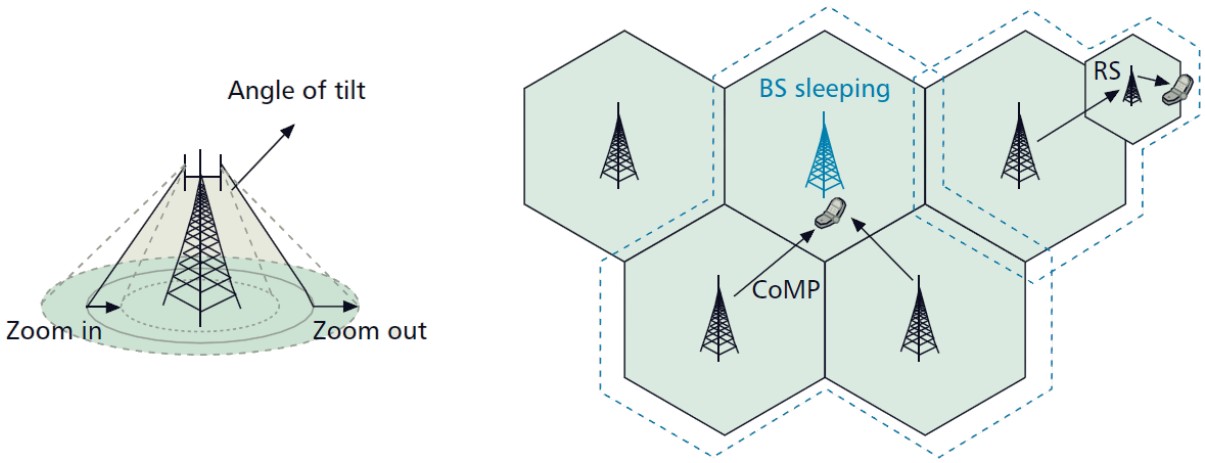

Figure 2.4: Low traffic cells switching off fully or zooming in while neighbor cells zoom out by antenna tilts, CoMP, or relaying approaches to serve the users located in the switched off cells as shown in [19].

them to the base stations, $n \in N$, such that the highest spectral efficiency can be offered by base station n to the user i, $SE_{n,i}$. After all the $i - n$ assignments, the base stations with the lowest traffic load are turned off and the users in those cells are assigned to the remaining neighbor cells. Load of the base station n, L_n, is defined as the ratio of utilized bandwidth, $W_{assigned}$, to the overall bandwidth of the network, W_{total}, as

$$L_n = \frac{\sum_{i \in I_n} w_{i,n}}{W_{total}} = \frac{W_{assigned}}{W_{total}}, \tag{2.7}$$

where I_n represents the set of users that are served by the base station n, and $w_{i,n}$ represents the allocated bandwidth by the base station n to the user i. This algorithm repeats until the load is fully concentrated over the active serving cells with the highest traffic loads that yield the best spectral efficiencies, and creates major energy saving in the access network compared to fixed cell size planning and static cell switch off/on algorithms. A distributed approach is mentioned in [20] without the involvement of a centralized server so that the information flow and the signaling overhead in the system is decreased. Each mobile user chooses the base station with the highest $L_n SE_{n,i}$ product as the serving cell while making sure the user does not drain the idle bandwidth of the base station:

$$W_{assigned} + w_{i,n} \leq W_{total} . \tag{2.8}$$

This algorithm also converges to mobile $i - n$ pairs that improve the energy savings in the network. Distributed cell zooming approach yields lower energy saving in the access network due to the lack of the centralized server; however, it creates a more energy saving environment in terms of reduced control plane and backbone

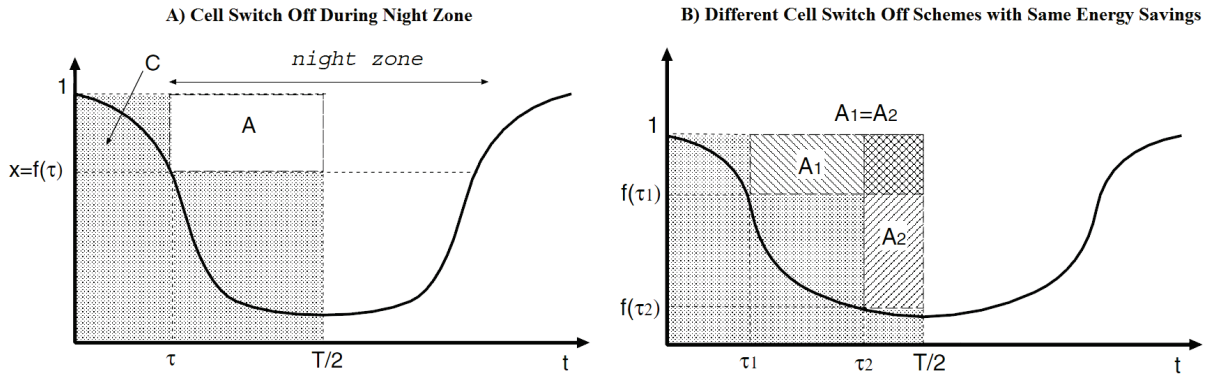

Figure 2.5: Daily traffic distribution and energy saving regions during night zones with low traffic periods shown in [21].

signalling. It should be noted that the granularity of the bandwidth assignments $w_{i,n}$ should be chosen according to the subcarrier spacing and resource block formats in LTE and beyond technologies which is described thoroughly in Section 2.2.1. These constraints have not been modeled in [19] and [20] and may lead to unrealistic scheduling decisions. Existing challenges in both of the algorithms are finding the optimum outage probability versus energy saving trade-off and dynamically configuring the network to maximize the energy saving performance according to the changing traffic load conditions in the network and expected quality of service by the users. The model also needs to be extended to take user mobility scenarios into consideration.

Adapting the cell switch off schemes to the daily traffic load has been investigated by [21] and [22], where a 24-hour traffic routine that monotonically decreases half of the day and symmetric around mid-day is analyzed to find the optimum time to start and stop the energy saving cell switch off period. Cellular access networks are usually statically configured to meet the peak traffic capacity constraints; however, there are significant traffic load reductions in office areas during night time and residential areas during day time. This makes the static cellular deployment schemes energy inefficient due to the redundant number of active base stations during low traffic periods. A basic traffic intensity distribution that is identical among all the cells in the network is assumed in [21] where the traffic load, denoted by $f(t)$ such that $t \in [0, T]$ and $T = 24$ h, is normalized with respect to the highest traffic load such that $f(0) = 1$. The paper suggests that the initial system which is configured with N cells to support the QoS at full load only needs xN cells to support the traffic when the traffic intensity declines by a factor of $x \in [0,1]$ while switching off the remaining $(1 - x)N$ cells. The proposed scheme consists of two states where the network operates with N cells switched on during the day zone, $t \in [0, \tau]$ and $t \in [T - \tau,\ T]$, and with xN cells switched on during the energy saving zone, $t \in [\tau,\ T - \tau]$.

Average daily energy consumption per cell in a network that uses the aforementioned two state cell switch off scheme is expressed as

$$E_{Switch-off} = 2P_{ave}[\tau + f(\tau)\left(\frac{T}{2} - \tau\right)], \tag{2.9}$$

where P_{ave} represents the average power consumption of a cell, and τ is the time when the network enters the energy saving period. Energy consumption during the night zone is reduced by $f(\tau)$ since only xN cells are actively operating and $x = f(\tau)$. The optimum τ is found simply by taking the derivate of $E_{Switch-off}$ to find the local minima for the daily energy consumption function as

$$\frac{dE_{Switch-off}}{d\tau} = 2P_{ave} * \left[1 + f'(\tau)\left(\frac{T}{2} - \tau\right) - f(\tau)\right] = 0, \tag{2.10}$$

$$1 + f'(\tau_{min})\left(\frac{T}{2} - \tau_{min}\right) - f(\tau_{min}) = 0, \tag{2.11}$$

which is same as maximizing the un-shaded area A in Figure 2.5 denoted derived as

$$Energy\ Saving\ Area = A = \left(\frac{T}{2} - \tau_{min}\right) * (1 - f(\tau_{min})) . \tag{2.12}$$

The advantages of the proposed scheme are not only increasing the energy saving of the access network and finding the optimum time to start the energy saving period but also the flexibility of implementation since the same energy saving can be obtained by either more number of switched off cells during a short period of time or by switching off small number of cells for a longer period of time which can be concluded from (2.12) and shown in Figure 2.5b. The choice of implementation can be done according to the slope of daily traffic distribution in which the choice of turning off small number of cells for a long period of time makes more sense if the traffic intensity $f(t)$ decays slowly, so that the time to wait to start the energy saving period is not too long. The major drawback for the scheme is the lack of cellular geometry constraints in the model since xN cells may not be able to serve the users in the network when the coverage areas of the cells are taken into consideration. The model can be enhanced by introducing a multi-state cell switch off model instead of the two state day/night scheme, and modeling accurate traffic distributions for each cell distinctly which do not necessarily decay monotonically but instead fluctuate over time.

An alternative way of energy saving via cooperation in cellular networks in demonstrated in [22], which extends the cooperation between access network components of the same provider mentioned in [21] to cooperation between multiple cellular network operators that are able to provide full service to a certain spatial

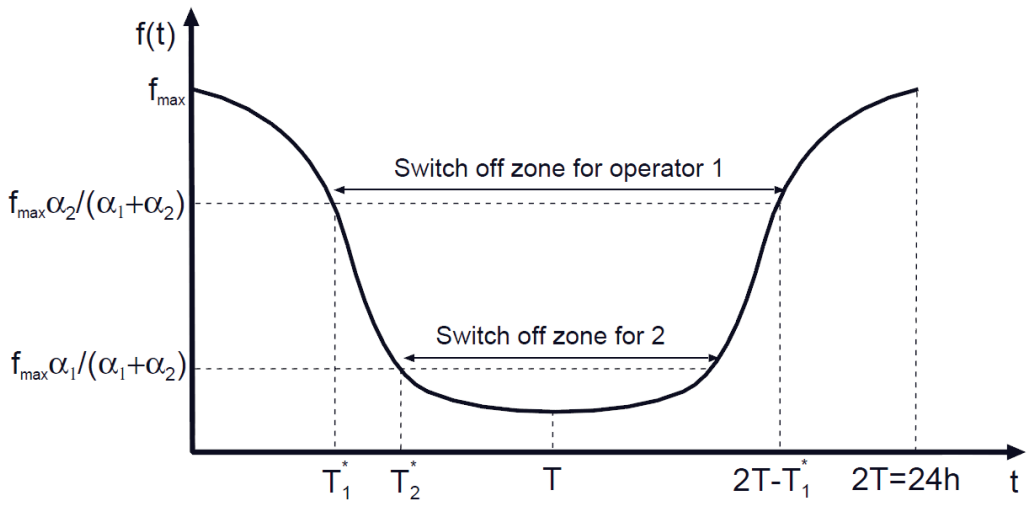

Figure 2.6: Cell switch off scheme enabled via cooperation among multiple network service providers shown in [22].

region. Proposed scheme suggests that network provider, $n \in N$, switches off completely at the optimal energy saving time τ_n derived as

$$\tau_n = f^{-1}\left(\frac{f_{max}\sum_{n\in N_{on}}\alpha_n}{\sum_{n\in N}\alpha_n}\right), \tag{2.13}$$

where N_{on} is the set of the active operators remaining after operator n switches off and α_n is the scaling factor for the number of users in each operator $n \in N$ as shown in Figure 2.6. The traffic load in the switched off operator n is transferred to the remaining active network providers N_{on} as roaming subscribers. It can be seen from (2.13) that the operators' switch off order follows an increasing traffic load pattern and the network operator with the highest traffic load is always on. The total energy consumption in the considered region that supports network operator coordination can be formulated as

$$E_{Operator-Coop} = \sum_{n=1}^{N} f^{-1}\left(\frac{f_{max}\sum_{n\in N_{on}}\alpha_n}{\sum_{n\in N}\alpha_n}\right) P_{ave}(n) + TP_{ave}(n), \tag{2.14}$$

where $P_{ave}(n)$ represents the average daily power consumption of an operator that does not use any switch off scheme. The clear advantages of network operators cooperating throughout the daily traffic are decreased OPEX for the networks and reduced carbon emission due to redundant resources being used by all the network operators that are statically configured to provide power according to peak traffic. The drawbacks of the scheme are the challenges of traffic transfers from one network operator to another such as extra signaling and forced handovers which can cause call drops and overload on the network, and the unfairness of the system for the network provider that has to always stay on and accept roaming subscribers. Energy saving advantage also

comes with a financial tradeoff where the network operators should accept the roaming subscribers without any extra cost to make the transitions in the network transparent, but this can create a significant decrease in network provider's profits. The system also requires updates for the core network (CN) components like the home location register (HLR), visiting location register (VLR), and billing center (BC), which need to be updated to only allow the roaming subscribers from the cooperated networks for no additional monetary cost.

Unlike the cell switch off methods mentioned in [21] and [22] which used simplistic monotonically decreasing traffic intensity functions to find the optimal periods to enter the energy saving mode, [23] tries to maximize the ratio of the switched off cells to the remaining active cells, $\frac{N_{off}}{N_{on}}$, using a traffic model across the cellular system based on an M/M/N/0 queue having an arrival rate of λ_k and incoming handover arrival rate of $\lambda_{h,k}$ modeled as a Poisson process, service time $1/\mu_i$ and time spent by users $1/\mu_h$ modeled with an exponential pdf in a single cell for class *k* calls. Different classes $k \in K$ represent different services offered in mobile networks such as voice, video call and packet data traffic in circuit switched (CS) and packet switched (PS) cores. The overall state space for *K* different classes offered is given as:

$$S = \{\bar{s} = (n_1, n_2, .., n_K) | \sum_{k=1}^{K} C_k n_k \leq C_T\}, \tag{2.15}$$

where n_k represents the number of active class *k* calls, C_k represents the amount of bandwidth required by class *k* calls and C_T represents the total available traffic rate capacity supported in the access network. The proposed scheme focuses on the outage probability calculation using the service blockage in M/M/N queue to decide on the feasibility of the switch off ratio rather than taking into consideration the signal strength outage as well. Therefore, the blocking probability for class *k* calls is defined as the state when no more class *k* calls can be accepted due to the bandwidth constraint as

$$S_{Blockage} = \{(n_1, n_2, .., n_K) | C_T - C_k < \sum_{k=1}^{K} C_k n_k \leq C_T\}. \tag{2.16}$$

Maximum feasible switch off ratio, $\frac{N_{off}}{N_{on}}$, in the access network is targeted to achieve optimum energy savings by switching off as many as redundant base stations as possible. The algorithm loops through different values of $\frac{N_{off}}{N_{on}}$ and calculates the new values for λ_k, $\lambda_{h,k}$, $1/\mu_i$ and $1/\mu_h$. Assuming that each class *k* has a different QoS constraint in terms of maximum service blockage probabilities, algorithm makes sure the new service blockage probabilities are within the constraints for each class after the new cell switch off ratio. Received power required for each active call in the system is calculated by dividing the current downlink power of the switched

on base stations by the mean number of active calls. Required downlink transmit power of the active base stations and the new radius of the cells are found using Cost-231 propagation model. If the new cellular radius is not within the cellular geometry constraints, algorithm either increases the downlink transmit powers of the switched on base stations or reduces the $\frac{N_{off}}{N_{on}}$ ratio. The algorithm eventually converges to an optimal switch off ratio with the necessary transmission power increase in the remaining cells to obtain the maximum energy savings in the access network. Although the proposed scheme assumes a more analytical way to model the traffic in the network to decide the switch off scheme, there is still room for improvement for more realistic modeling. The system should use a realistic 3GPP pathloss model instead of the theoretical Cost-231 propagation model and the outage probability calculations should be done by taking the downlink SINR ratios into consideration. The suggested schemes just focus on the power received per connection and ignore the inter-cell interference and the effect of SINR on the QoS provided to the users. Power per connection is assumed to be the downlink base station power divided by the mean number of active calls; however this assumption ignores the power control and scheduling in cellular networks.

The effect of dynamically changing traffic on the optimal base station sleeping strategy in a cellular network is studied in [16] and the decision parameter to maximize the energy savings is chosen as the power consumption ratio which is defined as the ratio between the dynamic and the fixed power consumption of a base station. Dynamic power consumption is defined as the required transmitted power by the base station that changes according to the traffic load in the cell, which is modeled as a Poisson process; whereas the fixed power consumption is independent of the load and covers the site cooling, power supply and signal processing. It is shown that the power ratio increases due to the rise in traffic load make the dynamic power component dominate over fixed power consumption, and more base stations should be active to save energy in the system. However, for low power ratio scenarios due to low traffic, the constant power dominates over the dynamic power component and less base stations should be active to save energy. Adjusting the base station sleep strategy according to the power ratio of the system is more realistic compared to the cell switch off/on schemes described in [19], [21], [22] and [20], which ignored the impacts of this ratio in the overall energy savings; however, the proposed system in [16] still needs some improvement. The downlink power control used for the modeling does not take the interference into consideration and aims to keep the received power at the mobiles at -110 dBm which might not be enough to sustain a successful radio link if the interference is high. For successful

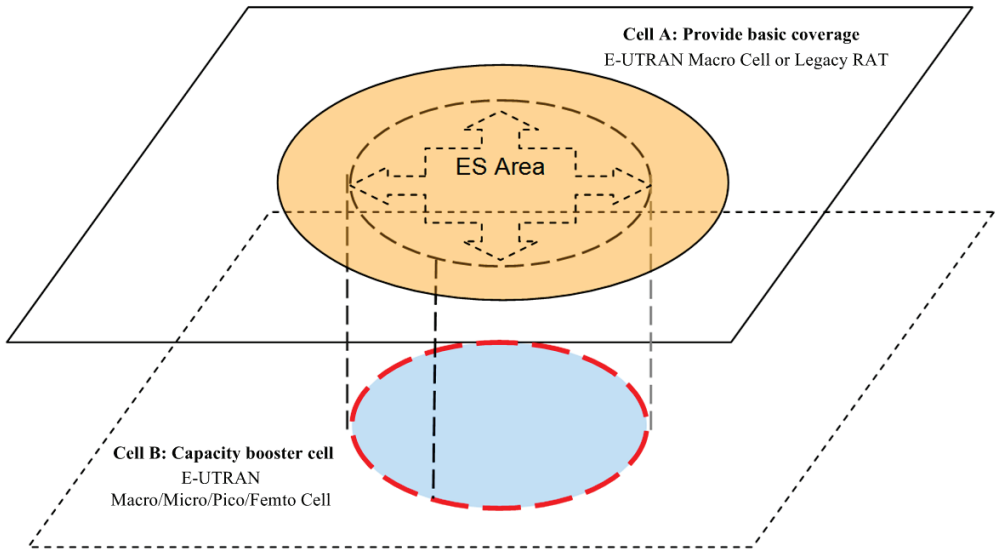

Figure 2.7: LTE cell switch off/on solution suggested in 3GPP release 8 workshops by [24].

communication in the downlink SINR ratio should be chosen as a reference point. Another assumption used in the model is the cells that remain active during the energy saving zone having equal cell radii. However, this assumption ignores the cellular geometry constraints completely since the cells that remain active need to be adjusted to provide coverage to the overall cellular region.

Cell switch off/on strategies to save energy has not only been the interest of academia, but have also been considered in the industry as part of the 3GPP standardization process. Huawei introduced an LTE energy saving solution with cell switch off/on schemes in 3GPP workshops for release 8 in [24]. A hierarchical cellular deployment with respect to LTE is assumed with an energy saving (ES) area that is covered by two different cells as shown in Figure 2.7. Energy saving scheme can be implemented either with inter-RAT or intra-RAT configurations. In the intra-RAT configuration, E-UTRAN macro cell is deployed for continuous coverage of the area and the pico/micro or femto cell, which is covered completely by the macro cell, is deployed to increase the capacity of special small areas or hotspots. The inter-RAT configuration has a cell using a legacy RAT such as UMTS/EDGE/GPRS, which is deployed for basic coverage of voice and medium speed data services and the E-UTRAN cell which is covered completely by the legacy RAT is deployed to provide high speed data or enhanced multimedia services that are offered by LTE. Proposed scheme only enables the energy saving capability in the capacity/data booster cells and the basic coverage supplying cells are prohibited from switching off. A pre-defined threshold is set in the network according to the observed traffic load so that the

capacity booster cells are deactivated when the observed traffic in the ES area is less than the threshold and re-activated when the observed traffic in the ES area is more than the set threshold. Proposed solution suggests two different implementation options: Operations, Administration and Maintenance (OAM) based and e-NB based. The e-NB based solution focuses on the real time traffic to set the threshold. Cell deactivation is initiated by e-NB's internal mechanism, whereas the cell activation is initiated by the neighbor eNB's trigger mechanism which keeps monitoring the ES area after the capacity booster cells are switched off. This option requires enhancements to the existing X2 interface since it depends heavily on inter e-NB communication to inform each other about cell status updates. The OAM based solution, on the other hand, sets the switch off thresholds according to observed statistics over time and the cell activation/deactivation procedures are completely controlled by the OAM through Itf-N interface. This option depends less on inter e-NB communication, but cell status notifications still need to be transmitted over the X2 interface. The OAM based solution is more feasible in cases where the capacity of X2 interface limited, however this topic should be considered under Self-Organizing Networks (SON), where the large scale OAM is done by controlling the element managers via network manager over the Itf-N interface as explained in [25].

All the schemes mentioned above focus on access network energy savings via various methods of cell switch off mechanisms using theoretical models for radio wave propagation and small scale fading. Authors of [26] analyzed the standalone energy efficiency of an upcoming radio technology feature in LTE-A, namely CoMP, and authors of [19] mentioned CoMP as an advantageous method for cells to zoom out, however, joint use of CoMP feature with traditional cell switch off schemes is not analyzed in any literature, to the best of our knowledge.

2.2 LTE – Advanced CoMP System Framework

2.2.1 Introduction to Downlink LTE Transmission

Major physical layer changes have been introduced while proceeding from 3GPP release 7 (HSPA+) to 3GPP release 8 (LTE). Multiple access technology used until release 7 HSPA+ schemes, CDMA, has been replaced with OFDM/OFDMA technology starting from release 8 LTE systems. OFDM takes advantage of both the simple receiver architecture of narrowband systems with the high capacity of wideband systems by utilizing many narrowband orthogonal subcarriers [27]. Orthogonal subcarriers are achieved by setting the center

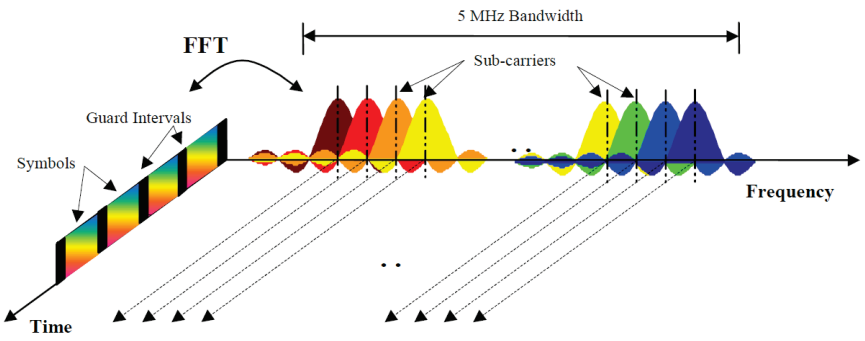

Figure 2.8: Time-Frequency domain representation of an OFDM signal shown in [28].

frequencies of subcarriers, which are also referred to as the frequency tones, to integer multiples of the base frequency [28]. It can be seen that the inter-frequency interference in minimized by using OFDM schemes since the center frequencies of the subcarriers do not interfere with the sidebands of the adjacent subcarriers as shown in Figure 2.8. This yields to spectrally efficient LTE downlink due to OFDMA use.

Multipath reception due to small-scale fading conditions for frequency selective channels, where the coherence bandwidth of the channel is smaller than the signal bandwidth and the multipath delay spread is greater than the symbol period, lead to inter symbol interference (ISI) and distortion in wireless systems as shown in Figure 2.9a. LTE OFDM schemes reduce the effects of ISI by utilizing narrow band subcarriers that go under flat fading. Symbol period is increased by a factor of the number of subcarriers, N_{sc}, after the serial to parallel conversion for sub-carrier modulation. Period of each OFDM symbol is extended by copying the final part of the symbol to the beginning of the OFDM symbol as shown in Figure 2.9b, which is known as the cyclic prefix (CP) or time domain guard interval addition. Serial to parallel conversion of the incoming serial bits belonging to the transport blocks from the MAC layer and addition of cyclic prefix by copying N_{CP} samples to do beginning of the OFDM symbol tackles the ISI in time dispersive domain. The length of N_{CP} should be larger than the length of the multipath delay taps, so that the receiver can just ignore the first N_{CP} samples from the received signal and eliminate the ISI completely. It should be noted that even for the cases where N_{CP} is larger than the number of delay taps, receiver still suffers from the intra symbol interference due to multipath. Addition of CP to each OFDM symbol not only decreases the inter symbol interference, but also enables the conversion of linear convolution to circular convolution so that the receiver can overcome intra symbol interference [29]. Due to the circular convolution property, receiver can just perform discrete fourier transform (DFT) to the received time samples to obtain the received signal in frequency domain for each subcarrier. These

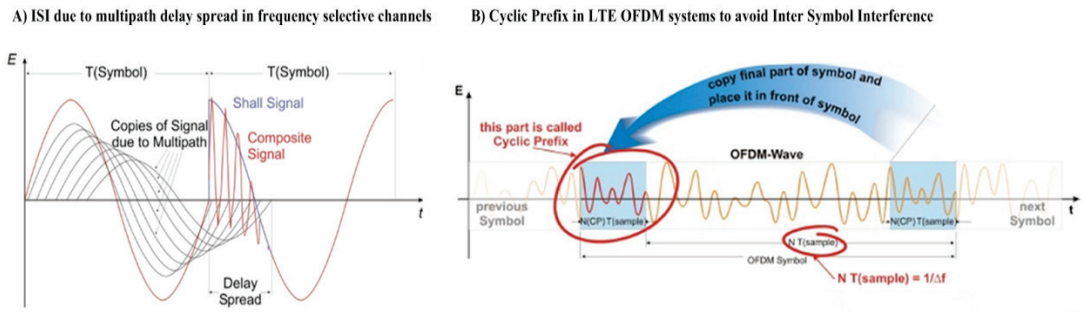

Figure 2.9: Cyclic prefix utilization in LTE systems to reduce ISI due to multipath reception, taken from [27].

mechanisms decrease the receiver complexity for the equalization procedures for LTE downlink. It should also be noted that increasing N_{CP} unnecessarily lead to transmission inefficient systems due to the overhead and increased symbol period can also lead to distortion due to the frequency dispersive nature of the channel resulting from UE mobility. This can be explained by the increased OFDM symbol period being larger than the coherence time of the fast fading channel with high Doppler spread. To overcome the signal distortion resulting from the time-varying nature of the channel, hybrid automatic repeat request (HARQ), cyclic redundancy check (CRC), and channel coding procedures still need to be used in LTE systems.

Block diagram of transmitter/receiver architecture for LTE DL OFDMA system is shown in Figure 2.10. The incoming bit stream at the transmitter is converted from serial to parallel for subcarrier mapping and then modulated accordingly. Serial to parallel conversion of the OFDM symbol in frequency domain makes the transmission robust against ISI. It should be noted that different subcarriers can be modulated with different schemes QPSK, 16-QAM or 64-QAM depending on the mapping of physical channels to various resource elements. For instance, when mapping PBCH channel on resource elements, the corresponding subcarriers should be modulated with QPSK whereas when mapping a PDSCH (Physical Downlink Shared Channel) channel on a resource element 64-QAM may be used depending on the channel feedback from UE [30]. Serving eNB (enhanced Node B) MAC scheduler may also choose different modulation schemes to be used for PDSCH to different served users according to received channel feedback from the users. OFDM symbol spanning N_{sc} subcarriers are expressed in complex In-phase and Quadrature (I/Q) plane after the adaptive modulation on each orthogonal subcarrier and passed to an N-point IFFT. The number of subcarriers is less than the N-FFT size; as a result, the remaining $N_{FFT} - N_{sc}$ input streams are padded with zero before the N-IFFT block. Orthogonal frequency bins are converted to time domain by creating orthogonal sine waves using the IFFT block that yields

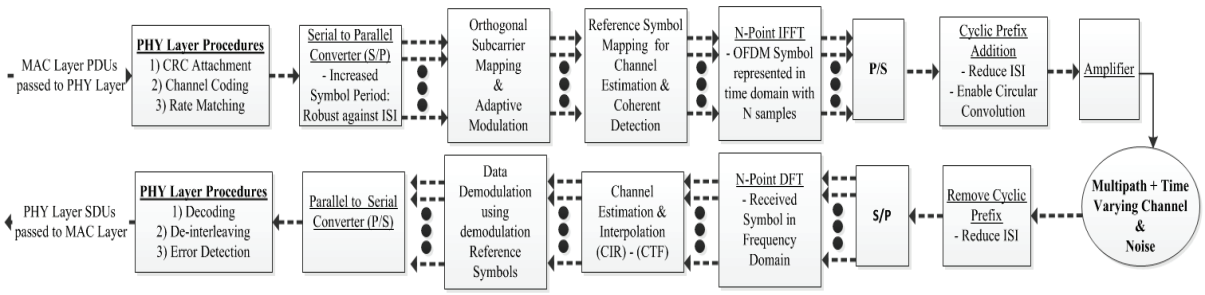

Figure 2.10: LTE downlink OFDMA transmitter and receiver architecture.

N_{FFT} samples in time domain. Time domain signal $x(t)$ containing N_{FFT} samples after performing IFFT to the modulated subcarriers is represented as

$$x(t) = \sum_{n=-\frac{N_{FFT}}{2}}^{\frac{N_{FFT}}{2}-1} I_{n(t)} \sin\left(2\pi t\left(f_{-\frac{N_{FFT}}{2}} + \Delta f\left(n+\frac{N_{FFT}}{2}\right)\right)\right) - j\, Q_{n(t)} \cos\left(2\pi t\left(f_{-\frac{N_{FFT}}{2}} + \Delta f\left(n+\frac{N_{FFT}}{2}\right)\right)\right), \quad (2.17)$$

where n denotes the index for the subcarrier frequency tone ($N_{FFT} - N_{sc}$ set to null), $I_{n(t)}$ and $Q_{n(t)}$ represent the modulated I/Q plane representations of the symbols according to the used modulation scheme on the corresponding subcarrier frequencies, $f_{-\frac{N_{FFT}}{2}}$ represents the base frequency tone and Δf represents the subcarrier frequency spacing. It should be noted that in Figure 2.10, the input to the IFFT block can come from the transport block data intended for different users in case of downlink multiple access, where the data intended for each user goes under separate encoding/interleaving/modulation procedures and eventually combine parallelly as inputs to the IFFT block. Relations between N_{FFT}, sampling frequency f_s, FFT duration T_{FFT}, sample period T_s and subcarrier spacing between different tones Δf are expressed below according to the downlink OFDM parameters specified in Table 2.1:

$$f_s = \Delta f\, N_{FFT}\ ; \quad (2.18)$$

$$T_{FFT} = {}^{1}/_{\Delta f}\ ; \quad (2.19)$$

$$T_s = T_{FFT}/N_{FFT}\ . \quad (2.20)$$

Depending on the FFT size and number of OFDM symbols per slot $N_{symbol/slot}$, number of samples per cyclic prefix N_{CP} can be varied to make sure the slot duration is set to 0.5 ms using (2.21) and (2.22):

$$T_{symbol} = T_s * (N_{FFT} + N_{CP}), \quad (2.21)$$

$$T_{symbol} N_{symbol/slot} = 0.5\ ms. \quad (2.22)$$

Table 2.1: LTE Downlink OFDM Parameters standardized in [31] assuming 15 kHz subcarrier spacing

Total Bandwidth	Available Bandwidth	Available Subcarriers (N_{sc})	FFT Size (N_{FFT})	Sampling Frequency (f_s)
5 MHz	4.5 MHz	300	512	7.68 MHz
10 MHz	9.0 MHz	600	1024	15.36 MHz
15 MHz	13.5 MHz	900	1536	23.04 MHz
20 MHz	18 MHz	1200	2048	30.72 MHz

The sampling frequency in LTE FDD systems is set as multiples of 3.84 MHz although it results in FFT sizes greater total number of available subcarriers. This is to simplify the implementation of dual stack UEs that support both UMTS with WCDMA chip rate set to 3.84 MHz and LTE at the same time as explained in [32].

Downlink OFDMA transmission shown in Figure 2.10 in a time-varying multipath channel can be formulated in time and frequency domains as

$$y_{Nx1} = x_{NxN} h_{Nx1} + n_{Nx1}\,, \tag{2.23}$$

$$\begin{bmatrix} y_1 \\ \vdots \\ y_N \end{bmatrix} = \begin{bmatrix} x_1 & x_N & \cdots & x_2 \\ \vdots & \vdots & \vdots & \vdots \\ x_N & x_{N-1} & \cdots & x_1 \end{bmatrix} \begin{bmatrix} h_1 \\ \vdots \\ h_N \end{bmatrix} + \begin{bmatrix} n_1 \\ \vdots \\ n_N \end{bmatrix}, \tag{2.24}$$

where y_{Nx1} is the received OFDM symbol with N_{IFFT} samples after cyclic prefix removal, h_{Nx1} is the multipath complex baseband channel impulse response (CIR) with delay tap length L, n_{Nx1} is the noise observed in the channel, first column of x_{NxN} matrix corresponds to the samples at the transmitter side shown in (2.17) after the N_{IFFT} block before the CP addition and the remaining columns are due to the multipath channel. It is clear from (2.24) that the receiver recovers completely from the inter symbol interference after removing first N_{CP} samples, assuming $N_{CP} > L$, but equalization is still needed to tackle the intra-symbol interference. Multipath CIR h_{Nx1} has a delay tap length of L, as a result the rows of h_{Nx1} and the columns of x_{NxN} are set to zero after h_L and x_{NxN}, respectively. It should be noted that the channel is assumed to be coherent within one OFDM symbol period; that is why the convolution of the samples is possible with the CIR. Due to the circular convolution property enabled after CP addition explained in [29], received OFDM symbol in time domain can be written as

$$y_{Nx1} = {F_{NxN}}^H X_{NxN} F_{NxN} h_{Nx1} + n_{Nx1}, \tag{2.25}$$

where F_{NxN} and ${F_{NxN}}^H$ denote the DFT and IFFT matrices, respectively, to represent the symbol in time and frequency domains as demonstrated in Figure 2.8, and X_{NxN} is a diagonal matrix with rows corresponding to the transmitted complex modulated symbols in frequency domain spanning over the orthogonal subcarriers before being inputted to the N_{IFFT} block. As a result, receiver can perform equalization by performing DFT on

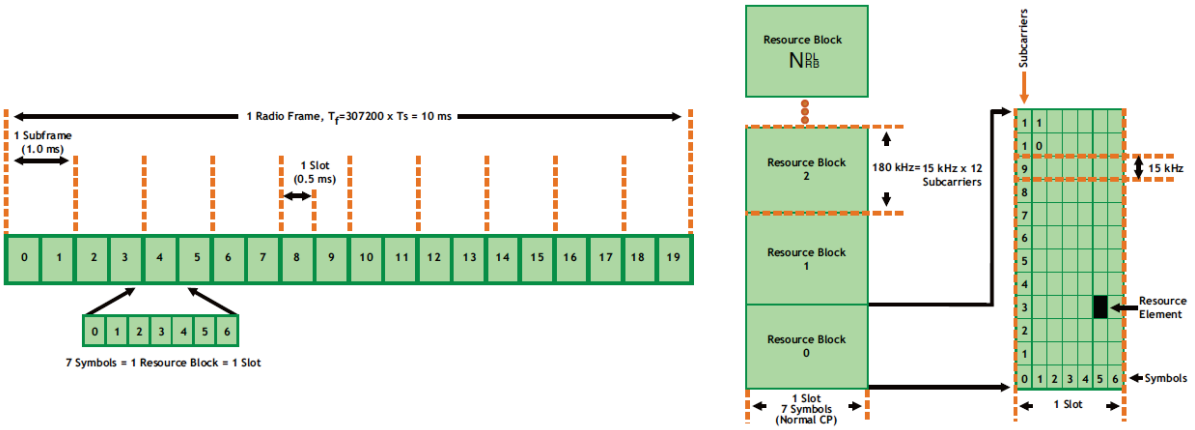

Figure 2.11: Frame structure and resource blocks in LTE FDD systems demonstrated in [33], assuming normal CP use.

(2.25). Received OFDM symbol in frequency domain over N_{IFFT} frequency tones, Y_{Nx1}, can be found after the N_{DFT} block as

$$Y_{Nx1} = X_{NxN}F_{NxN}h_{Nx1} + N_{Nx1}, \tag{2.26}$$

$$Y_{Nx1} = X_{NxN}H_{Nx1} + N_{Nx1}, \tag{2.27}$$

where H_{Nx1} represents the channel transfer function (CTF) and N_{Nx1} noise of the channel in frequency domain.

Multiple access in LTE is achieved by adaptively assigning predefined time-frequency resources called resource blocks (0.5 ms slots spanning over 12 subcarriers) to various UE every TTI according to required QoS and reported frequency selective channel feedbacks. Since both the uplink and downlink user plane data is carrier over shared physical channels (PDSCH/PUSCH), scheduling decisions are given every 1 ms at e-NB to meet the QoS requirements of the users in the cell by assigning necessary number of resource blocks to the served UEs. LTE downlink radio frame is 10 ms long and consists of 10 subframes that are 1 ms TTI each. Every subframe has two slots of 0.5 ms consisting of 6 or 7 OFDM symbols depending on the choice of extended or normal CP use, respectively, as formulated in (2.22). Frequency domain consists of narrowband subcarriers that are either 15 kHz or 7.5 kHz wide. Depending on the flexible bandwidth choice of implementation, 5 MHz, 10 MHz, 15 MHz and 20 MHz, total number of subcarriers available in the system varies. It should be noted that regardless of the choice of total bandwidth, 10% of the overall bandwidth is allocated as upper and lower guard-bands to avoid the interference between different LTE bands. Instead of assigning resources to UEs in time domain as slots or in frequency domain as subcarriers, UEs are assigned resource blocks consisting of 12 subcarriers and 1 slot (6 or 7 OFDM symbols). Since the scheduling decisions

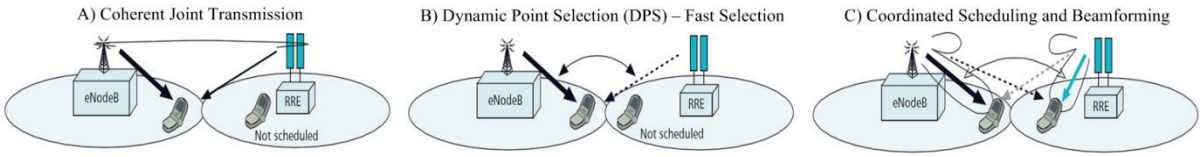

Figure 2.12: Downlink CoMP schemes demonstrated in [34].

are made every subframe, resource blocks of the same subframe are allocated in pairs to UEs in each TTI. Each subcarrier-OFDM Symbol pair is called a resource element, which is the smallest unit in downlink LTE transmission, as shown in Figure 2.11 displaying a 20 MHz FDD LTE system using normal cyclic prefix. Since frequency and time resources are scheduled adaptively according to the channel state feedback of various users, LTE downlink can be considered as a mixture of FDM and TDM (Time Division Multiplexing). The number of total resource blocks available in an LTE system can be found by taking into consideration the 10% bandwidth allocation for upper and lower frequency guardbands. As a result, in a 20 MHz system, only 18 MHz is the effective bandwidth which has 100 PRBs if $\Delta f = 15$ kHz.

2.2.2 CoMP Definitions and Standardization

Capacity and spectral efficiency of the cellular systems need to be increased in order to meet the increasing mobile data demand from users. Some of the proposed options that increase the capacity of cellular networks are listed in [35] as using more spectrum, increasing the number of transmit/receive antennas, using dedicated beams to serve the users, and enabling small cell deployment. However, none of these methods address inter-cell interference issue, which is the actual bottleneck for spectral efficiency, especially for LTE and beyond systems that have full frequency reuse. CoMP is listed as one of the key features and work items for LTE-A systems to improve cell edge performance, system throughput, received SINR and spectral efficiency by mitigating and exploiting the inter cell interference [6]. Scope of this thesis is limited to downlink CoMP usage in cellular networks. Definition of DL CoMP is explained initially in 3GPP 36.814 [36] as dynamic coordination among multiple spatially separated transmission points. CoMP coordinating set, N_{Coop}, is the overall master set of points that have logical/physical links enabling them to exchange channel feedbacks and/or user payloads to perform downlink joint transmission or make scheduling decisions in the access network over certain time - frequency resources. CoMP joint transmission set, N_{JT}, is a subset of N_{Coop} and corresponds the

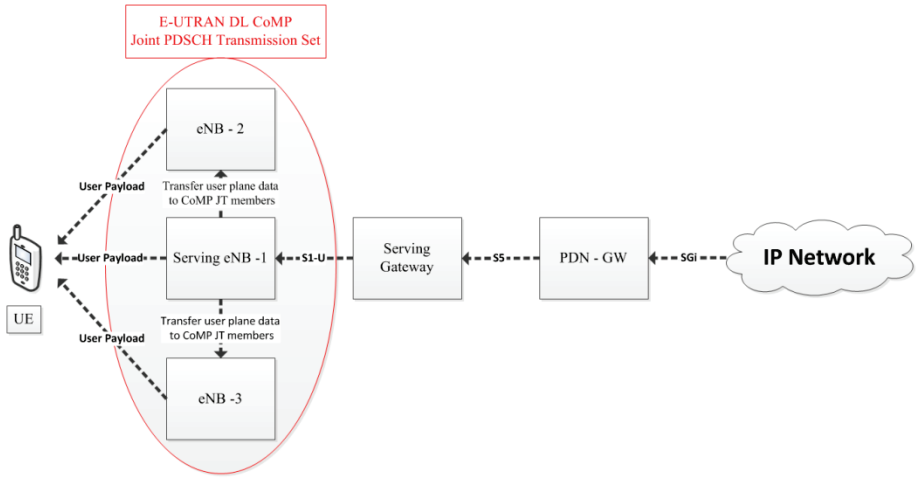

Figure 2.13: User plane data flow for downlink inter-eNB CoMP joint transmission scheme.

points that are directly participating in PDSCH transmission over the same resource blocks to the UE. CoMP measurement set, N_{meas}, includes the points about which the UEs report measured link qualities and CSI (Channel State Information) feedback. Downlink CoMP is categorized under two main categories as follows:

- Joint Processing: Downlink payload and user plane data intended for a UE is available at each point in the CoMP cooperating set. It can be implemented as joint transmission (JT), where downlink payload is transmitted on PDSCH from multiple points in the CoMP set to the UE by scheduling the same RBs as shown in Figure 2.12a. This is referred to as cross-point scheduling in [37], where the UE receives PDSCH assignments from multiple points in the same TTI as shown in Figure 2.13. An alternative scheme is dynamic point selection (DPS) where PDSCH transmission is done from the best point in the CoMP set. For DPS schemes, the transmission point can change every slot since different RBs in a certain subframe can be transmitted by different members of the N_{Coop}. It should be noted that the muted members of the N_{Coop} do not schedule any users over the RB where the best point is performing transmission as shown in Figure 2.12b.
- Coordinated Scheduling/Beamforming (CS/CB): Downlink payload is available at one point in the CoMP set, which is the serving eNB, and transmitted from this point. Rest of the points in the CoMP set indirectly participate in transmission by assisting the scheduling and beamforming decisions to mitigate the interference over the resource blocks where the serving eNB is performing PDSCH transmission as shown in Figure 2.12.c.

Serving cell is responsible for anchoring the PDCCH assignments, sending MIB/SIBs (Master Information Block/System Information Blocks) to the UE, controlling the resource allocation, HARQ information, transport format and power control. Serving cell also coordinates the other participants in the downlink cooperating CoMP set by manipulating DL channel feedback. Feedback mechanism in downlink CoMP can be either explicit where the UE's provide a channel information as observed by channel matrix, channel covariance, and covariance matrix of noise/interference, or implicit, where the UE reports channel quality indicator (CQI), precoding matrix indicator (PMI) and rank indicator (RI) for MIMO using the PUCCH (Physical Uplink Control Channel) or PUSCH (Physical Uplink Shared Channel). It should be noted that only the joint transmission scheme requires inter-point phase information, to align the phases of the transmitted and received signals from multiple points, as part of the CoMP feedback since it is the only scheme that performs coherent transmission using cross-point PDSCH scheduling.

There have been 5 different CoMP deployment scenarios provided in 3GPP 36.819 [37] as follows:

- Inter-eNB CoMP: Information and data exchange between the eNBs will be performed over the logical X2 interface.
- Intra-site CoMP: Coordination between different sectors of the same eNB in a homogeneous network.
- Intra RRH (Remote Radio Head) CoMP: Coordination between different RRHs in a homogeneous network.
- Intra cell eNB – RRH CoMP: Coordination between the macro eNBs and the RRH within the same cell.
- Inter cell eNB – RRH CoMP: Coordination between the macro eNBs and the RRH having different cell ids.

Inter-eNB CoMP deployment with downlink joint transmission is the most promising scheme in terms of performance gains, however it has the highest number of challenges to be addressed before commercialization due to the complexity of the protocol explained in Section 2.2.5.

2.2.3 Joint Transmission Procedures

Downlink CoMP joint transmission scheme is defined as multiple geographically separated points coordinating in terms of scheduling decisions and performing joint user plane data (payload) transmission to the UE over certain time/frequency resources called Resource Blocks for 3GPP Release 11 and beyond technologies. Inter-eNB coordination is one of the possible schemes which is heavily dependent on the X2 links between the eNBs.

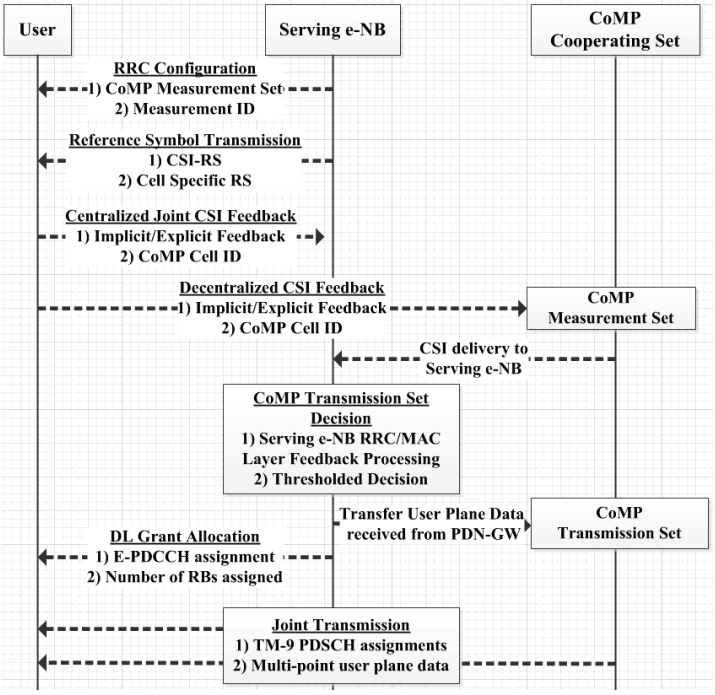

Figure 2.14: DL CoMP procedures for inter-eNB joint transmission schemes.

Procedures involved for the joint transmission scheme are demonstrated in sequential order in Figure 2.14. Serving cell acts as the anchor point of the CoMP transmission and can change with time and location due to UE mobility. Serving eNB sends the contents of the CoMP measurement set to the UE via downlink RRC signaling along with the measurement IDs (e.g. RSRP, RSRQ), and density/periodicity of the CSI-RS (Channel State Information Reference Signal). It should be noted that the CoMP measurement set is a subset of the overall CoMP coordinating set and the serving eNB may or may not perform down selection on coordination capable points to form the measurement set depending on the location of the UE and the feasibility of coordination. CSI-RS inserted into the resource blocks enable the UE to perform multi-point channel estimation for the member of the CoMP measurement set, N_{meas}. After performing multi-point channel estimation using CSI-RSs, UEs can either provide centralized or decentralized CSI feedback for each point of the CoMP measurement set. Channel feedback could either be explicit (complex channel impulse response seen by the user and the noise) or implicit (CQI, CSI value which can be used by the serving eNB to map to a certain downlink modulation scheme). In centralized multi-point feedback, UEs send the CSI for all the points in measurement set to the serving eNB. In decentralized multi-point feedback, user passes the measured/observed CSI to each point in CoMP set separately, and the members of the CoMP measurement set are required to transfer the received CSI feedback to serving eNB over the X2 link. It should be noted that, if the serving eNB

is providing the UL resources, UEs should send aggregate centralized feedback over PUCCH or PUSCH to the serving eNB containing measured results for all members of N_{meas}. A subset of the CoMP measurement set is chosen as the CoMP transmission set, N_{JT}. This decision is given by the RRC/MAC layer of the serving eNB, after consolidating the multi-point feedback for each member of the CoMP measurement set and performing a threshold-based decision on the approximated downlink received powers of each coordinating point – UE radio link. It should be noted that the joint transmission set clustering decision could also be based on the DL RRM measurement like RSRP/RSRQ as mentioned in [37]. After the joint transmission set clustering decision by the anchor, the downlink user plane payload coming from the PDN-GW targeted for a specific UE is transferred by the serving eNB to all the chosen members of the CoMP transmission set over X2 interface. Serving eNB transmits the DL CoMP grant allocation to the user over E-PDCCH (Enhanced Physical Downlink Control Channel) providing information about the system frame/sub-frames that are chosen for CoMP transmission, number of resource blocks assigned to the user and the members of the joint transmission set using a compact downlink control information (DCI) format. Then, user plane data is transmitted to the UE over PDSCH via TM (transmission mode) – 9 by all the members of the DL CoMP joint transmission set over the specified resource blocks.

2.2.4 Downlink Channel Estimation for Beyond LTE Systems

Both LTE and LTE-A systems use coherent detection and equalization methods to mitigate the ISI caused by multipath channel. Reference symbols known at both the transmitter and receiver ends, which do not carry data, are inserted to specific resource elements after subcarrier mapping and modulation shown in Figure 2.10. User estimates the radio channel and demodulates the data using these pre-known symbols. Release-8 LTE systems use the cell specific reference symbols both for demodulation and channel estimation; however these two procedures are decoupled in LTE-A schemes where the data demodulation is done using the UE specific RSs and complex multi-point channel estimation is done using CSI-RSs as shown in Fig. 2.15. Amplitude and phase of both CIR and CTF are estimated at resource elements containing reference symbols and the results are interpolated in time and frequency domains to predict the channel at resource elements carrying data. CSI-RS transmissions anchored by the serving cell are utilized by the UEs to estimate the channels for different points mentioned in the CoMP measurement set. Figure 2.15 shows a resource block pair over 1 TTI (1 sub-frame, 2 slots, 1 ms) spanning over 12 orthogonal subcarriers with normal cyclic prefix use (7 OFDM symbols per slot).

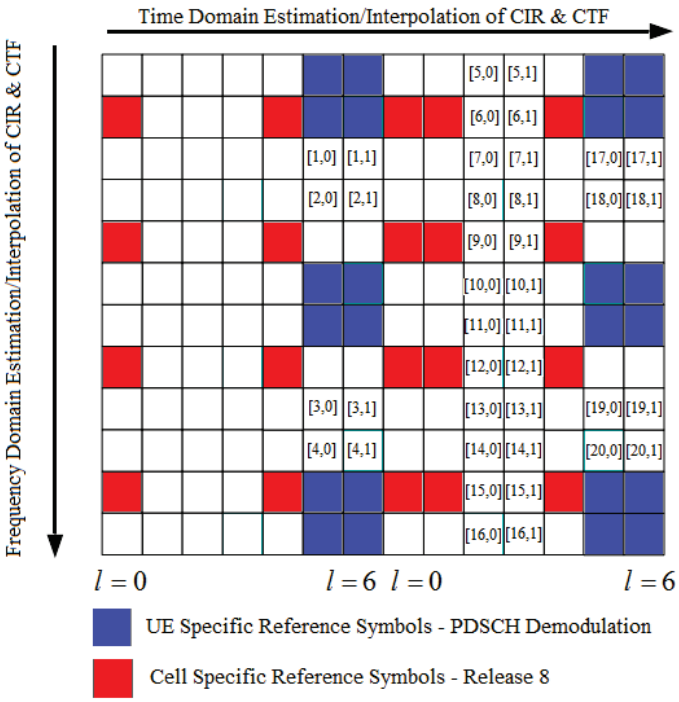

Figure 2.15: Reference symbol mapping in LTE-A DL CoMP systems, adapted from [30].

Single point channel estimation in pre-LTE-A networks for the serving eNB is done using cell specific reference symbols (CRS) marked in red. Both for normal and cyclic prefix use in single or two antenna port supporting eNBs, there are 8 reference symbols per resource block pair for the UE to perform single point channel estimation, in which the RS are placed every 6^{th} OFDM symbol in time domain and every 6^{th} subcarrier in frequency domain. As a result, UE has enough channel samples to perform both time and frequency domain interpolation to estimate and predict the channel samples for the resource elements not containing reference symbols. However, multi-point estimation cannot use the same framework in 3GPP release-8 since that would decrease the spectral efficiency of the system significantly. The trade-off between more accurate channel estimation versus system spectral efficiency according to the chosen density of the reference symbols is more crucial for LTE-A systems since UE needs to use CSI-RS to estimate multiple points. For LTE-A systems supporting CoMP, there will be 40 resource elements for an RB pair in a specific TTI allocated for multi-point channel estimation, so that the UE can perform coherent detection and equalization for each point mentioned in the CoMP measurement set. Assuming an inter-eNB CoMP measurement set of 20 eNBs, there will be only 1 reference symbol for each antenna port of each point of the measurement set assuming each eNB has two transmit antenna ports as shown in Figure 2.15. It can be seen that interpolation using the channel auto-

correlation functions in multiple domains for the serving cell (8 CRSs for each antenna port in each RB pair) will yield more accurate results compared to multi-point channel estimation (1 CSI-RS for each antenna port in each RB pair) in CoMP due to the scarce nature of reference symbols contained in resource block pairs for a particular member of the CoMP measurement set. As a result, multi-point channel estimation is more vulnerable to estimation errors due to the lack of reference symbols compared to single point channel estimation.

2.2.5 Technical Challenges and Discussion of Existing Literature

Technical challenges for DL CoMP are listed by [37], [35] and [38] as increased backhaul traffic, time/frequency synchronization of the cooperating points, multi-point channel estimation/prediction and feedback procedures, clustering of CoMP sets, feasibility of various deployment schemes, delays in the overall system and cross point scheduling of users. The effect of traffic intensity on the optimum downlink CoMP scheduling scheme is analyzed by Orange Labs in [39] where the multi-user joint processing with least interfering beams scheme is shown to outperform remaining cross-point scheduling single-user joint processing in terms of capacity gains. Assuming two eNBs using CoMP transmission in the downlink with the master and slave eNBs represent the eNB that has the served UE in the coverage area, and the eNB that does not have the scheduled UE in the ideal coverage region, respectively. The proposed scheme suggests that the slave eNB should schedule another UE within its own coverage area over the same RB using the least interfering beam with respect to the UE scheduled in the master eNB for CoMP transmission to increase the overall spectral efficiency of the system. To decrease the impact of signaling delays between the CoMP active set and the UE on UL capacity of the system, a centralized UL scheduling approach was demonstrated in [40] where the backhaul usage was tried to be minimized using pre-known statistical channel feedback information. Clustering decision delay is characterized as the time difference between the UL scheduling request and the scheduling grant provided by the serving e-NB. A prediction mechanism in implemented in the serving eNB to give UL scheduling decisions and cluster formation using the previously stored channel characteristics, so that the clustering decisions are not outdated at the time of the scheduling grants. Feasibility of various CoMP deployment scenarios is investigated in [41] to find the capacity maximizing clustering scheme and intra-cell cooperation is chosen to be a successful candidate for joint processing DL scheme, whereas the inter-eNB schemes are shown to require backhaul enhancements like capacity increases and latency reduction before commercialization. An energy efficient CoMP network backhaul design was proposed in [42], where the set of

points that can be used in the CoMP transmission set were pre-calculated and the remaining points were excluded from the CoMP measurement set due to network latency constraints. Proposed scheme minimized the unnecessary power consumption and traffic in the CoMP backhaul by taking network topology constraints, node processing and line delays into consideration before forming the CoMP measurement set. The scheme avoids unnecessary channel estimation at the UE, CSI exchange within the members of N_{meas} and user/control plane data exchange within the members of N_{JT}. Time and frequency synchronization within the members of N_{JT}, is another performance determining factor since unaligned joint transmission causes ISI and ICI (Inter carrier interference), respectively.

2.3 Summary

Motivations for green radio and the analysis for existing energy efficient schemes are presented in Section 2.1. LTE-A evolution for CoMP procedures and the discussion of the existing literature addressing CoMP technical challenges were presented in Section 2.2.

Although authors of [26] analyzed the standalone energy efficiency of an upcoming radio technology feature, namely CoMP, and authors of [19] mentioned CoMP as an advantageous method for cells to zoom out; joint use of CoMP feature with traditional cell switch off schemes is not analyzed in any literature, to the best of our knowledge. Joint use of traditional cell switch off schemes with CoMP transmission in the downlink is described along with the performance analysis in Chapter 3. All of the aforementioned methods explained in Section 2.2.5 including the 3GPP release 11 standardization for CoMP, [37] and [36], either focus on the effect of system delays, clustering strategies and scheduling schemes on CoMP system capacity or the power efficiency of the backhaul network. However, to the best of our knowledge, the impact of channel estimation errors and system delays on overall CoMP energy efficiency and capacity gains are not analyzed in existing works. The performance of this newly proposed scheme is heavily dependent on the accuracy of the selected CoMP joint transmission set. We model the multi-point channel estimation enabled via channel state information reference symbols (CSI-RS) introduced in 3GPP release 10 systems and simulate possible scenarios that would lead to inaccurate transmission set clustering: multi-point channel estimation errors and possible CoMP system delays due to CSI transfers, node processing delays and network topology limitations. Individual and joint impacts of system delays and estimation errors on energy efficiency and capacity performance for various mobility conditions are demonstrated in Chapter 4.

Chapter 3

Coordinated Multi-Point Aided Cell Switch Off Schemes

In recent years, the power consumption and energy efficiency of cellular networks have become important performance indicators. Various types of energy saving schemes have been proposed for cellular networks as explained in Section 2.1. However, most of these schemes do not take advantage of the advanced features offered by the recent cellular standards. CoMP is a key feature in LTE-Advanced and beyond technologies which is considered under the distributed antenna systems umbrella that needs to be analyzed for energy saving implementations. One of the recently proposed energy saving schemes in cellular networks is the cell switch off technique in which a lightly loaded cell is completely switched off and the traffic in that region is absorbed by the nearby cells with increased transmit powers. This chapter describes and analyzes the performance of a cell switch off scheme without increasing the transmit powers of the active cells; instead, using CoMP transmission to enable a sufficient DL received power levels. Formulation of capacity and energy efficiency metrics are presented and these metrics are used to compare the performance of the traditional versus the CoMP aided cell switch off schemes. The work explained in this chapter has been presented in the conference paper [43].

3.1 Cellular System Model

3.1.1 Cellular Layout and Uniform User Distribution

Hexagonal cellular network layout of 19 cells with base stations located in the center of the cells with omni-directional antennas is considered with a cluster size and frequency re-use factor of one. The center eNB represents the original serving cell and 18 remaining eNBs represent 3 tiers of co-channel interferers. According to the hexagonal cell geometry with cells having identical cellular radii *R,* the inter-eNB distance can be expressed as $R\sqrt{3}$. Inter-BS distance is taken as 500 m using the urban macro cellular layout from [44] and the cellular radius can be calculated as $R = \frac{500}{\sqrt{3}}$ m. UE location coordinates in the network are generated using polar coordinates. Angular coordinate, θ, is formulated by a uniform random variable such that $0 < \theta < 2\pi$ and the radial coordinate, *R,* is generated by modeling R^2 as a uniform random variable such that $0 < R^2 < \frac{500}{\sqrt{3}}$. Square of the radial coordinate is modeled as a uniform random variable to obtain perfect uniformity in a cellular spatial area. Described cellular layout is simulated as shown in Figure 3.1 with uniformly and randomly

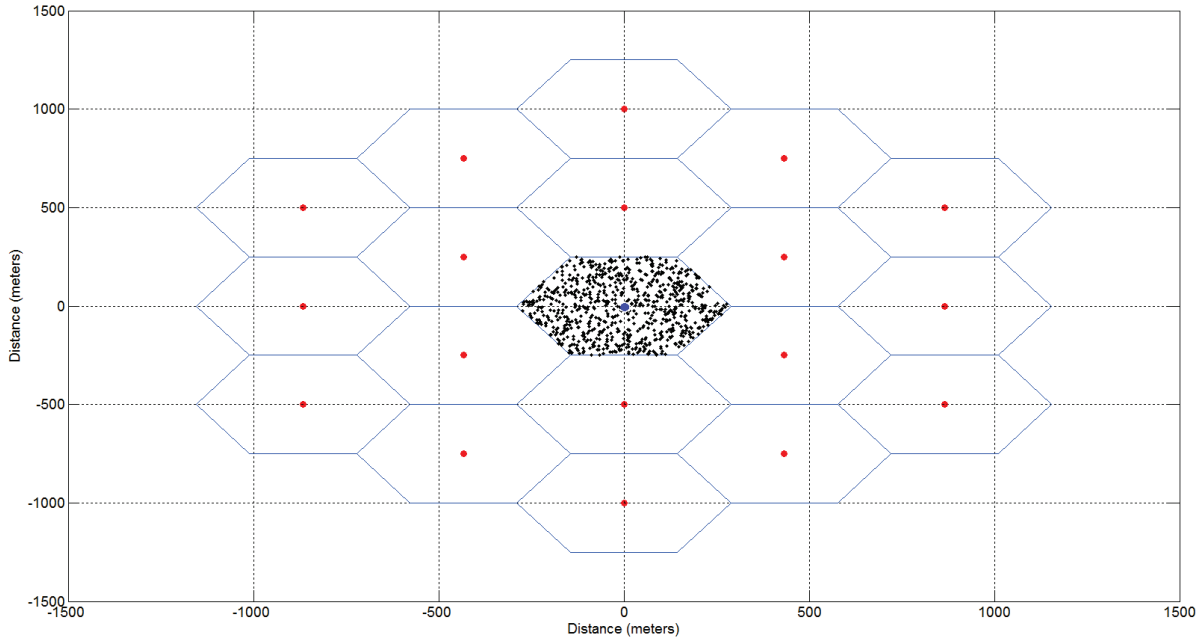

Figure 3.1: Uniform user distribution and hexagonal cellular layout.

distributed UE locations in the serving cell. Performance metric calculations are done for the original serving cell at the center which is switched off and the remaining 18 active eNBs marked in red have the capability of using downlink CoMP to serve the users in the switched off cell. Random user locations simulated in the switched off cell are denoted by $i \in I$, and the unique cell IDs of the eNBs are denoted as $n \in N = \{0,..,18\}$. Switched off center cell has the unique cell id $n = 0$ and the remaining eNBs are all part of the CoMP cooperating set which is denoted by $n \in N_{Coop} = \{1,..,18\}$. Although serving eNB can perform down selection on N_{Coop} before configuring the UE for multi-point measurements, we assume $N_{Coop} = N_{meas}$ for our simulations.

3.1.2 Large Scale Propagation and Pathloss Model

Pathloss in wireless communication is defined as the difference in dB between the transmitted and the received signal powers due to the attenuation during the propagation [45]. Most of the existing work explained Section 2.1.3 used the traditional log-normal shadowing for large scale pathloss modeling formulated as

$$P_{RX}\ (dBm) = P_{TX}(dBm)\ -\ PL(dB), \tag{3.1}$$

where P_{RX} represents the received signal power at the UE, P_{TX} represents the transmitted signal power at the eNB and the observed pathloss is denoted by PL which is derived as

Table 3.1: Simulation parameters for UMA pathloss model

Parameter	Value
Carrier Frequency (f_c)	2110 Mhz
BS (Base Station) Antenna Height (h_{BS})	24 m
User Terminal Antenna Height (h_{UT})	0.5 m
Average Street Width (L)	20 m
Average Building Height (h_B)	20 m
LoS Shadowing standard dev. (σ_{LoS})	4 dB
NLoS Shadowing standard dev. (σ_{NLoS})	6 dB
Break Point Distance (d_{BP})	337.6 m
Transmission Power (P_{TX})	20 W

$$PL(dB) = PL(d_0) + 10n \log\left(\frac{d}{d_0}\right) + X_\sigma, \tag{3.2}$$

where $PL(d_0)$ denotes the pathloss at the reference distance, d represents the propagation distance, n is the path loss exponent and X_σ is the Gaussian random variable with zero mean and standard deviation σ modeling the shadowing effect of the media. Pathloss models defined in the 3GPP specifications by ITU, which are formulated after actual field measurements are used in this thesis according to ITU-R report M.2135 for radio interfaces in [44], instead of the classical log-normal shadowing model to have a more realistic model and feasible results. Urban Macro (UMa) pathloss model is chosen for our model. Since the mobile antenna height is much smaller than the base station antenna height, non-line of sight (NLoS) propagation is also considered for realistic simulations along with the line of sight (LoS) model. Pathloss for LoS scenarios, expressed in dB scale, are given by

$$PL_{LoS} = 22\log_{10}d + 28 + 20\log_{10}f_c + X_{\sigma_{LoS}}, \quad 10m < d < d_{BP}; \tag{3.3}$$

$$PL_{LoS} = 40\log_{10}d + 7.8 + 2\log_{10}f_c - 18\log_{10}h_{BS} - 18log_{10}h_{UT} + X_{\sigma_{LoS}}, \quad d_{BP} < d < 5000 \text{ m}; \tag{3.4}$$

where the break point distance denoted by d_{BP} is calculated as

$$d_{BP} = \frac{4h_{BS}h_{UT}f_c}{c}, \tag{3.5}$$

where c represents the speed of light. It should be noted that the carrier frequency f_c used in (3.3) and (3.4) is given in GHz while being given in Hz for (3.5). Pathloss for NLoS propagation is calculated as

$$PL_{NLoS} = 161.04 - 7.1\log_{10}L + 7.5\log_{10}h_B - \left(24.37 - 3.7\left(\frac{h}{h_{BS}}\right)^2\right)\log_{10}h_{BS} + \left(43.42 - 3.1\log_{10}h_{BS}\right)(\log_{10}d - 3) + 20\log_{10}f_c - \left(3.2(\log_{10}11.75h_{UT})\right)^2 - 4.97) + X_{\sigma_{NLoS}}, \tag{3.6}$$

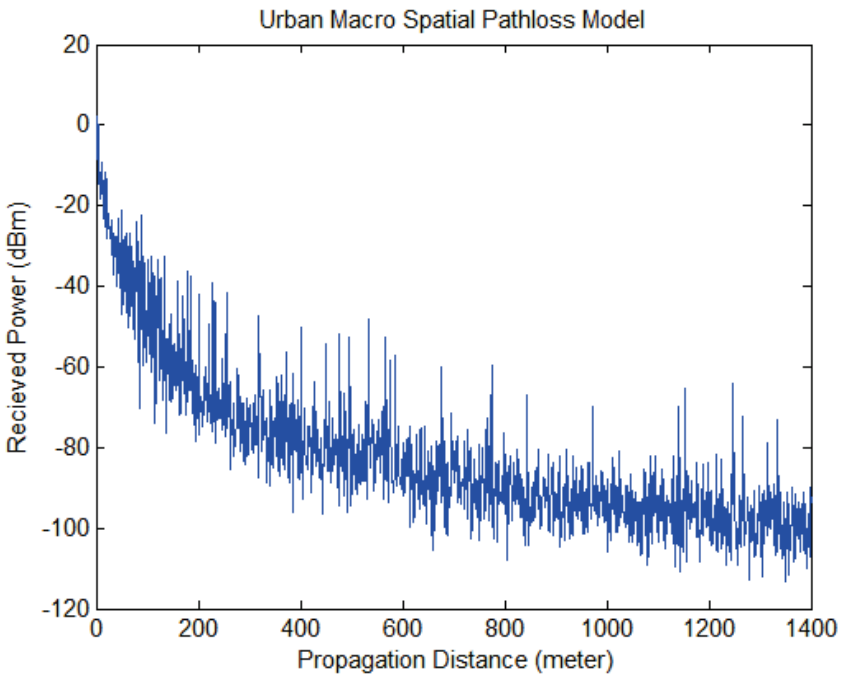

Figure 3.2: Large scale urban macro spatial pathloss model including both LoS and NLoS probabilities.

and LoS probability is modeled with a Bernoulli random variable as a function of the propagation distance,

$$Prob(LoS) = \min\left(\frac{18}{d}, 1\right) * \left(1 - e^{-\frac{d}{63}}\right) + e^{-\frac{d}{63}}. \tag{3.7}$$

Received signal power due to spatial pathloss versus propagation distance is obtained in Figure 3.2 using the equations (3.3) – (3.7) according to the parameters specified in Table 3.1. The shadowing effect is visible from the simulation results, where in some scenarios the UEs that are located further away from the base station have higher received powers. Received power attenuation after the break point d_{BP} has a lower decreasing slope as expected from (3.3), (3.4) and (3.5). It is also clear that the Bernoulli line of sight probability decreases with increasing propagation distance, *d,* due to (3.7); and the received signal power spikes due to LoS propagation decrease as expected. As a the NLoS probability increases for larger propagation distances, the signal fluctuations due to the shadowing effect become more clear since $\sigma_{LoS} = 4$ dB and $\sigma_{NLoS} = 6$ dB.

3.2 Downlink CoMP Performance Metrics Formulation

3.2.1 Capacity Calculation for CoMP Systems

The initial motivation for CoMP was to increase the cell edge user throughput/spectral efficiency by making use of inter-cell orthogonal resource assignments [34]. Inter-cell orthogonality in LTE-A is a major enhancement

compared to the legacy radio technologies to mitigate and exploit the inter cell interference. Received SINR in pre-LTE-A radio technologies is calculated as

$$SINR_{pre-LTE-A} = \frac{P_{RX}(n=j)}{\sum_{\substack{n\in N \\ n\neq j}} P_{RX}(n) + P_{noise}}, \tag{3.8}$$

where $P_{RX}(n=j)$ is the received signal power from the serving eNB $n=j$, the remaining eNBs act as co-channel interferers and P_{noise} represents the received noise power calculated as

$$P_{noise}\ (\text{dBm}) = N_0 + 10\log_{10} W(i), \tag{3.9}$$

where $N_0 = -174$ dBm/Hz is the noise spectral density and $W(i)$ is the frequency bandwidth assigned to the user *i*. In a cellular system using CoMP, members of the joint transmission set N_{JT} perform joint scheduling on PDSCH to transfer the user plane data using TM-9. Assuming the receiver UE performs perfect phase adjustment of sinusoidal crests, the received PDSCH power is calculated as

$$P_{JT} = \sum_{n\in N_{JT}} P_{RX}(n), \tag{3.10}$$

and the received downlink SINR in joint transmission systems is formulized according to [46] as

$$SINR_{CoMP-JT} = \frac{P_{JT}}{\sum_{n\in N\setminus N_{JT}} P_{RX}(n) + P_{noise}}, \tag{3.11}$$

where only the eNBs that are excluded from the joint transmission set due to measurement reports, $n \notin N_{JT}$ act as interference. Number of participating points in the joint transmission is called the clustering degree denoted by N_C. It is clear from (3.10) and (3.11) that the inter-cell interference is mitigated more as N_C increases. Downlink capacity perceived in bits/sec at each user location, *i,* is then derived as

$$C(i) = W(i)\log_2\left(1 + \frac{P_{JT}(i)}{\sum_{n\in N\setminus N_{JT}(i)} P_{RX}(n,i) + P_{noise}}\right), \tag{3.12}$$

where $P_{RX}(n,i)$ represents the received downlink power from the eNB *n* to UE *i* using the UMa large scale pathloss model explained in Section 3.1.2. It should be noted that each UE *i* has a distinct CoMP transmission set $N_{JT}(i)$ depending on the user location and mobility. Downlink capacity and spectral efficiency gains due to CoMP is directly related to the accuracy and the degree of the joint transmission cluster set as seen in (3.12).

3.2.2 Power Consumption Model

Spectral efficiency increase in downlink CoMP systems comes along with additional backhauling and signal processing trade-offs that increase the power consumption of a base station participating in CoMP. Total power consumption in Joules/sec for a base station using CoMP is calculated using the assumptions from [47] and [48] as

$$P_{Comp} = N_s N_{\frac{PA}{sector}} \left(\frac{P_{TX}}{PA_{eff}} + P_{SP} \right) (1 + C_C)(1 + C_{BB}) + P_{BH} \, , \tag{3.13}$$

where N_s is the number of sectors, $N_{PA/sector}$ is the number of power amplifiers per sector, P_{TX} is the transmit power of the base station, PA_{eff} is the power amplifier efficiency, P_{BH} is the power consumption due to CoMP backhauling, C_C and C_{PSBB} denote the cooling and battery backup losses in the system. In (3), P_{SP} is the signal processing power consumption in the base station which has a base value of 58W for an LTE e-NB mentioned in [16], however the signal processing increase due to CoMP is modeled in [47] with the below equation (3.14) as a quadratic function of the CoMP cluster set degree N_C for values of $N_C \geq 2$:

$$P_{SP-CoMP} = 58(0.87 + 0.1N_C + 0.03N_C^2) \text{ W} \, . \tag{3.14}$$

Backhauling power consumption P_{BH} for base stations using CoMP is modeled in [47] as

$$P_{BH} = \frac{C_{BH}}{100 Mbits/sec} 50 \text{ W} \, , \tag{3.15}$$

where C_{BH}, the additional backhaul data capacity needed, is expressed as

$$C_{BH} = \frac{N_c * (2N_C) * p * q}{T_S} \text{ bits/sec} \, , \tag{3.16}$$

where p and q represent the additional pilot density and excess CSI signaling due to CoMP joint transmission, respectively, and $T_S = 66.7$ μsec is the symbol period which is the reciprocal of the assumed OFDM sub-carrier spacing of $\Delta f = 15$ kHz using (2.19). None CoMP related contributing factors in the power consumption model are N_s, $N_{\frac{PA}{sector}}$, $\frac{P_{TX}}{PA_{eff}}$, C_C and C_{BB}, whereas P_{BH} and P_{SP} heavily dependent on $N_{JT(i)}$ as shown in (3.14) and (3.16), and demonstrated in Figure 2.14. While calculating the power consumption of the base stations that are not using CoMP joint transmission in the downlink, P_{Base}; signal processing power consumption $P_{SP-Base}$ is set to 58 W and P_{BH} does not exist. The total access network power consumption for each user i, $P_T(i)$, is found using (3.13) – (3.16) as

Table 3.2: Power consumption parameters for e-NBs using CoMP according to [47] and [48]

Parameter	Value
Transmission power (P_{TX})	20 W
Power amplifier efficiency (PA_{eff})	0.38
Cooling losses (C_C)	0.29
Battery backup losses (C_{BB})	0.11
Pilot density (p)	8/168
CSI signalling overhead (q)	8
Subcarrier spacing (Δf)	15 kHz
Power amplifiers per sector ($N_{PA/sector}$)	1

$$P_T = P_{Base}\,, \quad N_C = 1 \tag{3.17}$$

for traditional cell switch of schemes without CoMP, and as

$$P_T = P_{Comp} + (N_C - 1)\left(P_{Comp} - P_{Base}\right), \quad N_C \geq 2 \tag{3.18}$$

for the proposed CoMP aided cell switch off scheme. The scaling factor of $(N_C - 1)$ in (3.18) is used to make a fair power consumption comparison between the traditional and the proposed cell switch off scheme. For the user locations where CoMP is used (i.e. $N_C \geq 2$) to serve the cell switched off area, $(N_C - 1)\left(P_{Comp} - P_{Base}\right)$ is used to add up the additional power consumption of the base stations that are participating in the CoMP cluster as secondary cells and P_{Comp} is used to model the overall consumption of the main participant (serving cell) of the CoMP set.

3.2.3 Energy Efficiency Metric

Spectral efficiency and capacity metrics expressed in $\frac{\text{bits/sec}}{\text{Hz}}$ and $\frac{\text{bits}}{\text{sec}}$, respectively, are used as standardized KPIs (Key Performance Indicators); however, energy efficiency metric is not yet standardized across the literature. Green network deployment schemes generally use the cellular coverage area per power consumption ratio, m^2/W, as a metric to reflect the energy efficiency of the implementation [8]. This is more of a standalone energy efficiency KPI since it does not consider the user perceived quality of service. As mentioned in Section 2.1.2, energy efficiency and capacity performance metrics of the cellular network should be considered jointly to have a fair analysis of the system. Considering the all-IP network (AIPN) evolution with LTE and beyond technologies after the depreciation of circuit switched core, bits/Joule can be used as a generic metric for energy efficiency KPI to measure the amount of bits transmitted to the user per energy consumed in Joules. Capacity to

energy efficiency conversion is done using the capacity formulation from (3.12) and power consumption model from (3.17) and (3.18) as

$$EE(i) = \frac{C(i)}{P_T(i)}, \tag{3.19}$$

where $EE(i)$ represents the energy efficiency of the user i. It can be seen form (3.19) that the energy efficiency of the system is dependent on the trade-off between overall power consumption and the gain in the perceived capacity. As a result, unnecessary increases for the clustering degree N_C of the joint transmission set to include eNBs with low received power values could decrease the energy efficiency since the increases in the signal processing and backhauling power consumption are not compensated by an equal gain in downlink capacity perceived.

3.3 Simulation Results and Discussion

3.3.1 Traditional Cell Switch Off versus CoMP Aided Schemes

This section compares the performance of traditional cell switch off schemes with the proposed CoMP aided cell switch off scheme. Hexagonal cellular layout with 19 e-NBs, $n \in N = \{0,..,18\}$ are considered according to Section 3.1.1 and uniform random user locations $i \in I = \{1,..,500\}$ are simulated in the center eNB, $n = 0$. Traditional cell switch off scheme is modeled, where the original center serving eNB, $n = 0$, is switched off for energy saving and the remaining eNBs in the network zoom out by increasing their transmission power P_{TX} by 2 W to serve the users located in the switched off region. CoMP aided cell switch off scheme is modeled, where remaining active eNBs in the network use CoMP joint transmission technique in the downlink to serve the users while keeping the same transmission power levels. Stationary users are assumed in this section and the downlink received signal powers are calculated according to the UMa large scale pathloss model described in Section 3.1.2 as

$$P_{RX}(n,i) = P_{TX}(n) - PL_{UMa}(n,i), \tag{3.20}$$

where $P_{RX}(n,i)$ corresponds to the received downlink power by user i from eNB n. Although we assumed that all the remaining active eNBs in the network are members of both the CoMP cooperating and measurement sets, $n \in N_{Coop} = N_{meas} = \{1,..,18\}$, joint transmission cluster degrees from $N_c = 2$ up to $N_c = 6$ are simulated where N_C eNBs with the highest downlink received powers for each UE are performing cross-point PDSCH

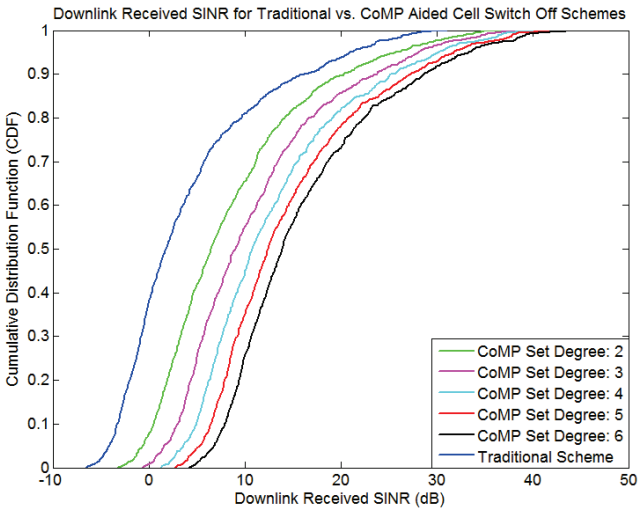

Figure 3.3: Received SINR CDF comparison between traditional and CoMP aided cell switch off schemes.

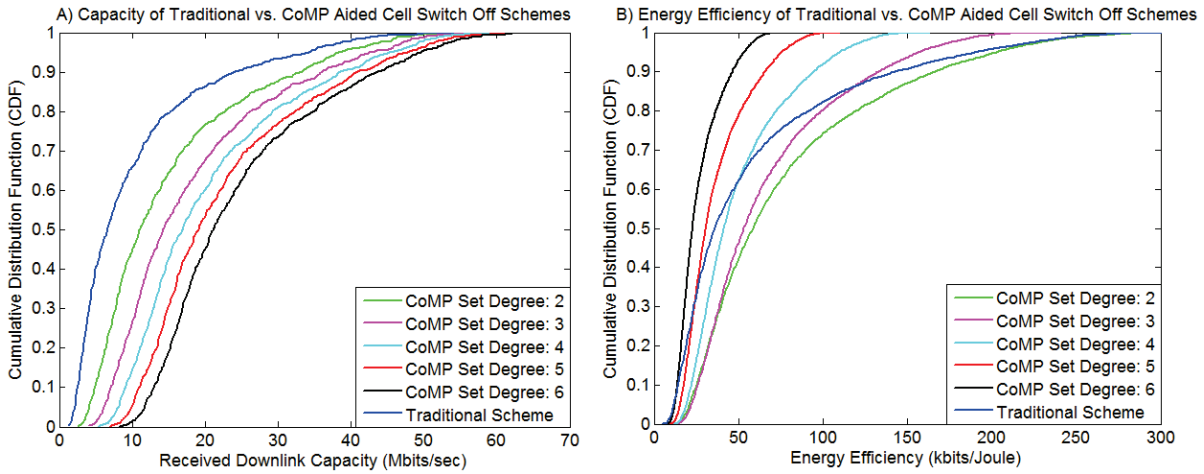

Figure 3.4: Energy efficiency and DL capacity comparison between traditional and CoMP aided cell switch off schemes.

transmission to serve the specific UEs. As a result, each user i can have distinct joint transmission sets $N_{JT}(i)$ depending on the user locations and various pathloss effects shown in (3.20). Received downlink SINR at each user location is calculated using (3.8) for traditional cell switch off schemes and (3.11) for CoMP aided schemes. Due to the inter cell interference mitigation effect, CoMP aided schemes yielded better received SINR values at each user and increasing the clustering degrees further improved SINR gains as shown in Figure 3.3. Significant cell edge performance improvements are observed in CoMP aided schemes, where the cell edge users are defined as the users receiving the lowest 5% of the received SINR values shown in the cumulative distribution function (CDF) displayed in Figure 3.3. Cell edge users in the traditional cell switch off schemes perceive DL SINR values lower than -7 dB, while in CoMP aided switch off schemes with $N_c = 6$,

Table 3.3: Mean system energy efficiency and user perceived DL capacity for cell switch of schemes

Simulated cell switch off scheme	Mean DL perceived capacity (Mbits/sec)	Mean system energy efficiency (kbits/Joule)
Traditional, $N_c = 1$	9.9737	59.5047
CoMP aided, $N_c = 2$	14.7906	78.0615
CoMP aided, $N_c = 3$	17.9528	67.2373
CoMP aided, $N_c = 4$	20.4614	50.3890
CoMP aided, $N_c = 5$	22.6593	36.4919
CoMP aided, $N_c = 6$	24.7179	26.6331

perceived SINR values increase to 6 dB. LTE-A and beyond technologies use adaptive modulation and coding (AMC) schemes, where the serving eNB adapts the used modulation scheme according to the downlink received SINR values. Spectral efficiency versus SINR comparison for LTE-A schemes using AMC were performed in [49] and shown that the users require at least 18 dB SINR values for the AMC scheme to boost up to 64-QAM with 0.8 coding rate. The CDF of the SINR for each cell switch off scheme can be used to find the probability of each modulation and coding scheme described in [49]. For example, the probability of using 64-QAM with 0.8 coding rate is found as

$$Prob(64-QAM, 0.8) = Prob(SINR > 17dB) = 1 - CDF_{SINR,N_C=1}(17) \sim 0.09 \quad (3.21)$$

for the users in the traditional switch off scheme, and as

$$Prob(64-QAM, 0.8) = 1 - CDF_{SINR,N_C=6}(17) \sim 0.09 \quad (3.22)$$

for the users in the CoMP aided switch off scheme using a static joint transmission clustering degree of $N_C = 6$. It is clear that the CoMP schemes make more use of the higher modulation schemes due to the decrease interference.

Received downlink capacity C_i for each user i and the energy efficiency of the access network, EE_i while scheduling the user are found using (3.12) and (3.19). CDF of the downlink capacity for each scheme is shown in Figure 3.4a, and it is clear that the proposed scheme of using CoMP jointly with traditional cell switch off schemes yields further improvement in the overall received QoS in terms of capacity. The surprising result of the simulations is that increasing the CoMP set degree blindly from $N_C = 2$ to $N_C = 6$, in fact, decreases the bits/Joule energy efficiency of the system proving that excess usage of CoMP in the downlink can lead to worse performance due to signaling and backhauling overhead in the network, as shown in Table 3.3 and Figure 3.4b. This can be explained by the power consumption of the access network increasing as a quadratic function of the

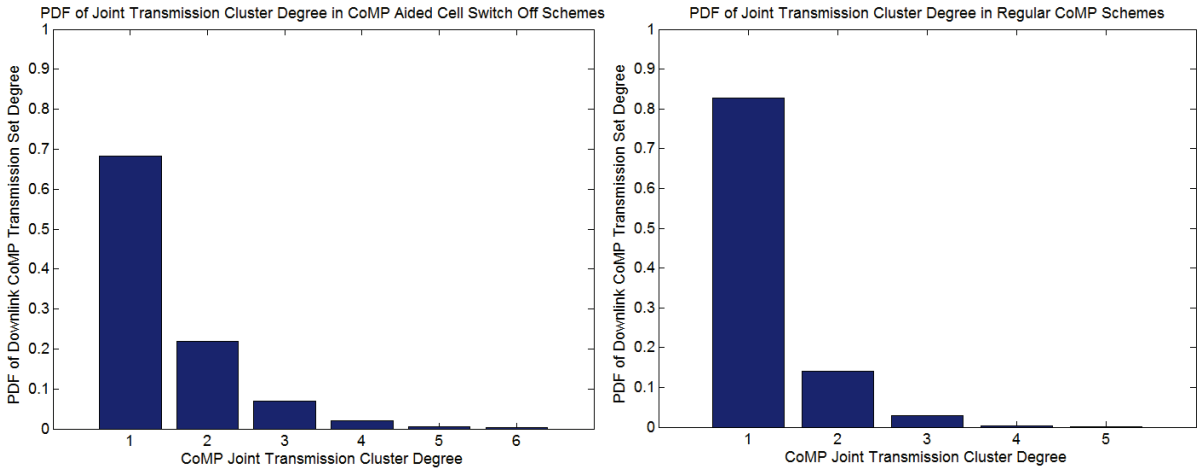

Figure 3.5: PDF of CoMP joint transmission cluster degrees for cell switch aiding versus regular CoMP schemes, simulated in stationary channels according to 3 dB clustering threshold.

clustering degree shown in (3.14) and (3.16) not being compensated enough by the DL CoMP capacity increases, which are derived in (3.12). Results summarized in Figure 3.14 prove that the CoMP aided cell switch off schemes yield better results in terms of both DL capacity and access network energy efficiency compared to the traditional cell switch off schemes assuming the correct clustering degrees are used. CoMP serving eNB should use adaptive joint transmission set degrees for each user not to create an energy inefficient system. This can be obtained by the serving eNB using a received power threshold to limit the CoMP cluster, which is explained in the next section.

3.3.2 Threshold-Based Joint Transmission Clustering CoMP Schemes

Advantages of receiving cross-point PDSCH scheduling with higher clustering degrees is very clear from the UE's perspective, however the cellular system should be considered as a whole by taking the energy efficiency of the access network into account. Proof of the need for a thresholding technique to form N_{JT} was performed in Section 3.3.1. E-NBs that do not yield enough capacity increases to compensate for the additional power consumption due to excess signalling and processing should be excluded from the transmission cluster. We simulated an ideal scenario where the serving eNB RRC/MAC layer performs the threshold-based CoMP transmission set decisions based on the received power values $P_{RX}(n,i)$ and the best member of the N_{meas} is found for each user i by $\arg\max_{n}\{P_{RX}(n,i)\} = n_{Best}(i)$. $P_{RX}(n,i)$ values are passed through a thresholding block

and the eNBs yielding DL received power values that are within a certain predefined threshold ∇_{NW-JT} compared to the best measured eNB are added to the clustering set for user i, $N_{JT}(i)$ as shown below:

$$\mathrm{n} \in N_{JT}(i) \quad if \quad |P_{RX}(n_{Best}, i) - P_{RX}(n, i)| \leq \nabla_{NW-JT}. \tag{3.23}$$

Received power threshold to form $N_{JT}(i)$ is chosen as $\nabla_{NW-JT} = 3$ dB, according to the parameters mentioned in [34]. Applying the 3 dB threshold rule to the regular CoMP systems with no energy saving adaptations and to the systems that use CoMP aided cell-switch off schemes for energy savings, discrete PDFs (Probability Distribution Functions) for the feasible cluster degrees, N_C, are obtained in a stationary wireless channel. It can be seen from Figure 3.5 that the probability of users utilizing CoMP increase by 50% when the center serving cell is switched off. Therefore, energy saving versus capacity gain trade-off in CoMP systems when they are used jointly with cell switch off/on schemes becomes more important.

3.4 Summary

This chapter analyzed an alternative way of improving the cell switch off schemes for further energy saving enhancements using CoMP transmission technique and proved the advantages in terms of both energy and capacity efficiency. Through simulations with realistic parameters, it is demonstrated that the cell switch off + CoMP combination used with proper CoMP active set degree yields a more energy efficient solution with better perceived DL capacity in comparison to the traditional cell switch off schemes. Performance of the joint transmission CoMP schemes is highly dependent on the clustering decisions. Excluding an eNB that yields received power levels within ∇_{NW-JT} to the best measured cell from N_{JT} will cause degradation in the DL capacity shown in Figure 3.4a, whereas including an eNB that does not meet the threshold constraint will degrade the overall energy efficiency of the access network as shown in Figure 3.4b. The trade-off between the network energy efficiency and the capacity can be balanced using the serving eNB thresholding mechanism explained in Section 3.2.2 by having adaptive $N_{JT}(i)$ clustering decisions for each user location i. It should be noted that threshold based transmission point selection has also been used for wireless relaying protocols as proposed by [50]. This chapter assumed stationary wireless channels and provided the proof of concept for user adaptive clustering decisions; however, joint transmission sets should be time adaptive according to the signal fluctuations due to small scale fading as well. Time adaptive clustering decisions will be discussed in Chapter 4 by simulating CoMP scenarios in time-varying multipath channels.

Chapter 4

Performance Analysis of Joint Transmission Scheme Subject to Imperfect CSI Feedback

This chapter enhances the stationary CoMP system modeled in Chapter 3 by analyzing the time-varying aspects of the performance metrics. Small scale fading effects are simulated for each radio link between the users and the members of the CoMP measurement set, N_{meas}. Various channel models are explained and discussed in Section 4.1 to model radio links accurately. Serving eNB performs joint transmission clustering by using the thresholding technique explained in Section 3.3.2 in a time varying fashion, distinctly for each UE, to adapt to the instantaneous received power fluctuations due to small scale fading. Possible multi-point channel estimation errors and system delays lead to inaccurate clustering decisions. Impacts of imperfect joint transmission set clustering decisions on energy efficiency and downlink capacity performance metrics are analyzed under various channel conditions using realistic models to simulate the time and frequency dispersive channel characteristics. Performance degradation sensitivities of various user locations in the cellular deployment are characterized both for low and high mobility conditions. The work explained in this chapter has been presented in the submitted conference paper [51].

4.1 Small Scale Fading Model

Propagation model described in Section 3.1.2 estimated the received signal power as a function of distance, simulated the large-scale path loss and shadow fading effect in the radio link. Large-scale path loss models are enough to have a basic understanding of the long term average received power of the static mobile users that are away from the base station by a large known distance. Received signal at the mobile receivers usually consists of multipath components, which are, radio waves propagating from different directions with different amplitudes and phases due to scattering, diffraction, reflection, refraction and absorption as demonstrated in Figure 4.1. Hence, rapid fluctuations in the received signal amplitude and phase are observed over short period of times and distances (order of wavelengths) due to the small scale fading effects. Apart from the natural phenomena in the transmission media, small scale fading arises due to the lack of a direct line of sight path between the transmitter and receivers due to the small height of the mobile receiver antennas compared to height of the base station transmitter antennas and the sizes of urban structures as described in Table 3.1.

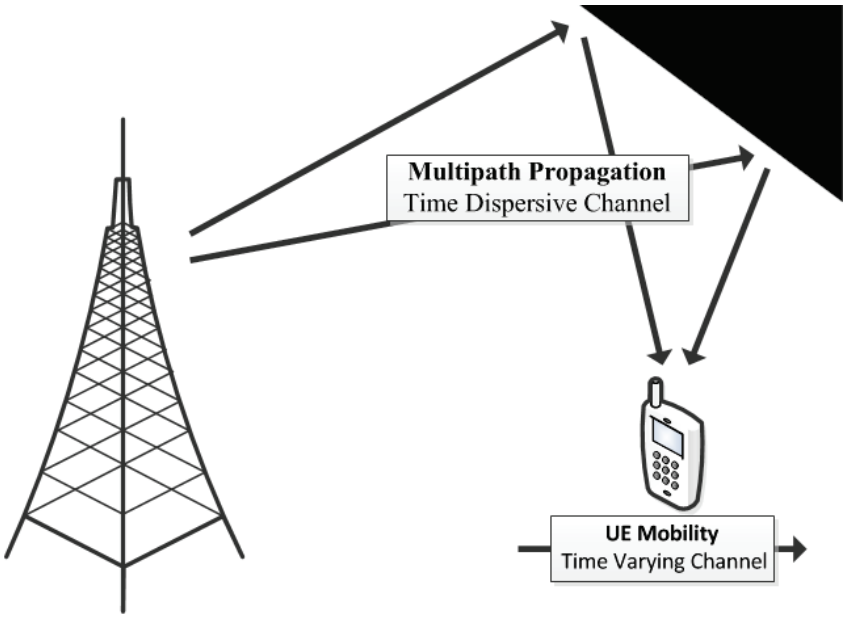

Figure 4.1: Demonstration of time dispersive and varying nature of the channel due to multipath propagation and mobility.

Radio channels between the UE i and each point in CoMP measurement set n ∈ $N_{meas}(i,t)$ are modeled independently and expressed by the time varying and dispersive complex baseband CIR as

$$h_{n,i}(t,\tau) = \sum_{l=1}^{L} A_l(t) e^{j2\pi f_{d_l} t} e^{j2\pi f_c \tau_l} e^{j\phi_l} \delta(\tau - \tau_l), \tag{4.1}$$

where L is the total number of multipath components, f_c is the carrier frequency, A_l, f_{d_l} and ϕ_l represent the time varying amplitude, Doppler frequency and additional phase shifts observed at the delay tap l, respectively. Amplitude and Doppler shift of each multipath component is represented as a function of time since the receiver velocity, spatial angle, θ_l between the mobile direction and the received wave of the multipath and the received power of each multipath are subject to change due to UE mobility. Main contributors to the phase shift of the multipath delay tap are f_{d_l} and $\emptyset_l$, however the difference in propagation of each multipath also contributes to the phase shift of each multipath component as

$$\Delta\varphi = \frac{2\pi d_l}{\lambda} = \frac{2\pi f_c d_l}{c} = 2\pi f_c \tau_l, \tag{4.2}$$

where d_l represents the additional distance travelled by the delay tap component l. It should be noted that the UE can face various phase shifts due to multipath propagation even under static conditions. Multipath radio channels are described with two major groups of parameters: Time Dispersive (Frequency Varying) and Frequency Dispersive (Time Varying).

Time dispersive nature of the mobile radio channel is due to the multipath components of the received signal over small periods of time because of the different propagation paths. Time dispersive nature is quantified in time domain by RMS delay spread of the channel of the channel as

$$\sigma_\tau = \sqrt{E(\tau^2) - E(\tau)^2}\,, \tag{4.3}$$

which is the variance of the power delay profile. Mean excess delay is the expected value of the power delay profile calculated as

$$E(\tau) = \sum_{l=1}^{L} |\, A_l \,|^2 \, \tau_l\,, \tag{4.4}$$

where A_l^2 and τ_l correspond to the received power levels and excess delays at each delay tap, respectively. Time dispersive nature of the channel is realized in the frequency domain by the coherence bandwidth of the channel. Coherence bandwidth of the channel, B_c, is inversely proportional to σ_τ and represents the spectral frequency range where the CTF has high correlation in terms of applying similar gain and phase differences to the passed radio waves.

Frequency Dispersive nature of the channel is due motion of the mobile users causing various Doppler shifts on the multipath components of the received signal. The relative motion of the mobile receivers with respect to the base station transmitters cause a phase change in the received signals due to the different paths lengths traveled by various radio waves. The change in received frequency or the Doppler shift observed at each delay tap *l* is found by

$$f_{d_l} = \frac{v}{\lambda}\cos(\theta_l)\,, \tag{4.5}$$

where *v* is the receiver velocity, which will be positive if the UE is travelling in the direction of the received signal from the delay tap *l,* and θ_l is the angle between the UE direction of travel and the received signal from the multipath component *l*. It is clear from (4.5) that each multipath component can face different Doppler shifts even if the UE is traveling at a constant velocity. Maximum spectral expansion is called the Doppler spread and expressed as $f_{d_{max}} = \frac{v}{\lambda}$, assuming $\theta_l = 0^o$. Impacts of the frequency dispersive channel in time domain are realized by the coherence time of the channel, T_c. Coherence time of the channel is inversely proportional to the Doppler Spread and represents the range of time period where the components of the radio waves are subject to CIRs with high correlation.

All the aforementioned parameters, both time and frequency dispersive characteristics, of the radio channel play a role in determining the type of small scale fading observed in the channel. Multi-path delay spread based fading is grouped as flat fading and frequency selective fading. Flat fading describes the scenario when the bandwidth of the signal B_{signal} is smaller than the coherence bandwidth B_c of the channel and accordingly the delay spread σ_τ of the channel being smaller that the symbol period T_{symbol} of the signal. Received symbol does not suffer from ISI since the delay spread is not significant. CTF applied to the various spectral components of the transmitted signal are highly correlated due to the narrowband signal. However, the received signal faces deep fades over time due to the narrowband signal. Frequency selective fading describes the opposite scenario where $B_{signal} > B_c$ and $\sigma_\tau > T_{symbol}$. Due to wideband signal, there are no significant amplitude fluctuations or deep fades, however the signal in the frequency domain is affected by changing CTFs since the wideband signal spectrum is larger than the flat bandwidth. As a result, UE may send different channel feedback to the serving e-NB since every assigned resource block may face different channel gains and phase shifts. Significance of σ_τ compared to T_{symbol} derived in (2.21) leads to inter symbol interference as demonstrated in Figure 2.9. Doppler spread based small scale fading is categorized as fast and slow fading. Fast fading represents the radio scenario where the mobile UE receivers have high velocities leading to a large Doppler spread and the data rate of the transmission is low. Coherence time of the channel T_c is smaller than the symbol period of the transmission T_{symbol} causing signal distortion since the CIR changes quicker than the symbol period. Slow fading represents the counter scenario where data rate of the transmission is fast and the mobile receiver is moving at slow velocities yielding a low Doppler spread. CIR does not change within the period of one symbol, and no distortion is observed at the receiver. Second order stochastic characteristics of CIR and CTF will be discussed thoroughly in Section 5.1.

4.1.1 Rayleigh Channel Model

Modeling and simulation of the small scale fading of the wireless channels has been an interest to both academia and the industry as explained in [52] and [53]. Theoretical approach to simulate a slow flat fading channel using the Rayleigh model is shown in [52]. Complex envelope received signal due discrete multipath channel impulse response and the Doppler shifts of each different multipath due to relative motion is derived by

convolution of the complex baseband CIR shown in (4.1) with the transmitted OFDM symbol shown in (2.17). CIR waveform is expressed in time domain by

$$h_s(t,\tau) = Re\{h(t,\tau)e^{j2\pi f_c t}\}, \tag{4.7}$$

$$h_s(t,\tau) = \sum_{l=1}^{L} A_l(t)\cos(2\pi f_{d_l} t \; + \; 2\pi f_c \tau_l + \phi_l + 2\pi f_c t)\,. \tag{4.8}$$

Using the cosine angle sum formula, (4.8) can also be written as below:

$$\cos(A+B) = \cos(A)\cos(B) - \; \sin(A)\sin(B); \tag{4.9}$$

$$A = 2\pi f_c t\,, \;\; B = \; 2\pi f_{d_n} t \; + 2\pi f_c \tau_l \; + \; \phi_n; \tag{4.10}$$

$$h_s(t,\tau) = \sum_{l=1}^{L} A_l(t)\cos(2\pi f_{d_l} t + 2\pi f_c \tau_l + \phi_l)\cos(2\pi f_c t) \; - \; \sin(2\pi f_{d_l} t + 2\pi f_c \tau_l + \phi_l)\sin(2\pi f_c t)\,. \tag{4.11}$$

It can be seen (4.11) that the received signal can be separated in to two parts that are 90^0 out of phase, hence it can be represented as a summation of in-phase and quadrature (I-Q) components:

$$h_s(t,\tau) = \sum_{l=1}^{L} I(t)\cos(2\pi f_c t) \; - \; Q(t)\sin(2\pi f_c t)\,. \tag{4.12}$$

Using the Central Limit Theorem (CLT) explained in [54], the sum of a large number of independently and identically distributed (iid) random variables lead to a Gaussian distribution. It can be seen above that both the in-phase and the quadrature component is a sum of independently and identically distributed random variables, A_l and ϕ_l, assuming a large number of multipath components L. The amplitude of the CIR in a multipath fading channel is found by calculating the envelope using the I-Q components as

$$|h_s(t,\tau)| = \; \sqrt{I(t)^2 + \; Q(t)^2}\,. \tag{4.13}$$

The sum of two iid Gaussian random variables that are 90^0 out of phase lead to a Rayleigh distributed random variable. As a result, the proposed model concludes that the PDF of the channel amplitude gain is going to follow the Rayleigh distribution

$$f(|h_s(t,\tau)|) = \; \frac{|h_s(t,\tau)|}{{\sigma_h}^2} e^{-|h_s(t,\tau)|^2 / 2{\sigma_h}^2}, \tag{4.14}$$

where σ_h is the RMS voltage of the received signal after propagation through the multipath channel. Although the theoretical Rayleigh model is successful at simulating flat fading channels, it is simplistic and cannot be used in a standalone way to simulate realistic radio wave transmission in a cellular environment since possible

Table 4.1: Simulation parameters for small scale fading model

Channel Parameters	Value
Number of multipath components (L)	6
Vehicular UE receiver velocity for high mobility (v_{high})	120 km/h
Pedestrian UE receiver velocity for low mobility (v_{low})	6 km/h
Sampling density for high mobility (η_{high})	2.13
Sampling density for low mobility (η_{low})	42.6
Number of UE-eNB radio links (N_{meas})	18
Number of time samples (T)	1000

cross-correlations within the underlying Gaussian processes shown in (4.12) were not taken into consideration and model does not provide flexibility to have time-varying Doppler spreads, power delay profiles.

An alternative Rayleigh channel model using a time-varying linear filter is proposed by authors of [53] by taking autoregressive channel properties, changing Doppler shifts and delay profiles into account. The proposed scheme simulates the channel as a none orthogonal Rayleigh process by modeling the cross correlations between the I-Q Gaussian processes shown in (4.12). Second order stochastic characteristics in time domain are used to generate the channel samples, where the current channel sample is dependent on the previously generated discrete samples according to the chosen filter length and the auto-correlation function of the CIR. The model is more advanced compared to [52], however is not flexible enough to involve various wireless channel parameters like antenna patterns, multipath component count, MIMO inputs, and channel sampling density.

4.1.2 Winner SCME Model

European WINNER project explained in [55] is a joint-effort project consisting of partners from both the telecommunications industry and the academia that aims to improve the existing performance of mobile communication systems. The main objectives of the project can be grouped under investigating and developing challenging scenarios is the radio interface, efficient cellular deployment techniques, cooperation schemes in the access networks, radio channel propagation models and efficient spectrum usage methods. There has been intensive work on creating realistic channel model implementations described in [56], [57], [58] and [59] for both small scale models as part of the Winner project. The model takes the 3GPP specification (25.996) as a basis for implementation and extends it to beyond 3G scenarios. MIMO parameters, radio link properties, antenna patterns, large-scale pathloss models, cellular layout, UE distributions, multipath delay spread and

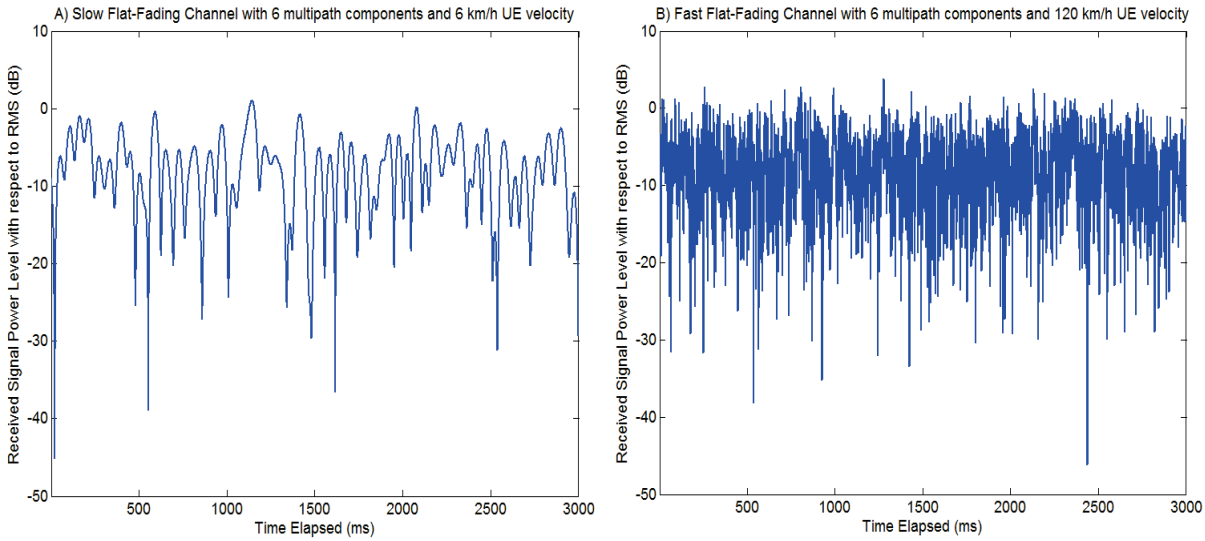

Figure 4.2: Small scale multipath fading model under different UE receiver mobility conditions.

Doppler spread are the inputs to the system to calculate the complex baseband channel impulse response for all the radio links and paths during the desired number of time samples according to the number of receiver and transmitter elements considered. Large scale pathloss and shadowing effects were already modeled in our simulation using the system described in [44], as a result [56]-[59] are just used to model the small scale fading effects in the system due to multipath and Doppler spread.

Input parameters to the SCME model are shown in Table 4.1 to generate complex channel impulse response $h(t, \tau_l)$ at each multipath tap l and time sample t. Spatial channel sampling density η is defined as the number of spatial samples per half wavelength $\lambda/2$. Channel samples, $t \in [1, .., T]$ are obtained with a 1 ms granularity to synchronize with the LTE MAC scheduling decisions that are performed every TTI at the serving eNB. As a result, η is tuned according to the receiver velocity to generate 1 channel sample for every TTI by converting the time sampling rate to spatial sampling rate according to

$$1\,ms = \frac{(\lambda/2)/\eta}{v} \quad . \tag{4.15}$$

Overall CIR at a particular TTI t is found by the superposition of all the multipath components l as

$$h(t) = \sum_{l=1}^{L} h(t, \tau_l) \, . \tag{4.16}$$

Instantaneous received signal power fluctuation at each channel sample due to small scale fading is found using (4.16) as

$$P_{Fading}(t) = 10\log_{10}\left[\left(\frac{\left|\sum_{l=1}^{L} h(t,\tau_l)\right|}{2}\right)^2\right], \tag{4.17}$$

expressed in dB scale. Received signal power level changes due to small scale fading are plotted against time elapsed both for high and low mobility scenarios according to 120 km/h vehicular and 6 km/h pedestrian receiver velocities, respectively. It is clear from the simulation results displayed in Figure 4.2 that high Doppler scenarios, which decrease the coherence time significantly, lead to major received power level fluctuations. Fast fading scenarios will induce additional challenges for UEs trying to perform multi-point channel measurements to help form the joint transmission clustering set. Serving eNB will need to adapt to the received power fluctuations due to small scale fading every TTI to update N_{JT}.

4.2 Formulation of CoMP Performance Metrics for Time-varying Channels

CoMP capable UE performs multi-point channel measurements for the eNBs that are part of the CoMP measurement set, $n \in N_{meas}$, every TTI unless otherwise specified by the serving eNB. Actual measured received power from eNB *n* by user *i* at TTI *t* is expressed as

$$P_{RX}(n,t,i) = P_{TX}(n) - PL(n,i) - P_{Fading}(n,i,t), \tag{4.18}$$

where $P_{TX}(n)$ is the transmitted power from the eNB $n \in N_{meas}$, $PL(n,i)$ is the large scale pathloss observed between user *i* and eNB *n* according to the UMa model explained in Section 3.1.2, and $P_{Fading}(n,i,t)$ is the time-varying power loss observed due to small scale fading at TTI *t* according to the model in Section 4.1.2. Small scale fading observed between every UE and eNB link, (n,i), is modeled independently, to have unbiased joint transmission clustering decisions. Due to the noisy channel expressed in (2.24) and scarce structure of CSI-RS for multi-point channel estimation demonstrated in Figure 2.15, the system is vulnerable to channel estimation errors. Joint transmission clustering decisions also suffer from the CoMP system delays due network topology constraints, feedback consolidation and processing procedures at the serving eNB. As a result, serving eNB RRC/MAC layer performs the threshold-based CoMP transmission set decisions based on the incorrectly estimated and outdated multi-point power measurements

$$P_{RX\_err}(n,t,i) = P_{RX}(n,t-\Delta,i) + P_{err}(\mu,\sigma), \tag{4.19}$$

where Δ is the delay observed in milliseconds during the CSI exchange and serving eNB feedback processing, and $P_{err}(\mu,\sigma)$ models the effect of channel estimation errors on measured received power calculation as a Gaussian random variable with mean μ and standard deviation σ expressed in dB scale. Time varying CoMP joint transmission set and cluster set degree for user *i* at TTI *t* are formed as

$$\text{n} \in N_{JT}(i,t) \quad if \quad |P_{RX_{err}}(n_{Best},i,t) - P_{RX_{err}}(n,i,t)| \leq \nabla_{NW-JT}, \tag{4.20}$$

$$N_C(i,t) = size(N_{JT}(i,t)\,), \tag{4.21}$$

respectively. Received joint PDSCH power, $P_{JT}(i,t)$, is calculated by plugging $N_{JT}(i,t)$ from (4.20) and $P_{RX\_err}(n,t,i)$ from (4.19) into (3.10). Downlink capacity observed, $C(i,t)$, is found by using $P_{JT}(i,t)$ in (3.12). Time varying power consumption of the access network is found by using $N_C(i,t)$ in (3.13). Accordingly, energy efficiency performance metric, $EE(i,t)$, is calculated as shown earlier in (3.19). Hence, imperfect CoMP clustering decisions due to the delayed and incorrectly estimated values of received power measurements shown in (4.19) will have impacts on all the aforementioned performance metrics. Time averaged energy efficiency, downlink capacity and cluster degree performance metrics for each user location *i* is denoted by $\overline{EE}(i)$, $\bar{C}(i)$ and $\overline{N_C}(i)$, respectively, calculated according to the multi-point channel samples over *T* TTIs.

4.3 Simulation Results and Discussion

4.3.1 Impact of Channel Estimation Errors

Cell switch off scheme aided with CoMP joint transmission technique is simulated with $i \in [1,\ldots,1000]$ user locations generated in the center switched off cell over $t \in [1,\ldots,1000]$ TTIs using the large scale UMa pathloss model from Section 3.1.2 and small scale fading model from Section 4.1.2. Sole Impacts of multi-point channel estimation errors on joint transmission clustering accuracy, energy efficiency and downlink capacity performance metrics are analyzed by assuming a CoMP system having no feedback delays, $\Delta = 0$ ms. Various channel estimation errors are introduced to the instantaneous received power measurements as Gaussian random variables, $P_{err}(\mu,\sigma)$, having $\mu = 0$ dB mean and $\sigma = [4\text{ dB}, 8\text{ dB}, 12\text{ dB}]$ standard deviation values. Moving average CoMP set degrees, $N_c(t)$, is plotted in Figure 4.3a, and it can be seen that the channel estimation errors result in a reduction in overall clustering degrees. Clustering degrees decrease further with increasing channel estimation errors. This can be explained by the incorrectly reported multi-point received

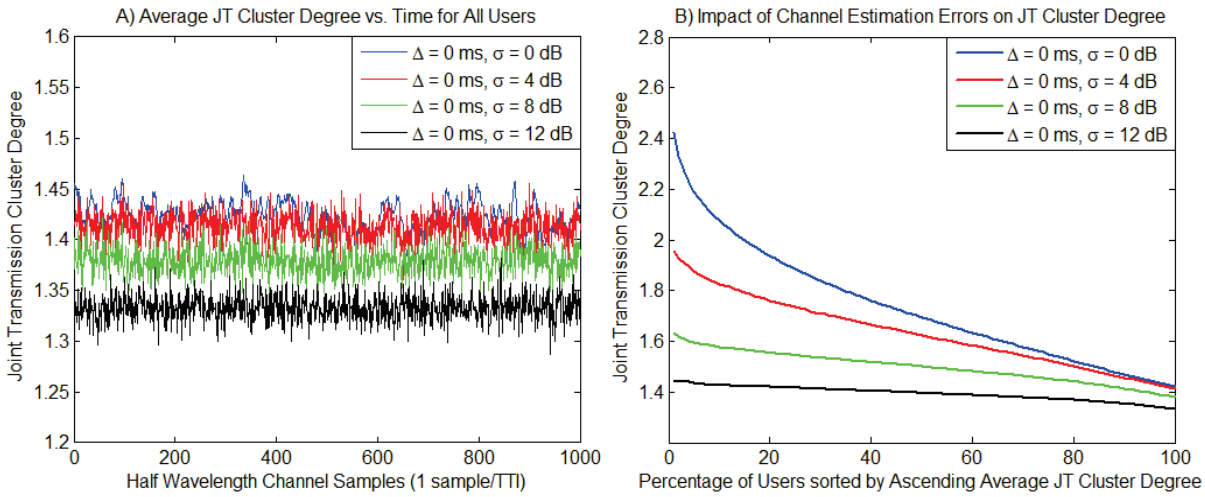

Figure 4.3: Joint transmission cluster degree changes due to channel estimation errors in fading channels.

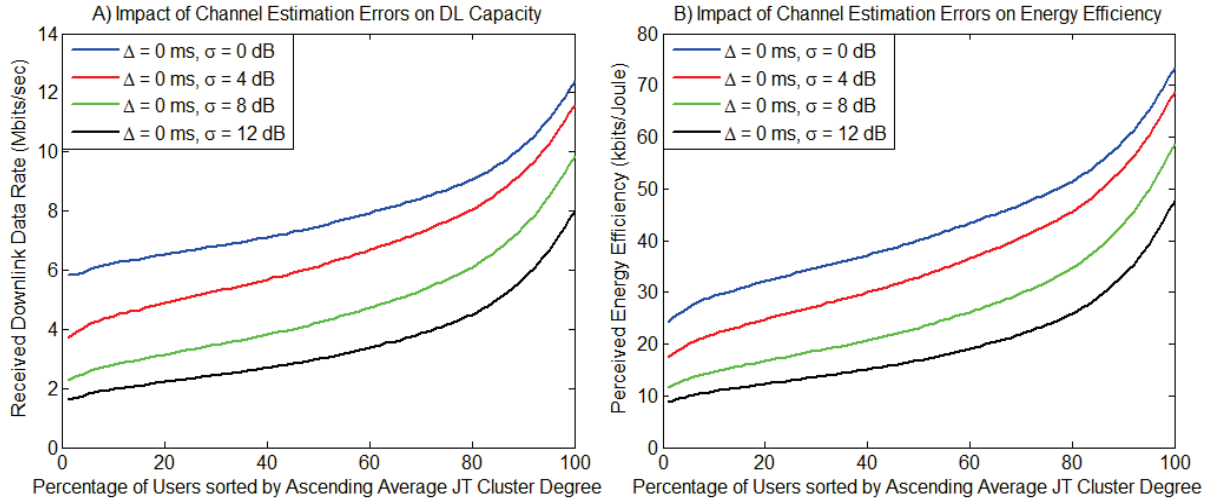

Figure 4.4: Downlink capacity and energy efficiency performance of CoMP schemes subject to channel estimation errors.

power measurements not being able to meet the ∇_{NW-JT} clustering threshold constraint in (4.20) as well as the perfectly performed measurements, $P_{err}(0\text{ dB}, 0\text{ dB})$. User locations i are sorted according to the clustering degrees that were supposed to be used in cases of ideal multi-point CSI feedbacks and plotted against the energy efficiency and downlink capacity metrics. The user locations i that correspond to the top p percent of the highest clustering degrees in ideal clustering conditions, $\Delta = 0\text{ ms}, P_{err}(0\text{ dB}, 0\text{ dB})$, are denoted by $i_{N_c,p\%}$. It can be seen from Figure 4.3b that the top 1% of the users that were supposed to have the highest clustering degrees in ideal feedback conditions, $i_{N_c,1\%}$, suffers from majorly decreased clustering degrees as opposed to the less CoMP dependent users. It should be noted that the clustering degrees partially represent the accuracy of the clustering decisions, since the clustering degrees may remain constant but the chosen members of the set N_{JT}

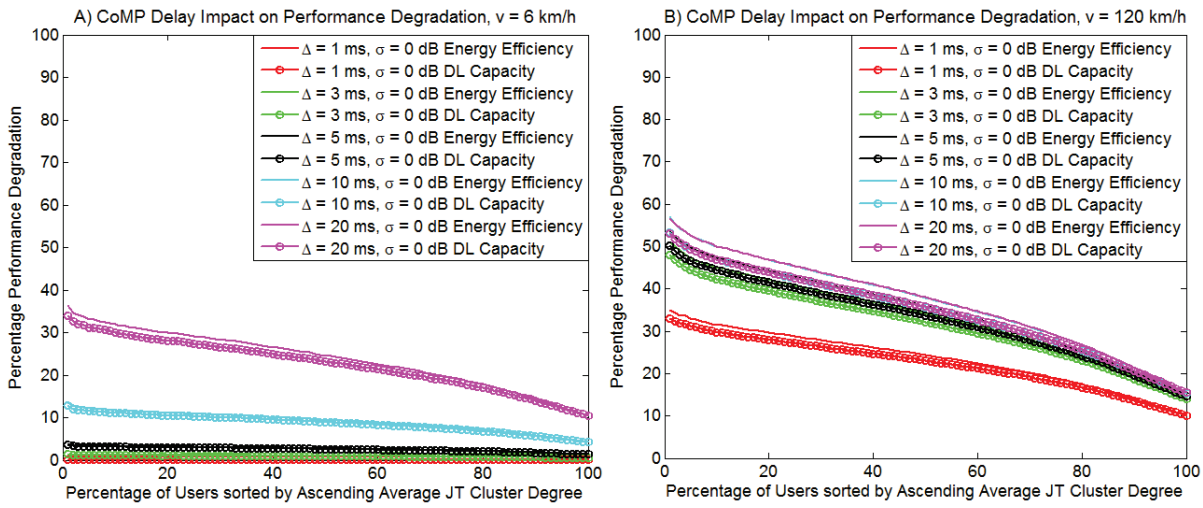

Figure 4.5: Performance degradation of CoMP schemes subject to system delays under various mobility scenarios.

may vary due to estimation errors. Downlink capacity losses up to 3.9 Mbits/sec and access network energy efficiency degradation up to 16.2 kbits/Joule are observed because of $P_{err}(0\text{ dB}, 12\text{ dB})$, when focused on user locations that were supposed to have the highest clustering degrees. It can be understood from the Fig. 4.4 that the impacts of passing incorrect CSI feedback to the CoMP serving eNB due to channel estimation errors become more severe for cell edge users that were supposed to receive PDSCH user plane data from joint transmission clusters with high degrees.

4.3.2 Impact of CoMP System Delay

Unlike the channel estimation errors, which are due to the noise of the channel and the scarce structure of CSI-RS to be used for multi-point measurements; system delays are due to the procedures involved during the feedback reporting shown in Figure 2.14. Decentralized feedbacks that extend the time to consolidate the CSI reports at the serving eNB due to X2 latency, feedback intervals chosen by the UEs, and the time it takes the serving eNB to process all the feedbacks to form the joint transmission cluster are some of the reasons for the outdated multi-point CSI to be used during the CoMP clustering decisions.

CoMP field trial results performed by EASY-C project reported that X2 latency of 0.5 ms, CSI feedback intervals of 10 ms and precoding delays of 20 ms were observed [38]. It was also mentioned during CoMP standardization process in 3GPP 36.819 that serving eNB processing delays of 4 ms are expected during operation [37]. Sole impacts of system delays, which cause outdated multi-point CSI feedback at the serving eNB, on overall energy efficiency and downlink capacity are evaluated both for high and low mobility scenarios

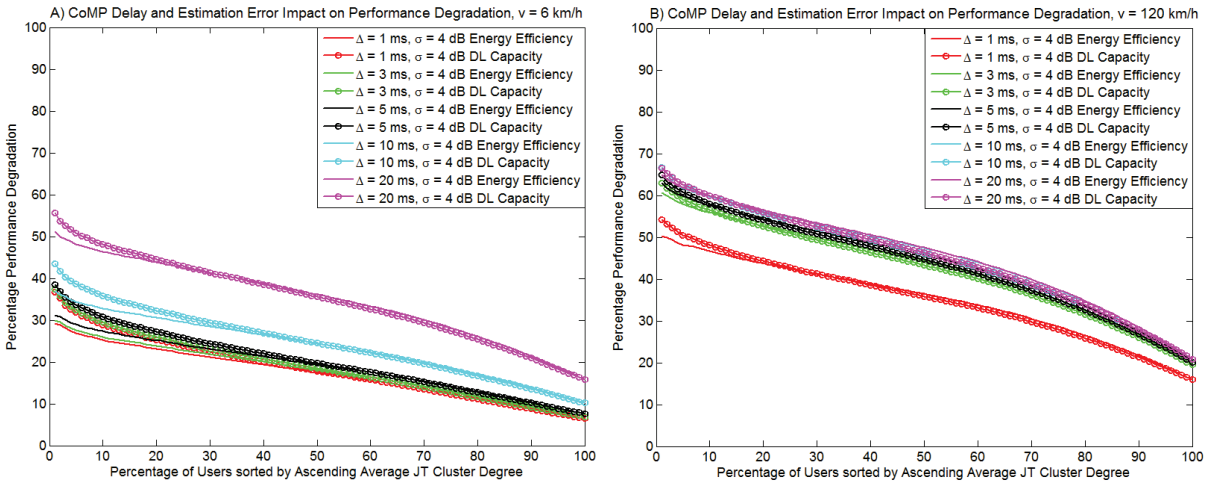

Figure 4.6: Performance degradation of CoMP schemes subject to both system delays and multi-point channel estimation errors under various mobility scenarios.

according to 120 km/h vehicular and 6 km/h pedestrian receiver velocities, respectively. Multi-point CSI aggregation and processing delays of $\Delta = [1\text{ ms}, 3\text{ ms}, 5\text{ ms}, 10\text{ ms}, 20\text{ ms}]$ are simulated assuming perfectly performed multi-point channel estimation procedures, $P_{err}(0\text{ dB}, 12\text{ dB})$, as shown in Figure 4.5. Users in low mobility conditions that were supposed to have the highest 1% of CoMP set degrees in ideal radio conditions, $P_{err}(0\text{ dB}, 0\text{ dB})$ and $\Delta = 0$ ms, face 32% system energy efficiency and 34% downlink capacity degradation when subject to 20 ms CSI feedback processing delays, whereas users in high mobility conditions suffer 35% $\overline{EE}$ and 37% $\bar{C}$ degradation even under 1 ms overall system delay. This is due to the steep decreasing slope of CIR auto-correlation function in high Doppler scenarios that reduce the coherence time of the channel causing inaccurate CoMP joint transmission clustering even under small system delays. Therefore, users in low mobility conditions start facing performance degradations after Δ = 10 ms, when the channel samples become less correlated. It is shown that the same CoMP system delay may have different impacts on users with different mobility conditions, since delays which are not high relative to the coherence time of the channel do not create major performance degradations as shown in Figure 4.5a for $\Delta = [1\text{ ms}, 3\text{ ms}, 5\text{ ms}]$. It should be noted that the influence of system delays on CoMP performance metrics are as vital as the channel estimation errors. Even if the UEs, which are in high mobility conditions $v = 120$ km/h, perform perfect multi-point channel estimation, overall system can still suffer from 55% $\bar{C}$ and 58% $\overline{EE}$ degradation due to Δ = 20 ms CoMP access network delays. Similar to the results from Section 4.3.1, users that are supposed to have higher clustering degrees get impacted more severely when the system is subject to access network delays during clustering decisions.

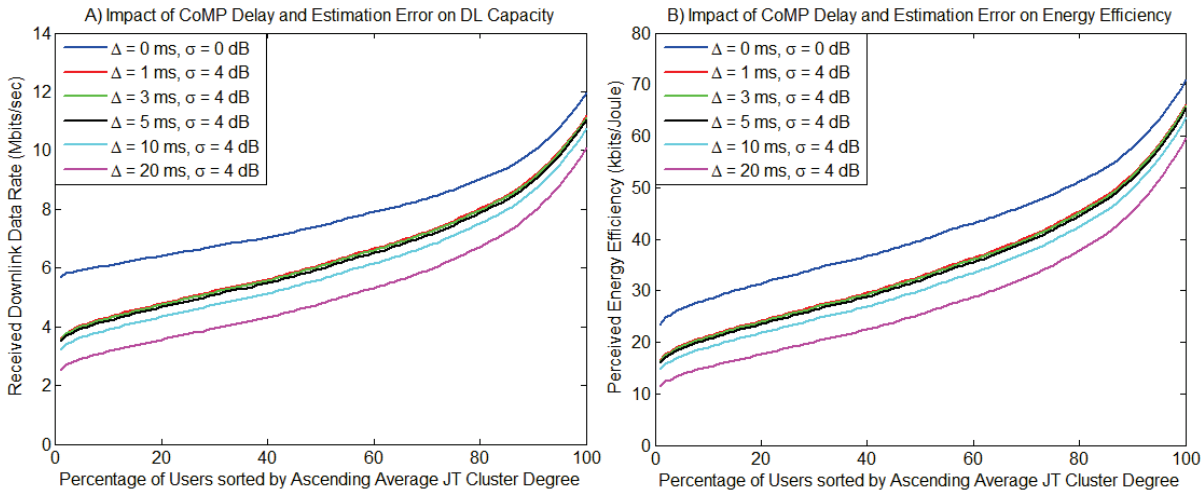

Figure 4.7: Downlink capacity and energy efficiency performance of CoMP schemes subject to both system delays and multi-point channel estimation errors under low mobility conditions, $v = 6$ km/h.

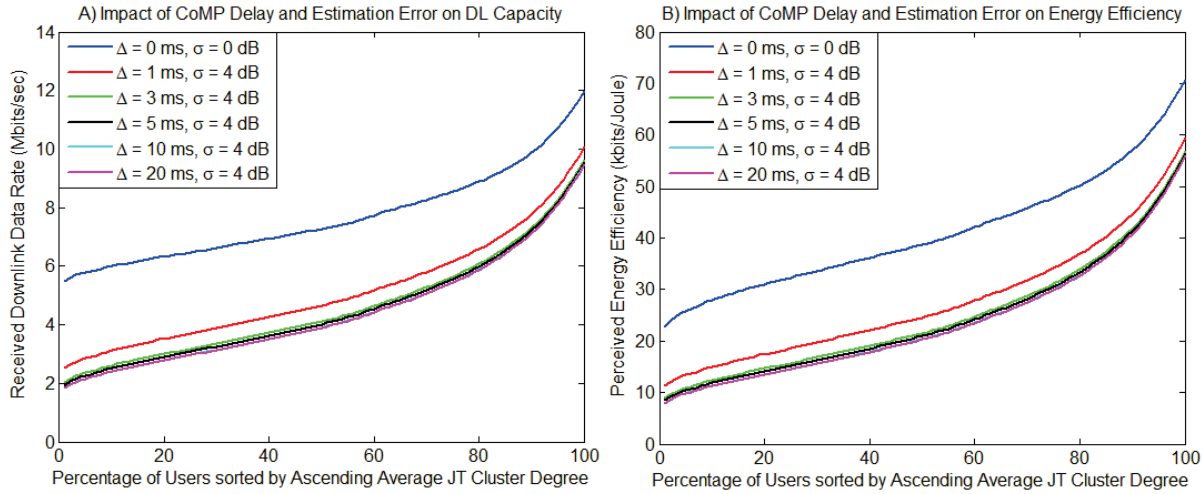

Figure 4.8: Downlink capacity and energy efficiency performance of CoMP schemes subject to both system delays and multi-point channel estimation errors under high mobility conditions, $v = 120$ km/h.

4.3.3 Joint Impact of Channel Estimation Errors and Delays

Realistic performance degradations of CoMP schemes with inaccurate clustering are revealed when estimation errors and systems delays are jointly considered according to (4.19) as shown in Figures 4.6, 4.7 and 4.8. $\overline{EE}$ and $\bar{C}$ degradations can reach up to 51% and 57% for low mobility users and 64% and 66% for high mobility users, respectively, for $P_{err}(0\text{ dB}, 4\text{ dB})$ and $\Delta = 20$ ms. The users having higher CoMP set degrees in ideal clustering conditions are more sensitive to delays and estimation errors and face major performance degradation due to inaccurate clustering. For instance, average energy efficiency and capacity degradation, considering all

the users in high mobility conditions $i_{N_c,100\%}$ for $P_{err}(0\text{ dB}, 4\text{ dB})$ and $\Delta = 20$ ms, reached around 9.2 kbits/Joule and 0.9 Mbits/sec; whereas for the user locations $i \in i_{N_c,1\%}$ access network energy efficiency degraded 14 kbits/Joule and downlink capacity performance decreased 3.8 Mbits/sec, as shown in Figure 4.7 and 4.8. It can be observed from Figure 4.6 that the main contributor to the performance degradation in low mobility conditions is the channel estimation errors, whereas system delay is the main performance determining factor in high mobility scenarios. It should be noted that the impacts of imperfect clustering on $\overline{EE}$ and $\bar{C}$ metrics slightly vary. This can be explained by the energy efficiency metric shown in (3.12) being dependent to the power consumption of the network which is solely a function of the CoMP cluster degree $N_c(i,t)$ rather than the clustering set member choices; whereas, capacity metric is dependent on both the number of the CoMP joint transmission points along with the choice of the points for N_{JT} as shown in (3.13).

4.4 Summary

Individual and joint effects of channel estimation errors and system delays on a DL CoMP system that is integrated to a cell switch off model are investigated by simulating a time-varying fading channel under various mobility scenarios. It is demonstrated that the accuracy of the joint transmission set clustering is a key performance determining factor both for the user perceived quality of service in terms of downlink capacity and the overall access network energy efficiency of CoMP supporting networks. Performance degradation due to CoMP systems delays is dependent on the coherence time of the channel, and it is shown that high mobility scenarios yield major joint transmission clustering inaccuracy due to high Doppler effect even under minimal system delays. Outdated CSI feedback reports do not decrease the CoMP performance in low mobility conditions as significantly as the high mobility conditions, since the channel samples that are used by serving eNB for clustering decisions are still correlated to the actual UE reported channel feedback due to the high coherence time. Realistic performance analysis for CoMP schemes is done by jointly considering the effects of channel estimation errors and system delays. It is observed that the users with higher CoMP cluster degrees are more sensitive to CSI delays and estimation errors yielding major performance degradations for access network energy efficiency and downlink capacity performance.

Chapter 5

Multi-Point Statistical Channel Estimation and Prediction Schemes

5.1 Stochastic Characteristics of CIR and CTF

Channel impulse response $h_{n,i}(t,\tau_l)$ formulated in (4.1) is a two dimensional complex stochastic process since various selections of the random variables A_l, f_{d_l}, $\emptyset_l$, and τ_l yield different realizations and an indexed family of random variables. The difference from regular stochastic processes lies within the fact that $h_{n,i}(t,\tau_l)$ is a random process in two different domains: time domain, *t*, and delay domain, τ. As a result, the first and second order stochastic characteristics of the random process should be modeled considering the different index domains to estimate and predict the amplitude and phase of the CIR and CTF to perform accurate coherent detection.

Auto-correlation function of the complex baseband channel impulse response, $R_h(t_1,t_2,\tau_1,\tau_2)$, with respect to both delay tap and time domains is expressed as

$$R_h(t_1,t_2,\tau_1,\tau_2) = E(h(t_1,\tau_1) * h^*(t_2,\tau_2)). \tag{5.1}$$

Wide sense stationary channel explained in [60] and [29] assumes that contributions from different multipath delay taps are assumed to be uncorrelated and the autocorrelation in time varying channel due to Doppler shift is assumed to be only dependent on the time difference of the between the instants of the CIR realizations. This assumption is consistent with the time-varying nature of the channel. As the difference between the CIR instants increase beyond coherence time, the instances become less correlated since the auto-correlation of any wide-sense stationary stochastic process is a decreasing function of as mentioned in [61]. Hence, (5.1) can be re-written as

$$R_h(t_1,t_2,\tau_1,\tau_2) = E\big(h(t_2+\Delta t\,,\tau_1)h^*(t_2,\tau_2)\big)\delta(\tau_1-\tau_2). \tag{5.2}$$

Similarly, autocorrelation function of the time-varying CTF, which is the Fourier Transform of the autocorrelation function of the CIR in delay domain, can be found as

$$R_H(\Delta t,\Delta f) = \int_0^\infty R_h(\Delta t,\Delta\tau)e^{-j2\pi f\tau}d\tau, \tag{5.3}$$

$$R_H(t_1,t_2,f_1,f_2) = E\big(H(t_2+\Delta t\,,f_2+\Delta f)H^*(t_2,f_2)\big). \tag{5.4}$$

Relation mentioned in (5.3) is due to the fact that the time varying CTF, $H(t,f)$, is the Fourier transform of the CIR with respect to the delay domain. As mentioned in Section 2.2.4, CSI-RS are only transmitted on specific resource elements. Thus, multi-point channel estimation is needed in order to obtain the channel impulse response of remaining resource elements by using an interpolation filter that makes use of the autocorrelation function of the channel. Considering a MIMO transmission, auto-correlation function is three dimensional: spatial correlation due to multiple transmitter antennas, time correlation due to Doppler spread and delay correlation due to multipath propagation. Spatial domain is assumed to be independent of the remaining two domains, and the delay versus time domains are separated to form single dimensional estimation/interpolation filters to track the time dispersive and varying characteristics of the channel separately.

5.1.1 Time Dispersive Characteristics

To estimate the CTF over a single OFDM symbol or a particular channel sample, the multipath characteristics of the channel need to be taken into consideration, which can be determined by the autocorrelation of the complex channel process with respect to the delay domain assuming no time domain difference between the instances. Auto-correlation of the CIR over a fixed time sample is expressed as

$$R_h(\Delta t = 0, \Delta\tau_L) = E(\boldsymbol{h}(\tau)\boldsymbol{h}(\tau)^H) = \begin{bmatrix} E[h(\tau_1)h(\tau_1)^*] & \cdots & E[h(\tau_1)h(\tau_L)^*] \\ \vdots & \ddots & \vdots \\ E[h(\tau_L)h(\tau_1)^*] & \cdots & E[h(\tau_L)h(\tau_L)^*] \end{bmatrix}, \tag{5.5}$$

where $\boldsymbol{h}(\tau)$ is the vector of the complex CIR at a particular time sample and the length of the vector L is dependent on the multipath delay spread of the channel. Since the autocorrelation function $R_h(\Delta t = 0, \Delta\tau = 0)$ gives the average power of the process $E[|h(\tau_l)|^2] = E[|A_l|^2]$ at each delay tap, the diagonal components of the matrix shown in (5.5) define the Power Delay Profile (PDP) of the channel at a particular time instant. Different multipath delay taps are considered uncorrelated, which means the CIR auto-covariance between different delay tap instants is zero. Hence, the autocorrelation function of the CIR at a particular time instant would be a diagonal matrix assuming the CIR process has zero mean at different delay taps. Mean excess delay and the delay spread can be determined using this matrix according to (4.3) and (4.4). Auto-correlation of the CTF in frequency domain, which is the Fourier Transform of the PDP with respect to the delay domain according to (5.3), is needed to characterize the frequency domain behavior of the channel due to multipath delay spread. Auto-correlation function of the frequency varying CTF is expressed as

$$R_H(\Delta t = 0, \Delta f) = E\big(H(f + \Delta f)H^*(f)\big)\,, \tag{5.6}$$

and the coherence bandwidth of channel is found by

$$\Delta f_c \geq \frac{cos^{-1}[R_H(\Delta f) = c_f]}{2\pi\sigma_\tau}\,, \tag{5.7}$$

where c_f defines the CTF correlation value for a certain coherence bandwidth Δf_c as derived in [62], and $R_H(\Delta f)$ forms the power delay spectrum of the channel. This is in correspondence with the fact that the Fourier transform of the autocorrelation function represents the power spectral density of the random process. It is clear from (5.7) that the CTF correlation c_f decays with increasing spectral differences Δf. Received signals within Δf_c will be observing similar CTF conditions in terms of applied amplitude gain and phase differences. This is the underlying reason for the frequency selective channel feedback, since various resource blocks assigned to the UE may get impacted by different CTF samples due to the 15 kHz subcarrier spacing shown in Figure 2.11. Subcarrier spacing in LTE-A and beyond schemes is chosen to be greater than the coherence bandwidth of the channel such that the CTF is relatively constant within a certain resource element and the individual subcarriers observe frequency flat fading.

5.1.2 Time Varying Characteristics

To track the multi-point CIR over different time samples, time-varying characteristics of the channel are needed to be considered, which can be determined by the autocorrelation function of the complex CIR over different time instances of the realization over each particular multipath delay tap separately. Auto-correlation of the CIR at a particular delay tap τ_l with respect changing time instances is called the delay-cross power density by the authors of [29] and found by

$$R_h(\Delta \boldsymbol{t_M}, \tau_l) = \begin{bmatrix} E[h(t_1,\tau_l)h(t_1,\tau_l)^*] & \cdots & E[h(t_1,\tau_l)h(t_M,\tau_l)^*] \\ \vdots & \ddots & \vdots \\ E[h(t_M,\tau_l)h(t_1,\tau_l)^*] & \cdots & E[h(t_M,\tau_l)h(t_M,\tau_l)^*] \end{bmatrix}, \tag{5.8}$$

where M depends on the chosen time domain interpolating filter length. Each element of the time autocorrelation matrix shown in (5.8) can be represented as a function of the time difference between the instances:

$$R_h(\Delta t, \tau_l) = E[h(t + \Delta t, \tau_l)h(t, \tau_l)^*]\,. \tag{5.9}$$

Overall time correlation matrix for the CIR is formed by integrating delay-cross power density in (5.8) over all the existing multipath delay taps as

$$R_h(\Delta t) = \int_{l=1}^{L} R_h(\Delta t, \tau_l)\, d\tau_l, \tag{5.10}$$

and the coherence time of the channel is found by

$$\Delta t_c \geq \frac{cos^{-1}[R_h(\Delta t) = c_t]}{2\pi f_{d_{max}}}, \tag{5.11}$$

where c_t defines the CIR correlation value for a certain coherence time Δt_c as derived in [62]. It should be noted that the coherence time of the CIR at a particular delay tap can be found by using (5.9) in (5.11). Coherence time quantifies the similarity channel impulse response samples in a time varying fashion. The received signals within the coherence time of a channel are highly likely to have similar amplitude correlations. When composing the CIR auto-correlation matrix in delay domain as shown in (5.5), UE can chose to include all the existing *L* delay taps, however the size of the time correlation matrix *M* can be updated dynamically according to the channel conditions.

The rate of change of the complex baseband CIR over time is limited by $R_h(\Delta t)$ as derived by the Markov inequality as

$$Prob\big(\big|h(t_i, \tau_0) - h\big(t_j, \tau_0\big)\big| > \varepsilon\big) \leq 2(R_h(|\Delta t = 0, \Delta\tau = 0|) - R_h\big(|t_i - t_j, \Delta\tau = 0|\big))/\varepsilon^2. \tag{5.12}$$

Thus, multi-point feedback with greater system delay or high Doppler scenarios will degrade the accuracy of the joint PDSCH transmission clustering significantly due to the decreasing nature of $R_h(\Delta t, \tau_l)$ that has a peak at $R_h(0, \tau_l)$, as demonstrated previously in Chapter 4. Similar to the delay domain procedure, Fourier transform of the delay-cross power density shown in (5.8) with respect to the time domain yields the scattering function at a particular delay tap and the Fourier transform of the time correlation function shown in (5.10) yields the overall Doppler spectrum which is the power spectral density of the stochastic process derived as

$$S(f, \tau_l) = \int_{\Delta t=0}^{\infty} R_h(\Delta t, \tau_l) e^{-j2\pi f \Delta t} d\,\Delta t, \tag{5.13}$$

and

$$S(f) = \int_{l=1}^{L} S(f, \tau_l) d\,\tau_l, \tag{5.14}$$

respectively. It should be noted that the CIR autocorrelation function at each particular delay tap can be used to accurately track the variations of each delay tap independently using (5.8). However, the implementation

complexity of such schemes is high due to the need to store separate autocorrelation functions and CIR samples for each tap. To reduce the computation complexity, UEs can choose to track the changes in the overall superimposed CIR shown in (4.16) by using the time correlation function from (5.10), instead of keeping track of the channel behavior at each multipath component individually.

5.2 Channel Estimation Techniques

5.2.1 Frequency Domain Estimation

CSI-RS mapping shown in Figure 2.15 indicates that the reference symbols that are used for channel estimation are not transmitted on every subcarrier. Motivation behind the frequency domain channel estimation is to exploit the CTF estimates calculated over the REs containing RSs and predict the CTF estimates at REs which do not contain any RS. CTF estimates over the subcarriers containing reference symbols for a single OFDM symbol or a particular TTI are expressed as

$$\widetilde{H}_{R\mathrm{x}1} = F_{R\mathrm{x}L} h_{L\mathrm{x}1} + H_{noise} \ , \tag{5.15}$$

where H_{noise} is the CTF estimation error due to the noisy transmission formulized in (2.25), $F_{R\mathrm{x}L}$ is the *RxL* portion of the *NxN* DFT matrix $F_{N\mathrm{x}N}$ that is used by the UE receiver to find the received signal in the frequency domain over all the allocated orthogonal subcarriers. It should be noted that $F_{N\mathrm{x}N}$ DFT matrix formulized in (2.25) is used to convert the OFDM symbol in time domain, which has *N* samples excluding the CP, to frequency domain correspondence over *N* subcarriers, $F_{R\mathrm{x}L}$ matrix represents the DFT matrix for the *R* rows containing the RSs, and *L* is the multipath delay tap length. Interpolation filter $A_{N\mathrm{x}R}$ that is used to estimate/predict the CTF at REs that carry user plane data can be found as

$$A_{N\mathrm{x}R} = F(S^H S + R)^{-1} S^H, \tag{5.16}$$

where the filter is configured according to the parameters shown in Table 5.1 depending on the chosen method for interpolation [29]. CTF estimates spanning all the *N* REs in frequency domain at a particular OFDM symbol is then found as

$$\widetilde{H}_{N\mathrm{x}1} = A_{N\mathrm{x}R} \widetilde{H}_{R\mathrm{x}1} \ , \tag{5.17}$$

$$\widetilde{H}_{N\mathrm{x}1} = F(S^H S + R)^{-1} S^H \widetilde{H}_{R\mathrm{x}1}. \tag{5.18}$$

Table 5.1: Time-invariant CTF interpolation filter coefficients for various estimation methods shown in [29]

Interpolation Method	F	S	R
IFFT	$\frac{1}{L}F_{N\text{x}\mathrm{L}}{F_{R\text{x}\mathrm{L}}}^{H}$	I_{RxR}	O_{LxL}
Least Squares	$F_{N\text{x}\mathrm{L}}$	$F_{R\text{x}\mathrm{L}}$	O_{LxL}
Regularized Least Squares	$F_{N\text{x}\mathrm{L}}$	$F_{R\text{x}\mathrm{L}}$	αI_{LxL}
MMSE	$F_{N\text{x}\mathrm{L}}$	$F_{R\text{x}\mathrm{L}}$	$\sigma^2_{Hnoise}(R_h(\Delta t = 0))^{-1}$
Mismatched MMSE	$F_{N\text{x}\mathrm{L}}$	$F_{R\text{x}\mathrm{L}}$	$\sigma^2_{Hnoise}/\sigma^2_h I_{LxL}$

Depending on the number of resource blocks scheduled for the UE at a particular TTI, number of REs that contain RSs can vary and (5.17) will adapt accordingly. It is clear from (5.18) that as the number of subcarriers containing RSs increases, the accuracy to estimate the CTF at the remaining $N - R$ subcarriers improves. Interpolation can be performed with both statistical and deterministic approaches, where the statistical approach yields better performance that comes along with a computation complexity trade-off. Unlike the deterministic CTF interpolation filters like IFFT, Least Squares and Regularized Least Squares methods which just need the DFT matrices $F_{N\text{x}\mathrm{L}}$ and $F_{R\text{x}\mathrm{L}}$, statistical CTF estimation heavily depends on the time dispersive stochastic characteristics of the channel as explained in Section 5.1.1. CIR autocorrelation function in delay domain $R_h(\Delta t = 0, \Delta\tau)$, CTF autocorrelation function in frequency domain $R_H(\Delta t = 0, \Delta f)$, variance of the CTF estimation error σ^2_{Hnoise}, and the variance of the complex CIR process in delay domain given by

$$\sigma^2_h = E(h(\tau + \Delta\tau)h(\tau)^H) - \mathrm{E}(h(\tau + \Delta\tau))E(h(\tau))^H \tag{5.19}$$

are utilized during statistical CTF interpolation methods like regular and mismatched MMSE. Although time-invariant frequency domain estimation methods mainly focus on CTF interpolation, CIR estimate at a particular time sample can be obtained using the same aforementioned methods by modifying (5.18) as

$$\tilde{h}_{L\text{x}1} = (S^H S + R)^{-1} S^H \tilde{H}_{R\text{x}1}, \tag{5.20}$$

where $\tilde{h}_{L\text{x}1}$ is the CIR estimate over L taps. This can be viewed as a time domain interpolation method used jointly with frequency domain estimation. CIR estimates obtained in (5.20) and the CTF estimates from (5.18) can then be utilized by the time-varying estimation methods to track the impacts of changing Doppler effect in the channel as mentioned in [63].

5.2.2 Time Domain Channel Estimation and Prediction

Due to the scarce structure of CSI-RS used for each CoMP measurement member's channel estimation, time-varying channel estimation and interpolation is very crucial for performance of Release 11 coordinated LTE-A systems. Each measured link should be estimated independently to correct the reported UE channel feedback and avoid inaccurate joint transmission clustering. Time invariant CTF and CIR estimates obtained by frequency domain estimation methods demonstrated in the previous section have to be complemented by time domain channel estimation and prediction methods to adapt UEs multi-point CSI feedback according to the time-varying characteristics of the channel. Two dimensional CIR and CTF estimation methods are needed to track both multipath and Doppler characteristics of the transmission.

One option is to first track the time varying CTF coefficients over OFDM symbols containing RSs and interpolating the CTF in time domain to obtain the CTF estimates for resource elements not containing reference symbols. Autocorrelation function of the CTF in temporal domain is needed to track the time-varying nature of the CTF. CTF autocorrelation function for a fixed subcarrier f_n in time domain is obtained by taking the Fourier transform of the CIR autocorrelation function from (5.9) as

$$R_H(\Delta t, f_n) = E[H(t+\Delta t, f_n)H(t, f_n)^*]\,. \tag{5.21}$$

The time domain CTF interpolation is done separately over different fixed subcarriers containing RSs using (5.21). These CTF estimates are then interpolated in frequency domain by utilizing the DFT matrices as shown in Section 5.2.1. Another option is to estimate the CIR on subcarriers with RS and then tracking the time-varying behavior of the CIR taps in time domain. Tracked CIR is then converted to CTF by FFT matrix to obtain CTF over all subcarriers. As a result, time-domain channel estimation can be done both for the CIR and CTF of the time-varying channel with possible interpolation in both domains.

CoMP supporting UEs perform time varying multi-point channel estimation, and the CIR at a particular delay tap l between the user i and CoMP measurement set member n $\in N_{JT}(i,t)$ at TTI t is estimated by using a weighted sum of the current observed channel sample at TTI t and previously estimated $M-1$ CIR samples as shown below:

$$\tilde{h}_{n,i}(t,\tau_l) = \sum_{m=0}^{M_{UE}-1} w(m)\hat{h}(t-m,\tau_l)\,, \tag{5.22}$$

where the weight coefficients *w(m)* are stored in a filter of length M_{UE}. A detailed representation of (22) for an auto-regressive minimum mean square error (MMSE) channel estimation is formulized as

$$\tilde{h}_{n,i}(t,\tau_l) = [(R_h(\Delta t,\tau_l) + \sigma^2_{noise} I_{MxM})^{-1} r_h(\Delta t,\tau_l)]^H \widehat{\boldsymbol{h}}_{t,\dots t-M+1;\tau_l}\,, \tag{5.23}$$

where the regularized time domain CIR autocorrelation function component, $R_h(\Delta t,\tau_l) + \sigma^2_{noise} I_{MxM}$, is formed using the variance of the channel estimation error for a particular tap of the CIR as

$$\begin{bmatrix} E[h(t,\tau_l)h(t,\tau_l)^*] + \sigma^2_{noise} & \cdots & E[h(t,\tau_l)h(t-M+1,\tau_l)^*] \\ \vdots & \ddots & \vdots \\ E[h(t-M+1,\tau_l)h(t,\tau_l)^*] & \cdots & E[h(t-M+1,\tau_l)h(t-M+1,\tau_l)^*] + \sigma^2_{noise} \end{bmatrix}. \tag{5.24}$$

Channel estimation filter of length M is formed by the product of the inversed regularized CIR autocorrelation function matrix for a particular delay tap τ_l shown in (5.24) and the autocorrelation vector between the most recent channel sample $h(t,\tau_l)$ and M previously estimated channel samples given by

$$r_h(\Delta t,\tau_l) = \begin{bmatrix} E[h(t,\tau_l)h(t,\tau_l)^*] \\ \vdots \\ E[h(t-M+1,\tau_l)h(t,\tau_l)^*] \end{bmatrix}. \tag{5.25}$$

The contents of the multipoint channel estimation filter of length M are used to take a weighted sum of the M most recent CIR realizations after RS decorrelation,

$$\widehat{\boldsymbol{h}}_{t_{n,\dots,n-M+1};\tau_l} = \begin{bmatrix} \hat{h}(t,\tau_l) \\ \vdots \\ \hat{h}(t-M+1,\tau_l) \end{bmatrix}, \tag{5.26}$$

to smoothen the CIR estimate at time t and delay tap l. Autoregressive coefficients of the multi-point channel estimation filter shown in (5.22) are formed using the MMSE criterion, where the more recent measured channel estimates are given higher weights as

$$w(j) > w(k) \qquad \forall\, j < k\,, \tag{5.27}$$

due to the decreasing nature of the CIR autocorrelation function in time domain as proven by (5.12) and explained in [64].

An alternative multi-point channel estimation method can be utilized by tracking the superimposed time-varying CIR coefficients instead of CIR realizations at each delay tap. Although this approach is be less accurate compared to tracking every multipath component, multi-point channel estimation complexity for the UE will be decreased significantly. Superimposed CIR estimate at TTI t is found by

$$\tilde{h}_{n,i}(t) = [(R_h(\Delta t) + \sigma^2_{noise} I_{MxM})^{-1} r_h(\Delta t)]^H \widehat{\boldsymbol{h}}_{t,\dots t-M+1} \tag{5.28}$$

where the used CIR samples that are used as inputs to the estimation filter are expressed as

$$\widehat{\boldsymbol{h}}_{t_{n,..,n-M+1}} = \begin{bmatrix} \hat{h}(t) = \sum_{l=1}^{L} \hat{h}(t,\tau_l) \\ \vdots \\ \hat{h}(t-M+1) = \sum_{l=1}^{L} \hat{h}(t-M+1,\tau_l) \end{bmatrix}. \tag{5.29}$$

Filter coefficients in (5.28) are formed using the superimposed CIR samples from (4.16) and the time auto-correlation function from (5.10) instead of the delay-cross power densities. Performance comparison of both the schemes shown in (5.23) and (5.28) is shown in Section 5.3.

Multi-point channel estimation procedures performed by the UE are enough to tackle the channel estimation errors; however CoMP system delays still create performance degradations as shown in Section 4.3.2. As a result, serving e-NB should perform channel prediction procedures using the CIR estimates reported by the UE to predict how the multi-point CIRs will change at the time of the joint PDSCH transmission. Multi-point channel prediction is performed by

$$\breve{h}_{n,i}(t+p) = \sum_{\substack{m=1 \\ p>1}}^{p-1} \breve{h}_{n,i}(t+p-m)w(m) \; + \; \sum_{m=p}^{M_{NW}} \tilde{h}_{n,i}(t+p-m)w(m) \quad | \quad p \in [1,\dots,P] \tag{5.30}$$

where $\breve{h}_{n,i}$ and $\tilde{h}_{n,i}$ represent the predicted CIR samples by the serving eNB and the estimated CIR samples by the UE, respectively, and $p \in [1,\dots,P]$ represents the prediction range in terms of number of TTIs. The prediction filter length used by the serving eNB is denoted by M_{NW} and the channel estimation filter length used by the UEs is denoted by M_{UE} to avoid confusions. It is assumed that the CIR prediction filter length is greater than the prediction range, $M_{NW} > P$, to track the time-varying behavior of the channel accurately. Serving eNB performs the prediction at P steps using (5.30) by updating the filter inputs, predicted CIR autocorrelation matrix and filter coefficients at every step. Currently predicted CIR sample replaces the most outdated CIR sample for the filter input at every step p. Prediction filter coefficients are generated similar to the estimation filters shown in (5.24), however the regularized CIR autocorrelation component is altered as

$$\begin{bmatrix} E[h(t,\tau_l)h(t,\tau_l)^*] + \varepsilon & \cdots & E[h(t,\tau_l)h(t-M+1,\tau_l)^*] \\ \vdots & \ddots & \vdots \\ E[h(t-M+1,\tau_l)h(t,\tau_l)^*] & \cdots & E[h(t-M+1,\tau_l)h(t-M+1,\tau_l)^*] + \varepsilon \end{bmatrix} \tag{5.31}$$

to replace the CIR estimation errors that were used for regularization by epsilon. Diagonals of the CIR autocorrelation matrix are summed with the epsilon to make sure the matrix is invertible, and since the CIR samples used by the serving eNB are already estimated by the UEs using (5.24), regularization for the prediction filter should not again utilize the variance of the channel estimation errors. It should be noted that both the channel estimation and the prediction filters, along with the CIR samples used as inputs, are time-varying in order to adapt to the small scale fading conditions of the channel.

5.3 CoMP Performance Gains due to Channel Estimation and Prediction

Multi-point auto-regressive MMSE filter is implemented to track and estimate the channel gains at each delay tap l for every CoMP measurement set member $n \in N_{meas}$ as formulated in (5.23). Multi-point channel estimation error for each delay tap l of every radio link is modeled independently as a complex circular additive Gaussian noise as

$$\hat{h}_{n,i}(t,\tau_l) = h_{n,i}(t,\tau_l) + h_{err}(\mu,\sigma), \tag{5.32}$$

where the estimation error is modeled as having 0 mean and 0.12 standard deviation both for the real and imaginary components of the complex CIR. Received power estimation error of $P_{err}(0\text{ dB}, 6\text{ dB})$ is obtained by plugging the complex circular Gaussian estimation error, $h_{err}(\mu = 0, \sigma = 0.12)$, into (4.17). Multi-point channel estimation filter length, M_{UE}, should be chosen with great attention as unnecessarily long estimation filters increases the complexity of the estimator and since the $R_h(\Delta t, \tau_l)$ decreases with increased time differences, enlarging the filter length increase does not bring much advantage to the estimator. Therefore, single point channel estimators determine the filter memory spans according to the receiver velocity and the coherence time of the channel. Multi-point tracking/estimation filters with memory spans, M_{UE}, of 6 and 30 TTIs are simulated with fixed lengths for each UE in the network regardless of the location and channel conditions. Average energy efficiency of the access network and the downlink capacity observed considering all the user locations, increased from 62 kbits/Joule to 70 kbits/Joule and from 10.2 Mbits/sec to 11.9 Mbits/sec, respectively, as the static filter lengths increased from $M_{UE} = 0$ to $M_{UE} = 30$. It is clear from Figure 5.1 that the multi-point channel estimation gains are more significant in terms of performance percentage improvements for users that are supposed to have higher CoMP joint transmission set degrees in ideal clustering conditions. Energy efficiency of the access network and the achieved downlink capacity considering the users $i \in i_{N_c,1\%}$

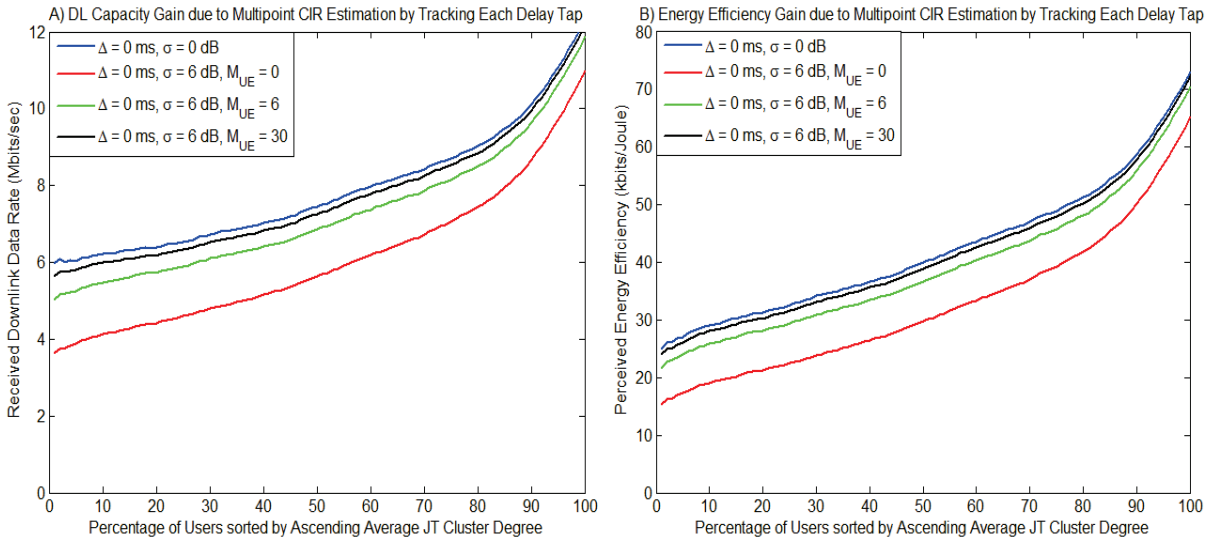

Figure 5.1: Downlink capacity and energy efficiency increases due to multi-point CIR estimation by tracking each delay tap, $\widetilde{\boldsymbol{h}}_{\boldsymbol{n,i}}(\boldsymbol{t},\boldsymbol{\tau_l})$, individually using the delay-cross power density functions formulated in (5.23).

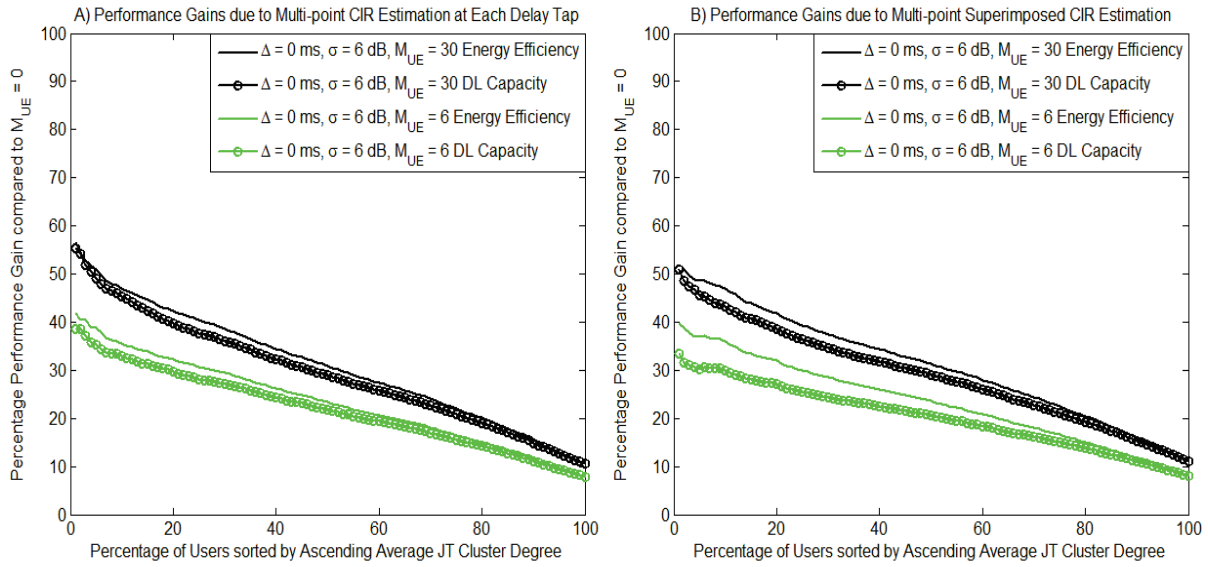

Figure 5.2: Comparison of multi-point channel estimation done by tracking CIR at each delay tap separately as shown in (5.23) versus tracking the superimposed CIR samples as shown in (5.28).

increased from 14.3 kbits/Joule to 25.1 kbits/Joule and from 3.82 Mbits/sec to 5.93 Mbits/sec, respectively, as the channel estimation filter lengths increased from $M_{UE} = 0$ to $M_{UE} = 30$. As a result, multi-point channel estimation filter lengths of LTE-A and beyond UEs should be chosen according to both the user velocity and the CoMP characteristics of the UEs, since increasing the memory span of the multi-point estimators yields major

performance improvements for users with higher joint transmission clustering sets compared to less CoMP dependent users.

UEs can perform CIR estimation either by tracking the time-varying behavior of each delay tap composing the CIR as simulated in Figure 5.1 or by just tracking the superimposed CIR samples to reduce the computation complexity as proposed in (5.28). Both schemes are simulated for low mobility conditions, $v = 6\ km/h$, where the serving eNB is assumed to form the JT clusters using the UE estimated multi-point CIR samples without any delay encountered as shown in Figure 5.2. Multi-point CIR estimation scheme that tracks each tap individually using $M_{UE} = 30$ yields energy efficiency and downlink capacity percentage performance improvements up to 56%; whereas multi-point superimposed CIR estimation scheme yields 51% improvement compared to CoMP schemes lacking any receiver memory span, $M_{UE} = 0$. At first, it may seem like tracking the CIR samples and the time-varying auto-correlation functions separately for each multipath component is a better performing scheme as opposed to schemes that just track the superimposed CIR using the overall time correlation functions. However, storing CIR at each delay tap for each CoMP measurement set member and forming individual auto-correlation functions for each multipath component places a huge computation complexity burden on the UE. As a result, UEs may choose to switch between the two schemes depending on the computation complexity versus CoMP clustering accuracy trade-off. It should also be noted that the increased computation complexity for CIR estimation may cause CSI feedback delays, which in fact decreases the clustering accuracy due to Doppler conditions.

Performance of comparison of CoMP systems under perfect clustering conditions having no estimation errors or systems delays, $P_{err}(\mu = 0\ \text{dB}, \sigma = 0\ \text{dB})$ and $\Delta = 0\ \text{ms}$; versus systems subject to inaccurate clustering conditions, $P_{err}(\mu = 0\ \text{dB}, \sigma = 6\ \text{dB})$ and $\Delta = 10\ \text{ms}$, which do not have any CIR estimation or prediction mechanisms, $M_{UE} = 0$ and $M_{NW} = 0$, are already performed in Chapter 4. Aforementioned simulation results demonstrated in Figure 5.1 and 5.2 assumed the system has no delays, and estimation error challenges are tackled by implementing multi-point CIR estimation filters. However, serving eNB channel prediction methods should be used jointly with UE multi-point channel estimation methods to tackle both the estimation error and system delay issues in CoMP schemes. Inaccurate CoMP transmission conditions are simulated with $\Delta = 10\ \text{ms}$ and $P_{err}(\mu = 0\ \text{dB}, \sigma = 6\ \text{dB})$, and the performance of schemes

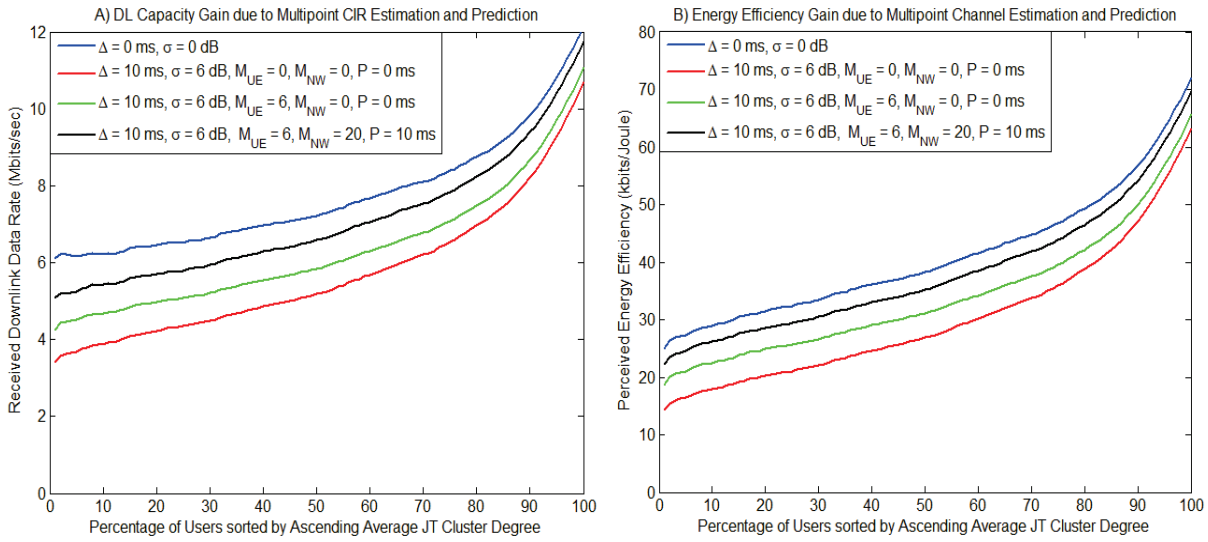

Figure 5.3: Downlink capacity and energy efficiency gains of the CoMP system due to UEs performing superimposed CIR estimation using (5.28) and serving eNB performing CIR prediction using (5.30).

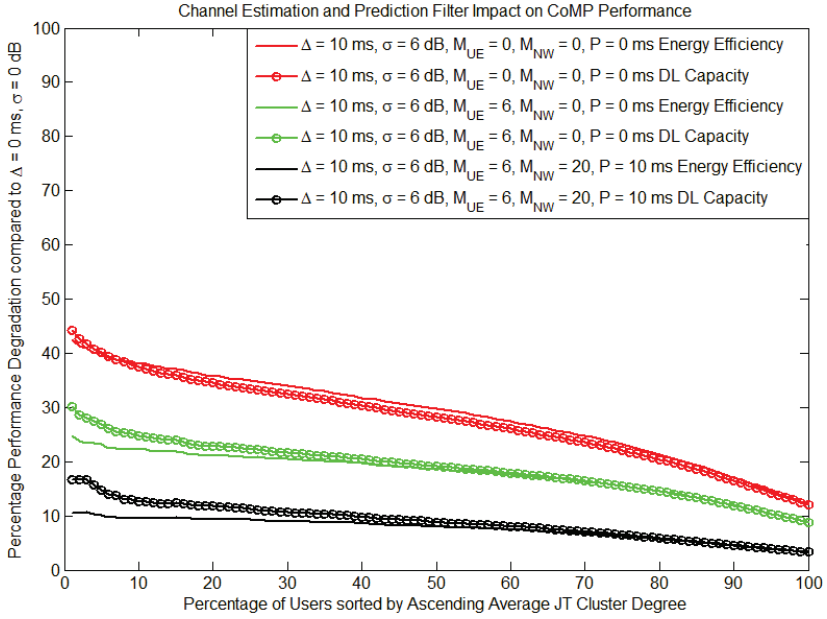

Figure 5.4: Performance improvement of the CoMP system by utilizing multi-point channel estimation and prediction schemes.

which only use multi-point channel estimation methods is compared to the schemes which use CIR estimation and prediction methods jointly. CIR prediction is performed using (5.30) and the simulation results are demonstrated in Figure 5.3 and 5.4. CoMP access network energy efficiency and downlink capacity percentage performance degradation of the schemes, which solely use multi-point channel estimation methods having

$M_{UE} = 6$ and $M_{NW} = 0$, reached around 25% and 31%, respectively, compared to the perfect clustering conditions. However, when the serving-eNB complemented the multi-point CIR estimation schemes by performing prediction using the estimated CIR samples using $M_{UE} = 6$, $M_{NW} = 20$, and $P = 10\,ms$, energy efficiency and downlink capacity percentage performance degradation reduced to 11% and 17%, respectively, compared to the ideal clustering conditions. It should be noted that the CIR prediction range P is set to the system delay observed in the channel to maximize the performance gains due to prediction. The ratio between the CIR prediction filter memory span and the prediction range, $\frac{M_{NW}}{P}$, can be fine-tuned to optimize the prediction accuracy. It can be concluded that the serving e-NB should adapt the prediction range P and the filter length M_{NW} according to the served UE's CoMP characteristics, since increased CIR prediction filter lengths while serving users with higher $N_C(i)$ aid the CoMP performance metrics more significantly as opposed to scenarios while serving users with lower clustering degrees.

5.4 CoMP Adaptive Channel Estimation Filter Design

Multi-point channel estimation filters at the UE should be designed according to the UE's CoMP parameters. None CoMP adaptive multi-point channel estimation filter length choices cause the below problems:

- Inaccurate multi-point CSI feedbacks result in exclusion of a potential joint transmission point from the CoMP cluster and decrease both the energy efficiency of the access network and the user perceived quality of service in terms of data rates.
- Inclusion of an incorrect point in the CoMP joint transmission cluster increases the downlink data rates slightly; however causes significant bits/Joule energy efficiency losses since the increased power consumption of the access network is not compensated by an equal amounts of downlink capacity gains for the served UEs.
- Chanel estimation filter length increases for less CoMP dependent UEs increase the computation complexity of the CIR estimation unnecessarily since JT clustering accuracy is not vital for UEs having lower N_C.values
- Using the same CIR estimation filter length for all the channels between the UE and the CoMP measurement set members increases the computation complexity unnecessarily for the points that are less likely to be included in the joint transmission set.

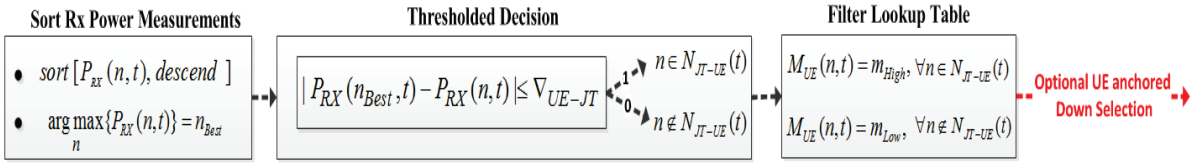

Figure 5.5: Instantaneous received power thresholding to predict the members of the joint transmission cluster and adapt the multi-point channel estimation filter lengths.

Unlike the currently existing channel estimation algorithms that adapt the memory span of the channel estimation filters according to the receiver velocity, coherence time, and noise of the channel; a new algorithm is proposed to adapt the memory span of the multi-point channel estimation filters according to both the current and previously observed time-varying CoMP characteristics of the UE.

5.4.1 User Driven Instantaneous Received Power Thresholding

Joint transmission clustering threshold is defined at the UE, $\nabla_{UE-JT} > \nabla_{NW-JT}$, to predict the members of the CoMP measurement set which will be chosen for PDSCH transmission. ∇_{UE-JT} is set to a higher value than ∇_{NW-JT} to account for channel estimation and measurement errors. After performing multi-point measurements for each member of the serving e-NB provided CoMP measurement set, UE *i* sorts the instantaneous received power values in descending order and chooses the best point in the measurement set for the current TTI *t*. UE, then performs a threshold-based decision according to ∇_{UE-JT} and forms a vector N_{JT-UE} with the predicted e-NBs that are highly likely to be included in the joint transmission set. According to the adaptive filter lookup table shown in Figure 5.5, filters with higher memory spans are chosen to estimate and smoothen the channel samples $\forall$ n $\in N_{JT-UE}$ while filters with shorter lengths are chosen $\forall$ n $\notin N_{JT-UE}$ not to increase the channel estimation computation complexity unnecessarily for points that are less likely to be included in N_{JT-NW} on the upcoming TTI. This is a straight forward method since the only parameters needed for computation are the instantaneous measured received powers for each n $\in N_{Meas}$, and the UE does not need to store the previously observed CoMP parameters. It should be noted that each network vendor or the carrier may have different joint transmission thresholds, ∇_{NW-JT}, and the user may approximate these thresholds by comparing the measured received powers for n $\in N_{Meas}$ with the chosen members of the joint transmission set after E-PDCCH or PDSCH decoding. As a result, UE utilized joint transmission clustering threshold $\nabla_{User-JT}$ is subject to change according to the clustering decision mechanism of the serving e-NB.

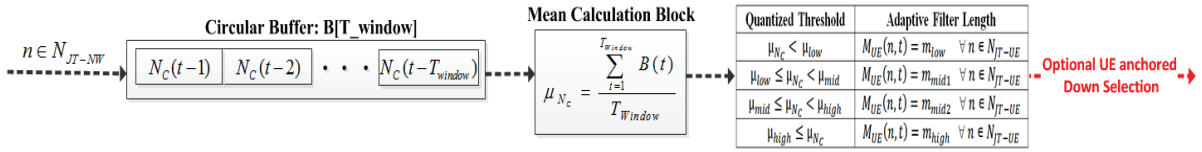

Figure 5.6: Tracking time-varying mean of the CoMP joint PDSCH transmission clustering degrees to adapt multi-point channel estimation filter lengths.

5.4.2 Moving Mean of Joint Transmission Cluster Degree

Single dimensional circular buffer, *B,* with size T_{window} is used to store the joint transmission clustering degrees, N_C, observed in the previous T_{window} TTIs. The contents of the circular buffer are passed to a mean calculation block, which finds the moving mean of the clustering degrees, μ_{N_C}, in the last T_{window} subframes. Quantized thresholding is then used to characterize the CoMP set degrees observed at the UE for PDSCH transmission and the channel estimation filters with larger memory spans are chosen for users that have higher μ_{N_C}. This method is consistent with the simulation results shown in Figure 5.2 proving that the users that have higher CoMP clustering degrees have better performance gains with larger channel estimation filter lengths. This method could be used jointly with the method mentioned in Section 5.4.1, since a user having a high μ_{N_C} should not increase the filter lengths for all the points in the measurement set. As a result, filter memory spans are increased for points that satisfy $n \in N_{JT-UE}$, for the users that have high mean of joint transmission clustering degrees observed in last T_{window} TTIs as demonstrated in Figure 5.6. Circular buffer and quantized threshold mechanisms help the user avoid sudden filter length changes in cases of fast fading scenarios with channel estimation errors, and create a robust environment for multi-point CIR estimation.

5.4.3 Independent Tracking of CoMP Measurement set points

Instead of tracking the mean CoMP clustering degrees as proposed by Section 5.4.2 or just using the instantaneous received power measurements for $n \in N_{meas}$ as proposed by Section 5.4.1, serving eNB joint transmission set clustering decisions can be tracked individually for each point. A time varying Boolean variable $x_n(t)$ is introduced, that will be set to 1 for the CoMP measurement set member $n \in N_{meas}$ which is also participating in joint PDSCH transmission on TTI *t,* and will be set to 0 if it is excluded from the joint transmission cluster formed by the serving e-NB, $n \notin N_{JT-NW}$. A time-varying two dimensional circular buffer, $B[N][T_{Window}]$, is used to store the values of $x_n(t)$ over T_{Window} TTIs for all the measured CoMP points. Contents of the circular buffer are sent to a summation block, which will sum the columns of *B* to find the total

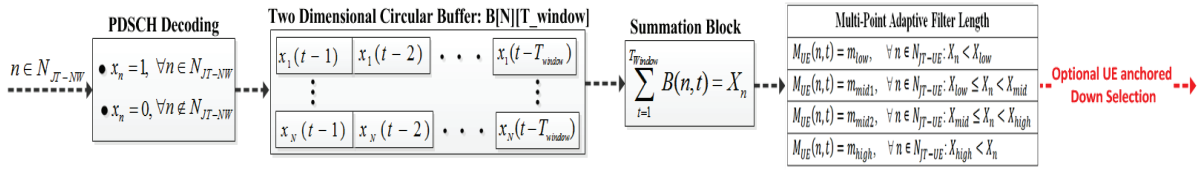

Figure 5.7: Independent tracking of time-varying CoMP Measurement set points to dynamically adapt the filter lengths separately for each $n \in N_{meas}$.

number of TTIs each point *n* has actively participated in joint PDSCH transmission over the last T_{Window} TTIs. Obtained values of X_n for each measured point are then sent to a multi-point adaptive filter length lookup table and the CIRs corresponding to the points that actively participated in joint PDSCH transmission in the recent TTIs will be estimated and predicted using filters with higher memory spans as shown in Figure 5.7. As a result, channel estimation filter lengths $M_{UE}(n,t)$ will be adapted separately for each point *n* in a time-varying fashion.

5.4.4 Adaptive Filter Lookup Table Formation

All the aforementioned CoMP adaptive channel estimation filter design techniques utilize an adaptive filter length look up table according to various inputs. Adaptive multi-point channel estimation filter lengths used by the UEs are set to $M_{UE} = [m_{low}, m_{mid}, m_{high}]$ depending on mean clustering degrees observed by the UE and the probability of each measured point n ∈ N_{meas} also being a member if the joint transmission set n ∈ N_{JT-NW}. It should be noted that the channel estimation filter lengths, M_{UE}, correspond to the number of stored CIR samples by the UE. Downlink RRC signaling provides the members of the CoMP measurement set as explained in Section 2.2.4. Each point may have different CSI-RS insertion density in the resource block pairs for multi-point channel estimation. Time –varying CSI-RS density of each e-NB in the CoMP measurement set is defined as the number of CSI reference symbols for each antenna port of each point per subframe as

$$d(n,t) = \frac{\#\ CSI-RS}{TTI}. \tag{5.33}$$

An example of a quantized mapping between the CIR autocorrelation value, corresponding coherence time, and the channel estimation filter length is shown in Table 5.2. Duration of the channel estimation filter can be obtained by using the auto-correlation between the first and the last members of the stored CIR values and modifying (5.11) as

$$\Delta t_c = t_1 - t_{M_{UE}} \geq \frac{\lambda cos^{-1}[R_h(\Delta t = t_1 - t_{M_{UE}}) = c_t]}{2\pi v}. \tag{5.34}$$

Table 5.2: Multi-Point adaptive estimation filter length lookup table using CIR autocorrelation values

CIR Auto-correlation	Coherence Time	Filter Length (Memory Span)
c_{high}	$\Delta t\_low_{c_{high}}$	m_{low}
c_{mid}	$\Delta t\_mid_{c_{mid}}$	m_{mid}
c_{low}	$\Delta t\_high_{c_{low}}$	m_{high}

For less CoMP dependent UEs that have smaller joint transmission clustering degrees, the CIR auto-correlation value between the first and the last members of the stored CIR samples, $\hat{h}(t,\tau_l)$ and $\hat{h}(t-M+1,\tau_l)$, can be set to a higher value that yields lower coherence time for the filter memory span and shorter channel estimation filter lengths. Hence, for UEs having higher N_C degrees, autocorrelation between the first and the last stored CIR estimates will be set to lower values to enlarge the filter lengths and increase the clustering accuracy. Filter lengths can be found by using the CSI-RS density formulated in (5.33) as

$$m(n,t) = d(n,t)\Delta t_c \,. \tag{5.35}$$

As a result, the adaptive channel estimation filter lengths stored in the quantized lookup tables are subject to change with varying receiver velocities.

5.5 UE Anchored Down-Selection for CoMP Joint Transmission Cluster

CoMP system delay between the time UEs send multi-point CSI feedback and the time serving e-NB forms the joint transmission cluster to transfer the user plane data to the UEs is the bottleneck for energy efficiency and downlink capacity performance as proved in Section 4.3.2. Clustering decisions taken according to the outdated versions of the CSI feedbacks degrade the performance of CoMP systems. Serving e-NB can perform CIR prediction methods to tackle the challenges caused by the system delays as shown in Section 5.3. However, consolidating all the CSI reports for n ∈ N_{meas} and predicting the CIRs for each radio link create a huge computation burden on the serving e-NB.

UE aided joint transmission clustering scheme is proposed, where the UE first applies CoMP adaptive multi point channel estimation procedures mentioned in Section 5.4 and then re-sorts the smoothened received power estimates, $\tilde{P}_{RX}$, in descending order for all the members of the CoMP measurement set. Best CoMP measurement set member is found by $arg\ max_n\{\tilde{P}_{RX}(n,t)\} = n_{best}$, using the received power measurements according to the estimated multi-point CIR values. UE, then performs a threshold-based decision to predict the possible members of the Joint Transmission set cluster as

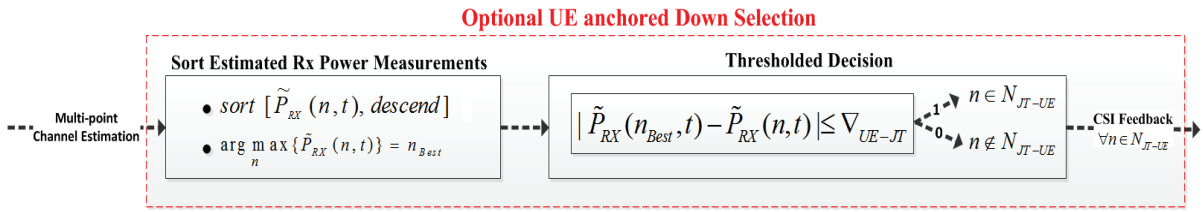

Figure 5.8: CoMP joint transmission cluster down-selection anchored by the UE after performing multi-point channel estimation and thresholding the received power estimates for each measured point.

$$\text{n} \in N_{JT-UE} \quad if \quad |\tilde{P}_{RX}(n_{best},t) - \tilde{P}_{RX}(n,t)| \leq \nabla_{UE-JT} \ , \tag{5.37}$$

$$\text{n} \notin N_{JT-UE} \quad if \quad |\tilde{P}_{RX}(n_{best},t) - \tilde{P}_{RX}(n,t)| > \nabla_{UE-JT} \ . \tag{5.38}$$

∇_{UE-JT} is the UE defined threshold to predict the members of the joint transmission set after performing channel estimation. It is determined by using the serving e-NB clustering threshold, the standard deviation of the received power measurement errors, $P_{err}(\mu,\sigma)$, resulting from channel estimation discrepancies, and a tuning parameter, s, as

$$\nabla_{UE-JT} = \nabla_{NW-JT} + s\sigma_{P_{err}} \ . \tag{5.39}$$

Both ∇_{NW-JT} and $\sigma_{P_{err}}$ are approximated by UE using a finite buffer storing the instantaneous ∇_{NW-JT} values observed in the recent TTIs by checking the difference between the best and the worst received powers from points performing joint PDSCH transmission. By this method, UE adapts to various network/carriers that have different clustering threshold configurations. UE predicted cluster threshold is made robust to the possible channel estimation errors by adding $\sigma_{P_{err}}$ as a security margin, and can be tuned according to various multi-point channel estimation schemes. UE then sends out multi-point CSI feedbacks only for CoMP measurement set points that satisfy $\text{n} \in N_{JT-UE}$ as shown in Figure 5.8. This scheme reduces the uplink payload for multi-point CSI feedbacks and decreases the heavy processing and clustering decision burden on the serving eNB by performing down-selection on the joint transmission set for the upcoming TTI. CSI feedback for the points that are less likely to be a part of the joint transmission set are not transferred over the access network or between the CoMP nodes. Hence, serving e-NB avoids unnecessary processing for these points and reduces the overall computation time for CIR prediction. As a result, the clustering decisions become more accurate at the time of PDSCH transmission. It should be noted that the thresholding procedures described in (5.37) and shown in Figure 5.5 share the same logic. However, (5.37) is performed after channel estimation procedure to limit the

number points about which UE sends CSI feedback for, while the method explained in Section 5.4.1 performs thresholding on the measured received power values to adjust the channel estimation filter lengths.

5.6 Summary

Channel estimation errors and system delays, which cause inaccurate CoMP joint transmission clustering decisions, are tackled using a holistic approach where UEs perform multi-point channel estimation and serving e-NB performs multi-point channel prediction procedures. Time domain channel estimation and prediction algorithms both utilize the time-varying second order stochastic characteristics of the CIR. UEs can perform multi-point CIR estimation either by tracking each delay tap individually or by tracking the overall superimposed CIR. It is demonstrated that although the latter mentioned scheme yields less accurate estimation results, it reduces the computation time significantly. CIR prediction gains are maximized by setting the prediction range equal to the observed CoMP system delays and making sure there are enough CIR samples stored by the serving e-NB to track the time-varying nature of the radio links. Novel multi-point channel estimation filter designs are proposed, where the UE adapts the estimation filter lengths according to the observed CoMP clustering degrees and the likelihood of each measured point being included in the joint transmission cluster on the upcoming TTI. This method makes sure the UEs with higher clustering degrees utilize estimation filters with larger memory spans for points that are more likely to be included in the joint transmission set. UE aided down-selection methods should be used jointly with the CoMP adaptive channel estimation procedures to decrease the multi-point CSI processing times at the serving e-NB. CoMP clustering accuracy is improved and the CIR estimation/prediction computation complexities are reduced with the proposed schemes.

The work explained in this chapter is part of the patent filings [65] and [66]. A journal paper is also under preparation.

Chapter 6

Conclusion and Future Work

6.1 Thesis Conclusions

Cell switch off schemes, which aim on decreasing the power consumption of the access networks by turning off the cells with low traffic loads, are used jointly with the LTE-A CoMP technology, which primarily targets on improving the cell edge performance in terms of achieved capacity rates. It is shown that the CoMP aided cell switch off schemes are superior to the traditional cell switch off schemes in terms of both energy efficiency and downlink capacity rates achieved in the network.

Performance of the proposed CoMP scheme is heavily dependent on the accuracy of the joint transmission clustering decisions given by the serving e-NB. Inclusion of an incorrect point in the CoMP cluster decreases the bits/Joule energy efficiency of the network since the increased downlink capacity rates are not enough to compensate for the additional power consumed in the network due to CoMP backhaul data transfers and signal processing. On the other hand, excluding a correct candidate from the joint transmission cluster degrades both the energy efficiency and the downlink capacity performance metrics. To balance the trade-off between the energy efficiency and the capacity KPIs, serving e-NB should perform threshold-based clustering decisions depending on the received downlink power levels between the members of the CoMP measurement set and the served UE. Threshold-based clustering method makes sure that the energy efficiency of the CoMP access network is not degraded while trying to improve the cell edge data rates.

Realistic performance gains of the CoMP schemes are revealed by simulating dynamic small scale fading channels for multi-point radio links and jointly considering the possible system delays and channel estimation errors that can occur prior to PDSCH user plane data transfers. High mobility scenarios lead to major joint transmission clustering inaccuracy due to the decreasing nature of the CIR autocorrelation functions, which create outdated CSI feedbacks in CoMP systems with delays. Multi-point channel estimation errors result in performance degradation since both the clustering degrees and the chosen members of the transmission cluster are affected. It is shown that the UEs with higher CoMP set degrees are more sensitive to CSI delays and estimation errors yielding inaccurate clustering decisions at the serving e-NB.

Channel estimation procedures performed by the CoMP supporting UEs via time-varying auto-regressive MMSE filters are enough to tackle the challenges introduced by faulty multi-point received power measurements. Multi-point channel estimation can be implemented either by tracking the overall superimposed CIR or by tracking the decomposed CIR at each multipath delay tap. It is shown that the latter scheme yields more accurate CIR estimates but comes along with increased computation complexity. LTE-A serving e-NBs, anchoring the joint transmission CoMP procedures, can address the discrepancies caused by the outdated CSI feedbacks due to system delays by performing CIR prediction for each $UE-n \in N_{meas}$ link before forming the N_{JT} clusters.

Existing channel estimation filter memory spans implemented by the UEs are adapted according to the observed CoMP characteristics. CoMP dependent UEs, which are served with higher clustering degrees, need to have filters with increased lengths to avoid inaccurate clustering decisions; whereas the UEs subject to PDSCH transmission from smaller clusters can decrease the auto-regressive filter lengths to avoid the computation complexity overhead. Dynamic filter lengths for each point in CoMP measurement set are utilized, so that only the points that are more likely to be included in the joint transmission sets are estimated with larger filter memory spans. It should be noted that all the aforementioned methods for CoMP adaptive channel estimation filters can be adapted by serving e-NBs for multi-point CIR predicting filters. Processing burden on the anchor e-NB is further decreased by the UEs taking initiative on the clustering decisions by sending out CSI feedbacks only for a subset of the CoMP measurement set which has high potential of taking active role during joint PDSCH transmission.

6.2 Possible Enhancements and Future Work

Proposed schemes for CoMP aided cell switch off technique and CoMP adaptive channel estimation and prediction methods have been presented with formulation, analysis and simulation results; however, there is still room for enhancements. Future work and interesting open research topics are listed as follows:

- Dynamic switching between the traditional and CoMP aided cell switch off schemes can be implemented, since it might not be worthy in some scenarios to involve CoMP unnecessarily. LTE-A access networks can implement a dual mode operation between the traditional and CoMP aided cell

switch off schemes. Adaptive changes between the two schemes can be performed according to the UE distribution and scheduling in the access network.

- DL Capacity performance for the CoMP schemes used Shannon's model for calculations, as presented in Section 3.2.1. More realistic data rate calculations can be performed by taking LTE-A AMC schemes into consideration and using actual CSI feedback versus PDSCH modulation scheme mapping table. It should be noted that the existing AMC tables have to be altered for joint transmission CoMP schemes.
- Multi-point channel estimation schemes utilized the time-varying characteristics of the channel to track the CIRs, as described in Section 5.2. An alternative method can be implemented by tracking the time-varying CTF in frequency domain using the time dispersive characteristics of the channel assuming uncorrelated scattering between the multipath delay taps. Time varying CTF autocorrelation function for a particular subcarrier frequency tone f_0 is formed as

$$R_H(\Delta \boldsymbol{t_M}, f_0) = \begin{bmatrix} E[H(t_1, f_0)H(t_1, f_0)^*] & \cdots & E[H(t_1, f_0)H(t_M, f_0)^*] \\ \vdots & \ddots & \vdots \\ E[H(t_M, f_0)H(t_1, f_0)^*] & \cdots & E[H(t_M, f_0)H(t_M, f_0)^*] \end{bmatrix}. \quad (5.40)$$

  It would be interesting to see the performance differences in terms of estimation accuracy and computation time of the CTF tracking scheme as opposed to the superimposed and decomposed time-varying CIR tracking schemes explained in this thesis. CTF autocorrelation function shown in (5.40) has to be used for all the subcarriers containing reference symbols and the frequency interpolated CTF is tracked in a time-varying fashion. Examples of CTF tracking using Slepian sequences and Wiener interpolators have been demonstrated in [63]. Depending on the number of resource blocks assigned to the UE per TTI, UEs may choose to switch between the decomposed CTF and CIR tracking schemes. If the number of subcarriers assigned to the UE per TTI is more than the number of multipath components L, it would be wiser to use the CIR tracking method to reduce the computation complexity.
- Auto-regressive channel estimation/prediction filters satisfying the MMSE criterion have been considered in Section 5.2.2; however more advanced schemes like Kalman filters can be utilized, as mentioned in [67] and [68].

- Section 5.4.3 proposed CoMP adaptive channel estimation filter length decisions, where the eNBs that are highly likely to be a part of the N_{JT} are estimated with larger memory spans. This scheme can be enhanced further for decomposed CIR estimation technique. Each multipath component of every $UE - N_{JT}$ radio link can be estimated with adaptive filters, $M_{UE}(n,t,l)$. UEs should only enlarge the CIR estimation filter memory spans for the major contributing multipath components belonging to the members of the N_{meas}. This method will balance the computation complexity versus accuracy trade-off for the decomposed CIR tracking scheme, by slightly reducing the estimation accuracy and reducing the computation time significantly.
- Computation complexity versus performance gain trade-offs for CoMP adaptive channel estimators predictors can be analyzed further by comparing the real time computation times for each tracking scheme. Although accurate channel estimation schemes implemented by the UE tackles the incorrect received power measurements, additional delays introduced due to the estimation computation times may in fact degrade the CoMP performance due to the outdated CSI feedbacks.
- MAC layer scheduling decisions should be integrated to the proposed schemes to get the optimum CoMP cluster degree every TTI. It should be noted that if multiple eNBs that are participating in joint PDSCH transmission assign the same resource block to the UE. The slave eNB of the cluster cannot use the same resource block to schedule UEs located in its own coverage region. Simulations shown in Chapters 3, 4 and 5 performed performance analysis by focusing on the UEs located in the CoMP serving eNB. However, overall cellular layout should be considered to obtain fair performance gains. Certain number of RRC connected UEs getting different UL/DL grants every TTI can be simulated in the whole cellular layout to obtain the energy efficiency and downlink capacity maximizing clustering decisions under dynamic scheduling conditions.

Future work will focus on enhancing the proposed schemes in this thesis by taking the above mentioned research topics into consideration.

Bibliography

[1] A. Nolan, "Global action plan: An inefficient truth," Internet: http://www.globalactionplan.org.uk/green-it, Dec. 2007.

[2] *Node B datasheets*, http://www.motorola.com/, 2008.

[3] J. T. Louhi, "Energy efficiency of modern cellular base stations," in *Proc. IEEE INTELEC'07*, Rome, Italy, Sept. 2007.

[4] ICT-EARTH. "Energy aware radio and network technologies." Internet: https://www.ict-earth.eu/, 2010 [Jan. 31, 2012].

[5] ICT-C2POWER. "Cognitive radio and cooperative strategies for power saving in multi-standard wireless devices." Internet: http://www.ict-c2power.eu/, 2011 [Jan. 31, 2012].

[6] T. Abe, "Further enhancements for LTE-Advanced," Internet: http://www.3g4g.co.uk/LteA/, Sept. 2010 [Dec. 20, 2011].

[7] Z. Hashmi, H. Boostanimehr, and V. Bhargava, "Green cellular network: A survey, some research issues and challenges," *IEEE Communications Surveys & Tutorials*, vol. 13, no. 4, pp. 524-540, Fourth Quarter 2011.

[8] L. M Correia, et. al, "Challenges and enabling technologies for energy aware mobile radio networks," *IEEE Commun. Mag.*, vol. 48, no. 11, pp. 66-72, Nov. 2010.

[9] Alcatel-Lucent and Vodafone Chair on Mobile Communication Systems, "Study on energy efficient radio access network (EERAN) technologies," Unpublished Project Report, Technical University of Dresden, Dresden, Germany, 2009.

[10] H. Claussen, L. T. W Ho, and F. Pivit, "Effects of joint macrocell and residential picocell deployment on the network energy efficiency," in *Proc. IEEE PIMRC'08*, pp.1-6, Sept. 2008.

[11] R. Baines, "Femtocells - the green solution," Internet: http://www.ecnmag.com/blogs/2010/09/femtocells-green-solution, Sept. 24, 2010 [Nov. 27, 2011].

[12] D. Ferling, T. Bohn, D. Zeller, P. Frenger, I. Godor, Y. Jading, and W. Tomaselli, "Energy efficiency approaches for radio nodes," in *Proc. Future Net. Mobile Summit '10*, pp. 1-9, June 2010.

[13] B. Badic, T. O'Farrell, P. Loskot, and J. He, "Energy efficient radio access architectures for green radio: Large versus small cell size deployment," in *Proc. IEEE VTC'09*, Anchorage, AK, Sept. 2009.

[14] Y. Chen, S. Zhang, S. Xu, and G. Y. Li. "Fundamental trade-offs on green wireless networks," *IEEE Commun. Mag.,* vol. 49, no. 6, pp. 30-37, Jun. 2011.

[15] C. E. Shannon, "A mathematical theory of communication," *The Bell System Technical Journal*, Vol. 27, pp. 379-423, 623-656, July 1948.

[16] L. Xiang, F. Pantisano, R. Verdone, X. Ge, and M. Chen, "Adaptive traffic load-balancing for green cellular networks," in *Proc. IEEE PIMRC'11,* Toronto, ON, Canada, Sept. 2011.

[17] W. Cheng, X. Zhang, H. Zhang and Q. Wang, "On-Demand based wireless resources trading for green communications," in *Proc. Infocom'11 Workshop on Green Commun.*, Shanghai, China, Apr. 2011.

[18] R. Schoenen, G. Bulu, A. Mirtaheri, and H. Yanikomeroglu, "Green communications by demand shaping and User-in-the-Loop tariff-based control," in *Proc. 2011 IEEE Online Green Communications Conference (IEEE GreenCom'11)*, Online, 2011.

[19] Z. Niu, Y. Wu, J. Gong, and Z. Yang, "Cell zooming for cost-efficient green cellular networks," *IEEE Commun. Mag.,* vol. 48, no. 11, pp. 74-79, Nov. 2010.

[20] S. Zhou, J. Gong, Z. Yang, Z. Niu and P. Yang, "Green mobile access network with dynamic base station energy saving," in *Proc. ACM MobiCom*, Beijing, China, Sept. 2009.

[21] M. Marsan, L. Chiaraviglio, D. Ciullo, and M. Meo, "Optimal energy savings in cellular access networks," in *Proc. ICC'09 Workshop on Green Commun.,* Dresden, Germany, June 2009.

[22] M. Marsan and M. Meo, "Energy efficient wireless Internet access with cooperative cellular networks," *Computer Networks*, vol. 55, no. 2, pp. 386-398, Feb. 2011.

[23] L. Chiaraviglio, D. Ciullo, M. Meo, and M. Marsan, "Energy-aware UMTS access networks," in *Proc. 11th Int'l Symposium on Wireless Personal Multimedia Communications*, Lapland, Finland, Sept. 2008.

[24] 3GPP R3-100162, "Overview to LTE energy saving solutions to cell switch off/on," *3GPP RAN3 Meeting*, Valencia, Spain, Jan. 2010.

[25] NEC Corporation. *NEC's proposals for next-generation radio network management* [Online]. Available: http://www.nec.com/en/global/solutions/nsp/lte/pdf/son.pdf, Feb. 2009.

[26] D. Cao, S. Zhou, C. Zhang, and Z. Niu, "Energy saving performance comparison of coordinated multi-point transmission and wireless relaying," in *Proc. IEEE Globecom'10*, Miami, FL, Dec. 2010.

[27] S. Bahrenburg. *Long Term Evolution from A-Z.* Karlsruhe, Germany: Inacon Gmbh, 2010, pp. 1-107.

[28] C. Gessner, "UMTS Long Term Evolution (LTE) technology introduction application note," Internet: http://www.3g4g.co.uk/Lte/LTE_WP_0703_RandS.pdf, Mar. 2007 [Sept. 12, 2011].

[29] S. Sesia, I. Toufik, and M. Baker. *LTE, The UMTS Long Term Evolution: From Theory to Practice*. Croydon, UK: Wiley, 2011, pp. 121-246.

[30] 3GPP TS 36.211 V10.4.0, "Physical channels and modulation," Dec. 2011.

[31] 3GPP TS 36.213 V10.0.1, "Physical layer procedures," Jan. 2011.

[32] Alcatel-Lucent. *LTE technical principles* [Online]. Available: http://www.scribd.com/doc/529-26489/LTE-Technical-Principles, 2008.

[33] Anritsu Corporation. *LTE resources guide* [Online]. Available: http://www.anritsu.com/en-GB/Media-Room/Newsletters/files/anritsu_lte_guide.pdf, Jan. 2011.

[34] M. Sawahashi, Y. Kishiyama, A. Morimoto, D. Nishikawa, and M. Tanno, "Coordinated multipoint transmission/reception techniques for LTE-advanced," *IEEE Wireless Commun.,* vol. 17, no. 3, pp. 26-34, Jun. 2010.

[35] P. Marsch and G. P. Fettweis. *Coordinated Multi-Point in Mobile Communications*. New York, USA: Cambridge University Press, 2011, pp. 1-460.

[36] 3GPP TR 36.814 V1.2.1, "Further advancements for EUTRA: Physical layer aspects," June 2009.

[37] 3GPP TS 36.819 V11.1.0, "Coordinated multi-point operation for LTE physical layer aspects," Dec. 2011.

[38] R. Irmer, H. Droste, P. Marsch, M. Grieger, G. Fettweis, S. Brueck, H.-P. Mayer, L. Thiele, and V. Jungnickel, "Coordinated multipoint: Concepts, performance, and field trial results," *IEEE Commun. Mag.*, vol. 49, no. 2, pp. 102–111, Feb. 2011.

[39] A. Vergne and S. E. Elayoubi, "Evaluating the capacity gains from coordinated multipoint transmission and reception," in *Proc. IEEE WiOpt'10,* Avignon, France, June 2010.

[40] F. Diehm and G. Fettweis, "On the impact of signaling delays on the performance of centralized scheduling for joint detection cooperative cellular systems," in *Proc. IEEE WCNC'11,* Cancun, Mexico, Mar. 2011.

[41] X. Shang-hui and Z. Zhong-pei, "Coordinated multipoint transmission systems with the clustered super-cell structure configuration," in *Proc. IEEE WiCOM'09*, Bejing, China, Sept. 2009.

[42] L. Scalia, T. Biermann, C. Choi, K. Kozu, and W. Kellerer, "Power efficient mobile backhaul design for CoMP support in future wireless access systems," in *Proc. Infocom'11 Workshop on Green Commun.*, Shanghai, China, Apr. 2011.

[43] **G. Cili**, H. Yanikomeroglu, and F. R. Yu, "Cell switch off technique combined with coordinated multi-point (CoMP) transmission for energy efficiency in beyond-LTE cellular networks," in *Proc. IEEE ICC'12 Workshops,* Ottawa, ON, Canada, June 2012.

[44] International Telecommunication Union, "Guidelines for evaluation of radio interface technologies for IMT-Advanced," Rep. ITU-R M.2135, 2008.

[45] T. S. Rappaport. *Wireless Communications: Principles and Practice*, Upper Saddle River, NJ: Prentice Hall, 1996, pp. 57-248.

[46] S. Brueck, L. Zhao, J. Giese, and M. Amin, "Centralized scheduling for joint transmission coordinated multi-point in LTE-Advanced," in *Proc. 2010 International ITG Workshop on Smart Antennas*, pp. 177-184, Feb. 2010.

[47] A. J. Fehske, P. Marsch, and G. P. Fettweis, "Bit per joule efficiency of cooperating base stations in cellular networks," in *Proc. IEEE Globecom'10 Workshops,* Miami, FL, Dec. 2010.

[48] O. Arnold, F. Richter, G. Fettweis, and O. Blume, "Power consumption modeling for different base station types in heterogeneous cellular networks," in *Proc. Future Network and Mobile Summit 2010*, pp. 1-8, June 2010.

[49] R. Schoenen, A. B. Sediq, H. Yanikomeroglu, G. Senarath, and Z. Chao, "Fairness analysis in cellular networks using stochastic Petri nets," in *Proc. IEEE PIMRC'11*, Toronto, Canada, Sept. 2011.

[50] V-A. Le, R-A. Pitaval, S. Blostein, T. Riihonent and R. Wichmant. "Green cooperative communication using threshold-based relay selection protocols," in *Proc. ICGCS'*10, pp. 521-526, June 2010.

[51] **G. Cili**, H. Yanikomeroglu, and F. R. Yu, "Energy efficiency and capacity evaluation of LTE-Advanced downlink CoMP schemes subject to channel estimation errors and system delay," submitted to *IEEE ICC'13*, Budapest, Hungary, June 2013.

[52] G. Prabhu and P. Shankar, "Simulation of flat fading using Matlab for classroom instruction," *IEEE Trans. Educ.*, vol. 45, no. 1, pp. 19–25, Feb. 2002.

[53] K. E. Baddour and N. C. Beaulieu, "Autoregressive models for fading channel simulation," *IEEE Trans. Wireless Communications*, vol. 4, no. 4, pp. 1650–1662, Jul. 2005.

[54] K. Siegrist, "Central limit theorem," Internet: http://www.math.uah.edu/stat/sample/CLT.html, Jan. 16, 2012 [Feb. 01, 2012].

[55] 6th Framework Programme, Information Society Technologies, Wireless World Initiative New Radio (WINNER), IST-2003-507591, [Online]. Available: https://www.ist-winner.org/, 2006.

[56] "Spatial channel model for multiple input multiple output (MIMO) simulations", 3GPP TR 25.996 V6.1.0, Sep. 2003. [Online]. Available: http://www.3gpp.org/ftp/Specs/html-info/25996.htm

[57] J. Salo, G. Del Galdo, J. Salmi, P. Kyösti, M. Milojevic, D. Laselva, and C. Schneider. (2005, Jan.). MATLAB implementation of the 3GPP Spatial Channel Model (3GPP TR 25.996) [Online]. Available: http://radio.aalto.fi/en/research/rf_applications_in_mobile_communications/

[58] D. S. Baum, J. Salo, G. Del Galdo, M. Milojevic, P. Kyösti, and J. Hansen, "An interim channel model for beyond-3G systems," in *Proc. IEEE VTC'05*, Stockholm, Sweden, May 2005.

[59] D. S. Baum, J. Salo, M. Milojevic, P. Kyösti, and J. Hansen, "MATLAB implementation of the interim channel model for beyond-3G systems (SCME)," May 2005. [Online]. Available: http://radio.aalto.fi/en/research/rf_applications_in_mobile_communications/

[60] M. Garg, "Statistical wireless channel model," Internet: http://www.mohrahit.in/find/wireless-ChannelModel.html, Oct. 09, 2005 [Oct. 14, 2011].

[61] A. Leon-Garcia. *Probability and Random Processes for Electrical Engineering.* Reading, MA: Addison-Wesley, 1994, pp. 330-389.

[62] B.H. Fleury, "An uncertainty relation for WSS processes and its application to WSSUS systems," *IEEE Trans. Commun.*, vol .44, no. 12, pp. 1632-1634, Dec. 1996.

[63] L. Somasegaran, "Channel Estimation and Prediction in UMTS LTE," M.S. thesis, Institute of Electronic Systems, Aalborg University, Denmark, 2007.

[64] A. Duel-Hallen, "Fading channel prediction for mobile radio adaptive transmission systems," *Proc. IEEE*, vol. 95, no. 12, pp. 2299-2313, Dec. 2007.

[65] **G. Cili**, H. Yanikomeroglu, and F. R. Yu, "CoMP adaptive channel estimation prediction filter design," Filed by Apple Inc., U.S. Patent Application No: 61/674,852 (filing date: July 23, 2012).

[66] **G. Cili**, H. Yanikomeroglu, and F. R. Yu, "UE anchored down-selection for CoMP joint transmission cluster," Filed by Apple Inc., U.S. Patent Application No: 61/674,854 (filing date: July 24, 2012).

[67] R. A. Olesen, "Channel Prediction for Coordinated Multipoint Transmission," M.S. thesis, Dept. of Engineering Sciences, Uppsala University, Sweden, 2011.

[68] D. Aronsson, "Channel Estimation and Prediction for MIMO OFDM Systems Key Design and Performance Aspects of Kalman-based Algorithms," M.S. thesis, Dept. of Engineering Sciences, Uppsala University, Sweden, 2011.